KAUNAS UNIVERSITY OF TECHNOLOGY

IEVA MILAŠAUSKAITĖ

RESEARCH OF DYNAMICS OF PIEZOELECTRIC ENERGY HARVESTERS

Doctoral Dissertation
Technological Sciences, Mechanical Engineering (09T)

2014, Kaunas

This dissertation was prepared at Kaunas University of Technology, Institute of Mechatronics, during the period of 2010 – 2014.

Scientific Supervisor:

Prof. habil. dr. Vytautas OSTAŠEVIČIUS (Kaunas University of Technology, Technological Sciences, Mechanical Engineering – 09T).

KAUNO TECHNOLOGIJOS UNIVERSITETAS

IEVA MILAŠAUSKAITĖ

PJEZOELEKTRINIŲ ENERGIJĄ GENERUOJANČIŲ SISTEMŲ DINAMIKOS TYRIMAI

Daktaro disertacija
Technologijos mokslai, mechanikos inžinerija (09T)

2014, Kaunas

CONTENT

4

NOMENCLATURE

FE – Finite Element –modelling technique;
IoT – Internet of Things;
OPT 0 – typical piezoelectric energy harvester/cantilever beam with constant cross-section;
OPT II – piezoelectric energy harvester/cantilever beam optimal for operation at its second resonant frequency;
OPT III – piezoelectric energy harvester/cantilever beam optimal for operation at its third resonant frequency;
OPT RAT – piezoelectric energy harvester/cantilever beam of rational configuration
PEH – Piezoelectric Energy Harvester;
PMN-PT - lead magnesium niobate-lead titanate – piezocrystal;
PVDF - polyvinylidene fluoride – piezoelectric polymer;
PZT - lead zirconate titanate – piezoceramic material;
VIPEH – Vibro-Impacting Piezoelectric Energy Harvester;
VIS - Vibro-Impacting System;
V_{RMS} – Root Mean Square voltage generated by piezoelectric energy harvester;
WSN – Wireless Sensor Network.

LIST OF FIGURES

LIST OF TABLES

INTRODUCTION

Research Relevance, Aim and Objectives

In relation to decreasing power consumption for electronic devices ambient energy harvesting un-cease being at the focus of research community for well more than a decade. The focus in the subject is such long-lasting, as researchers are aiming to offer alternatives for batteries (or, at least, augment their use) for wireless systems and devices, which may be further connected to the wireless sensor networks (WSNs) or become a part of the Internet of Things (IoT). Self powered devices are desirable, since on board power supply would eliminate heavy expenses of battery replacement and environment contamination. Employing benefits offered by new fabrication as well as device technologies, self powered systems possess advantages of low weight and volume, ease of integration with other micro mechanical and electrical components, and can be widely applied in monitoring/control of various subjects, ranging from structural soundness of buildings to manufacturing processes or even human health condition.

Solar, thermal and vibration energy are considered as main ambient energy sources. Photovoltaic and thermoelectric effects are employed to harvest solar and thermal energies respectively, while vibration energy is harvested harnessing electromagnetic, electrostatic or piezoelectric effects. Energy harvesting from vibrations is currently capturing the most of researchers' interest, as vibrations are most ubiquitous and energy may be harvested in dark and inhospitable environments.

However, there are still quite many issues associated with vibration energy harvesters, on the top of which being low harvester efficiency (5-20 %), particularly prominent in practical applications. For typical harvester designs the maximum generated power is achieved when natural frequency of harvester matches dominant vibration frequency of environment it operates in. Therefore, if resonant frequency of harvester does not match that of its' operating environment, level of harvester generated power decreases dramatically. Thus, a number of various methods and strategies are sought for to improve efficiency of energy harvesters.

The aim of this research is to develop, analyze and elaborate enhanced configuration energy harvester prototypes that would ensure effective electrical energy generation under varying mechanical excitation conditions.

To achieve the aim, the following objectives were raised:

1. Perform literature review of the research ongoing in the field of energy harvesting, placing the greatest emphasis on piezoelectric energy harvesters and determine the main issue associated with them.
2. Develop a universal finite element model of piezoelectric energy harvester, which would allow investigations of harvester dynamic and electric response when it is excited by harmonic or random excitation signal and operating in non-impacting or vibro-impacting modes.

3. Evaluate effects of piezoelectric energy harvester's excitation and constructional parameters variation to dynamic and electric response of harvester by means of developed FE model.
4. Adapt experimental measurement stands that would allow evaluating dynamic and electric characteristics of harvester prototypes and verifying adequacy of developed FE model.
5. Suggest enhanced piezoelectric energy harvester prototype configuration that would ensure effective energy generation under varying mechanical excitation conditions via self-excitation of higher vibration modes.

As it is already stated above, one of the thesis objectives is to review and summarize recent publications related to/analyzing the field of energy harvesting. Thus, sections of the thesis describe not only to available energy harvester configurations, but also numerical as well as experimental testing techniques of energy harvesters. It is worth noting that this thesis is focused on harvesting energy from mechanical vibrations and excludes other alternative energy sources, such as solar, wind or thermal energy. Main vibration energy to electricity conversion methods are covered shortly, summarizing their basic operation principles as well as advantages and disadvantages. Only piezoelectric transduction mechanism (as well as the main properties of piezoelectric materials) is described and analyzed in more detail, since objects of this research are operating on the basis of this conversion principle.

Earliest configurations of vibration energy harvesters focused on simple oscillators aiming to exploit resonance phenomenon under harmonic excitation. However, nowadays, researchers have directed their attention towards more sophisticated energy harvester configurations that could as well harvester energy from random ambient vibrations. As a result, a part of recent research in harvesting of vibration induced energy has thus focused on nonlinear and complex scavenging systems. As compared to their liner counterparts, non-linear energy harvesters demonstrate improved performance under broadband excitation as well as longer device operation lifetime. Thus, not only typical piezoelectric energy harvester designs, but also recent non-linear design implementations are discussed in the first section of the thesis.

Object of this research - vibro-impacting piezoelectric energy harvester (VIPEH) - consists of relatively flexible cantilever beam covered with piezoelectric material, which is in turn enveloped with electrodes enabling to collect charge developed across deformed piezoelectric material. This cantilever beam may be/may not be impacting on a rigid mechanical support, which is incorporated to harvester with the aim to widen its' operational frequency range and prolong lifetime. It is important to note, that, in such case, maximal displacement of vibrating device is limited by the stopgap size (i.e., distance between incorporated support and beam at rest). If beam is not hitting incorporated support, harvester frequency response function demonstrates typical linear behaviour. For sufficiently high harvester excitation amplitudes, cantilever beam starts impacting on incorporated support and higher modes of device vibration may be excited.

Thus, the proposed configuration of piezoelectric energy harvester is regarded as distributed parameter system, concerning not only its first but also higher vibration modes. The topic of harvester efficiency improvement via excitation of higher vibration modes is very important, since currently available energy harvesters, although showing high efficiency results in publications, are not commonly used in practical applications (e.g., wireless sensor powering) due to inefficiency under varying excitation conditions.

Dynamic and electric characteristics of the above described piezoelectric energy harvester prototypes are analyzed employing numerical and experimental methods. Finite Element model of the object is created with Comsol Multiphysics software, meanwhile experimental measurements are performed with adapted holographic measurement and laser Doppler vibrometry stands.

Statement of novelty

The following scientific novelties are presented in the thesis:
1. Universal Finite Element model of piezoelectric energy harvester, which allows integrated investigations of harvester dynamic and electric response when it is excited not only by harmonic, but also by random excitation signal and is operating in non-impacting or, moreover, vibro-impacting modes.
2. Experimental and theoretical proof of feasibility to use enhanced vibro-impacting harvester configuration with incorporated supports located at the nodal points of harvester vibration modes. This configuration of harvester allows exploiting higher modes of vibration which self-excite when harvester is operating in vibro-impacting mode. Thus, efficiency of harvester is improved, especially when harvester is excited by random signals, predominant in real environments;
3. Concepts of optimal and rational piezoelectric energy harvesters are introduced, with numerical and experimental proofs that rational piezoelectric energy harvester prototype (based on simplified optimal piezoelectric energy harvester configuration, which is obtained by thickening the cantilever substrate at particular cross-section point) outperforms piezoelectric energy harvester of typical (i.e., constant cross-section) configuration.

Document structure

The thesis is divided into six sections. Research development pathway presented in Figure 1 illustrates the sequence of actions taken to meet the research objectives and achieve the final aim of the study.

Section 1 introduces the reader to the performed research, presenting research development pathway, research background, main aim as well as objectives.

Section 2 presents main topics related to the field of the energy harvesting with the review of recent and most relevant literature and discussions on works performed in this area. This covers introduction to wireless sensors, IoT and common as well as alternative ways to power them. Summary on different methods that can be used to convert vibration energy into electricity is presented, with particular emphasis on piezoelectric transduction. The latter is followed by broad

review of piezoelectric energy harvester configurations, highlighting main issues associated with the most popular harvester designs.

Issue: inefficiency of piezoelectric energy harvesters

Aim: development of the enhanced energy harvester

Review & analysis of wireless devices, their powering requirements, common as well as alternative energy sources and energy conversion mechanisms

Decision to employ vibration energy to drive piezoelectric energy harvester

Review and analysis of piezoelectric materials, piezoelectric energy harvester configurations as well as main issues associated with these harvesters

Decision to concentrate the research on cantilever type piezoelectric energy harvester

Review & analysis of available methods used to enhance design and efficiency of cantilever type piezoelectric energy harvesters

Suggestions for enhanced piezoelectric energy harvester design

Development of FE model of piezoelectric energy harvester which would allow evaluating effects of different variables to harvesters' performance

Numerical simulations completed with the developed FE model of piezoelectric energy harvester

Adaptation of experimental measurement stands and conduct of experimental studies to verify theoretical discussions as well as simulation results

Development of enhanced piezoelectric energy harvester prototype

Figure 1. Research development pathway

Section 3 introduces the developed finite element model of piezoelectric energy harvester and describes all numerical simulations performed during the research period. Numeric research was completed with a number of different piezoelectric energy harvester configurations - varying harvester's dimensions and shape, piezoelectric material, pattern of piezoelectric layer segmentation, parameters of the connected electric circuit, and rigid support location - finally introducing an enhanced design of piezoelectric energy harvester. This enhanced harvester design is based on simplified optimal piezoelectric energy harvester configuration, which is obtained by thickening cantilever substrate of harvester at particular cross-section point (i.e., varying its' cross-section).

Section 4 is devoted to present all experimental studies completed during the research period as well as covers fabrication processes of piezoelectric energy harvester prototypes. Experimental studies were completed employing adapted holographic measurement and laser Doppler vibrometry stands, with a number of piezoelectric energy harvester prototypes of different configurations. Comparative experimental studies were focused on dynamic and electric response of prototypes in order to prove benefits of suggested enhanced harvester configurations.

Section 5 is devoted for the case study of enhanced piezoelectric energy harvester prototype, describing its development stages, numerical simulations, fabrication processes and experimental research.

Section 6 summarizes conclusions drawn both from theoretical and experimental studies with the suggestions for future research and development in this area.

To whom it might concern

The possible readers of the thesis may include other students and academic community involved in the research of wireless sensors, alternative power supplies and micro-power energy harvesting. It may also capture the interest of energy scavenging technology developers or even those, who are seeking for cooperation partners in the scientific research.

Future work

Future work might include further optimization of piezoelectric energy harvester configuration (e.g., multilayered devices) besides development of sophisticated mathematical and numerical models to predict lifetime of operating vibro-impacting devices.

Research approbation

Theoretical and experimental studies were performed at Kaunas University of Technology, Institute of Mechatronics. Some of the research results were obtained and reclaimed implementing research project "Development and research of untraditional energy source for autonomous microelectromechanical systems" (No. MIP-060/2012), financed by Research Council of Lithuania.

Research results were already presented in a number of international conferences. Main research results were published in 13 scientific papers: 6 papers

with impact factor are listed in the database of the Institute for Scientific Information (ISI), 3 papers are available in ISI database referred editions and 4 papers in the conference proceedings. The detailed list of all publications is available below.

List of Publications

„ISI Web of Science" publications with citation index

1. V. Ostasevicius, I. Milasauskaite, R. Dauksevicius, V. Baltrusaitis, V. Grigaliunas, I. Prosycevas, Experimental characterization of material structure of piezoelectric PVDF polymer // Mechanika / 2010, no. 6(86), p. 78-82.
2. R. Dauksevicius, G. Kulvietis, V. Ostasevicius, R. Gaidys, I. Milasauskaite, Multiphysical modeling of a contact-type piezotransducer for the analysis of micro-energy harvesting from ambient vibrations // Journal of Vibroengineering / 2011, Vol. 13, no. 2, p. 342-351.
3. R. Dauksevicius, G. Kulvietis, V. Ostasevicius, I. Milasauskaite, Numerical study of cantilevers with non-uniform width for enhancing the performance of vibration-driven micropower generator based on piezoelectric conversion // Journal of Vibroengineering / 2011, Vol. 13, no. 3, p. 578-585.
4. R. Dauksevicius, I. Milasauskaite; V. Ostasevicius, V. Jurenas, S. Mikuckyte, Experimental study of coupled dynamic and electric characteristics of piezoelectric energy harvester under variable resistive load // Journal of Vibroengineering / 2012, Vol. 14, iss. 3, p. 1435-1443.
5. G. Janusas, I. Milasauskaite, V. Ostasevicius, R. Dauksevicius, Efficiency improvement of energy harvester at higher frequencies // Journal of Vibroengineering / 2014, Vol. 16, no. 3, p. 1326‑1333.
6. I. Milasauskaite, R. Dauksevicius, V. Ostasevicius, R. Gaidys, G. Janusas, Influence of contact point location on dynamical and electrical responses of impact-type vibration energy harvester based on piezoelectric transduction // ZAMM, Z. Angew. Math. Mech., 2014, no. 11 (94), p. 1-6.

International database issues

1. V. Ostasevicius, I. Milasauskaite; R. Dauksevicius; V. Baltrusaitis, V. Grigaliunas, I. Prosycevas, Fabrication and analysis of piezoactive structure used for energy microharvesters // Mechanika 2010: proceedings of the 15th international conference, April 8-9, 2010, Kaunas, Lithuania / 2010, p. 332-337.
2. R. Dauksevicius, G. Kulvietis, V. Ostasevicius, I. Milasauskaite, Finite element analysis of piezoelectric microgenerator–towards optimal configuration // Procedia Engineering: Eurosensors XXIV, September 5-8, 2010, Linz, Austria: proceedings / 2010, Vol. 5, p. 1312-1315.
3. R. Dauksevicius, I. Milasauskaite, V. Ostasevicius, R. Gaidys. Investigation of piezoelectric bending actuator for application in kinetic energy harvesting // Mechanika 2012: proceedings of the 17th international conference / 2012, p. 48-51.

Proceedings

1. I. Milasauskaite, V. Grigaliunas, D. Virzonis, Optical interferometry for displacement measurement of a microelectromechanical membrane // Mechatronic Systems and Materials: scientific papers / 2008, p. 8-9.
2. I. Milasauskaite, V. Ostasevicius, V. Grigaliunas, R. Gudaitis, Polyvinylidene fluoride (PVDF) films for radioactive source powered piezoelectric microgenerator // Mechatronic Systems and Materials: scientific papers / 2009, p. 13-18.
3. R. Dauksevicius, G. Kulvietis, V. Ostasevicius, I. Milasauskaite, Design and Development of Vibrational Mechanoelectrical MEMS Transducer for Micropower Generation // Design, Test, Integration and Packaging of MEMS/MOEMS (DTIP), 2011 Symposium on, p.164-169.
4. G. Janusas, I. Milasauskaite, V. Ostasevicius, V. Grigaliunas, R. Dauksevicius, R. Gaidys, Output power optimization of energy harvester, employing segmentation of its electrodes /Vibroengineering PROCEDIA: international conference / 2013, vol. 1, p. 103-106.

1.   LITERATURE REVIEW

In relation to decreasing power requirements for electronic devices, energy harvesting continues to be at the focus of research community for more than a decade. Interest in the subject is long-lasting since researchers are aiming to offer alternatives for conventional batteries (or, at least, augment their use) in miniaturized wireless systems, which may further become a part of the Wireless Sensor Networks (WSN) or Internet of Things (IoT).

This section presents a review of publications as well as main theoretical concepts and principles used in the field of energy harvesting. The section starts with the basic introduction of Internet of Things, Wireless Sensor nodes, their possible applications and typical powering requirements. These are followed by a brief review of electrochemical batteries, renewable energy sources, energy conversion principles and commonly met energy scavengers, with a particular emphasize on piezoelectric energy harvesters (PEHs). The most common configurations of PEHs with their capabilities, limitations as well as areas of design improvement are elaborated.

In general, the aim of this section is to introduce reader to the field of energy harvesting, outlaying its basic principles, recent research achievements and commonly met issues or, in other words, lay a steady theoretical ground to understand numerical and experimental research presented in the subsequent sections of the thesis.

1.1. Wireless Sensor Networks, Internet of Things and Wireless Nodes

Immense advances in electronics with decreased device size and modest power consumption have led to the vast development of various sensors facilitating our lives. One may encounter Wireless Sensor Network (WSN) nodes almost everywhere, their application spreading over variety of different fields, ranging from structural health monitoring to medical implants, e.g., WSNs are used for structural monitoring of buildings; status monitoring of machinery; monitoring of domestic environments to make them more comfortable; military tracking; security; personal tracking and recovery systems [1] (some examples of nodes, their measured parameters and power requirements are presented in Table 1 [2]). There are many companies worldwide that are working with WSNs, including Crossbow, Picotux, Sentilla, Gumstix, Libelium, GE Energy and others. The most famous WSNs so far are ExScal (a 1000+ node WSN in remote area in Florida, USA to monitor intrusion activities), Argo (a global array of 3,000 drifting floats that measure temperature and salinity of the ocean) and GLACSWEB (WSN aimed for glacier behaviour monitoring). The main advantage of all these networks is that they can significantly improve accuracy of scientific measurements of physical phenomena since they are deployed directly and densely in experimental areas.

The other extensive and promising area for applications of wireless sensors and other wireless devices lies within the Internet of Things (IoT). The basic concept of IoT relies on the abundant presence of a variety of subjects/objects – i.e., sensors and actuators – which (given defined addressing schemes) are able to communicate

and interact with each other in order to meet common goals. WSN and IoT application areas coincide at a lot of instances, as IoT may be as well used for environment monitoring, medical and health care, industrial, transport and etc. systems. However the main difference between WSN and IoT is that IoT systems are responsible for performing actions, not just sensing things. The further sections of this thesis will refer to the wireless sensor nodes that could further become a part of both WSNs and IoT.

In general, a wireless sensor node (scheme of which is presented Figure 2) is a device made of i) a sensing element which will capture required physical or chemical parameters; ii) a processing element consisting of microprocessor or microcontroller that will process measurement data and store them in memory; iii) a communication element which will allow communication with external portable devices; iv) a power supply element, which will include both power source and converter.
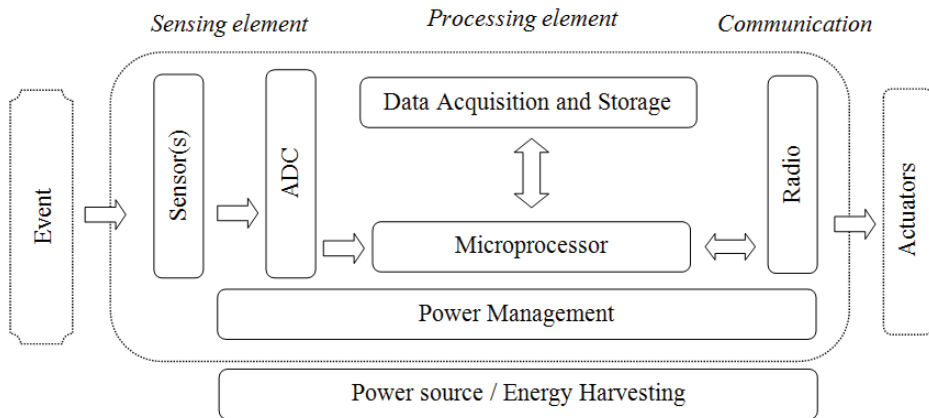
Figure 2. Typical architecture of wireless sensor node (after [3])
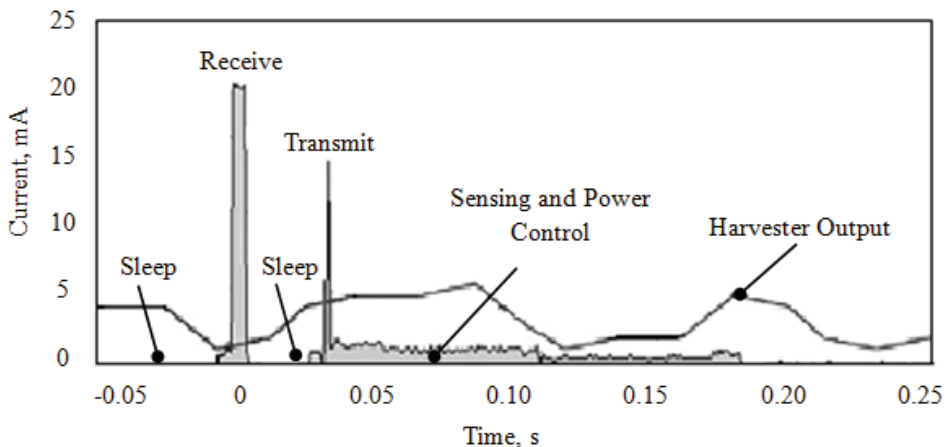
Figure 3. Typical scenario for power consumption in a wireless sensor node (after [5])

17

Power consumption of wireless sensor node was estimated by various authors [2 - 5] presenting different values, yet it usually ranges between 10 and 100 µW. Let us consider a typical case of power demand of wireless sensor node depicted in Figure 3. As per common scenario, every node communicates only at a small portion of its life. In most of operation time the only activities occurring in a node are background tasks. Combining peak and standby power dissipation leads to an average power dissipation of approximately 100 microwatts. It goes without saying, that consumption strongly depends on the complexity of sensed quantity and on the number of times per second it has to be transmitted as well as the other factors summarized in Table 2.

The main issue associated with wireless nodes is their powering. Most often electrochemical batteries are used to power the nodes, yet this imposes device operation lifetime limit and/or increases device cost if battery replacement is needed. The subsequent chapters present most commonly met electrochemical batteries, however it is important to emphasize that conventional batteries would not meet powering requirements for most of WSN and IoT devices, thus alternative and renewable energy sources for wireless nodes powering are analyzed as well.

Table 1. Examples of wireless sensors, parameters they measured and their powering requirements

Applications	Type of sensors in the node	Measured parameters	Power requirements (mW)
Habitat monitoring	Ultrasonic, pressure, vibration	Tracking numbers, distribution	6000, 10
Structural health monitoring	Ultrasonic, piezoelectric	Cracks in structure	-
Military service	Acoustic, vibration	Intruder	28
Environment applications	Electrochemical, thermocouple, seismic, barometric	Trace chemicals, measure temperature, pressure, turbidity, humidity	50-450
Agricultural monitoring	Thermocouple, electrochemical	Temperature, soil moisture	0.01-50

Table 2. Factors affecting power consumption of different wireless node elements

Power supply	Sensors	Signal conditioning	Radio
Discharge rate; battery type & dimensions; Supply voltages.	Physical to electrical signal conversion; Complexity of supporting components; Signal sampling.	Sampling rate.	Modulation scheme; transmission range; Operational duty cycle.

1.2. Electrochemical Batteries

Nowadays electrochemical batteries are most popular power sources for such small scale, low-power systems like wireless sensors. The popularity of this power source has resulted from their relatively low costs, commercial availability in various sizes, power densities as well as ease of fabrication and integration (no moving parts are involved, no need for voltage converters). Batteries are typically classified in two main categories: i) primary (disposable), and ii) secondary (rechargeable). Chemicals of the disposable batteries are designed to complete irreversible reactions, thus such batteries may only be used once and have a very limited lifetime. Chemical reactions in rechargeable batteries are reversible, thus it is possible to recharge the battery running current of opposite direction through it.

Much research is focused to improve battery components, yet battery capacity improvements are slow and their lifetime is still relatively short. Battery miniaturization without reducing their lifetimes is a great obstacle as usually battery capacity is a function of its size. For example, at an average power consumption of 100 µW a wireless sensor node needs slightly more than 1 cm^3 of lithium battery volume for one year of operation, assuming that 100 percent of the battery's charge is used. So, given a 1 cm^3 size constraint, standard sensor node batteries would have to be replaced at least every nine months [7]. Thus, regular battery replacement is an inevitable part of node maintenance. It is a major, costly and time-consuming task. Besides, there are also many devices where battery replacements are particularly intricate – e.g., biomedical heart stimulation implants; corrosion sensors embedded in concrete; or in remote locations (e.g. oil rig undersea). Moreover, size of batteries (literature review suggests that battery for an analogue transceiver of the 1920's may have occupied 5% of the device volume, the Crossbow mica mote is powered by two AA size batteries that occupy 90% of the device volume [8]) and their disposal after use become great issues, making battery usually the largest and most expensive component of the wireless sensor node.
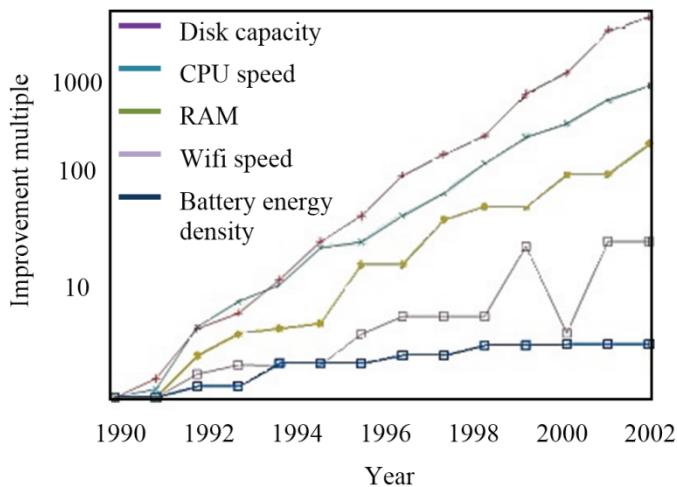
Figure 4. Advances in computer and battery technology since 1990 (after [9])

Literature review on the use of batteries for low-power electronics and remote sensors performed by Paradiso and Starner [9] concluded that progress in battery technologies is much slower than that of electronics in terms of energy density and operation life time, e.g., between 1990 and 2003, disk capacity increased by a factor of thousand; CPU speed was increased by almost as much, meanwhile battery energy density only increased about three times during the same period. This trend of increasing "energy gap" may be seen in Figure 4. Reliability of batteries is not sufficient to satisfy increasingly demanding powering requirements of wireless devices. Thus, alternative methods to power wireless devices are needed. The possible approaches to this challenge are: i) to use new fuels for local energy supplies, ii) to develop novel methods to distribute power for nodes from a nearby active source, or iii) to develop technologies that enable node to generate or harvest its own power. While research efforts have been made in i) and ii), the most promising solutions appear to be in the area of energy harvesting, which is further on described and analyzed in the thesis.

1.3. Renewable power sources

As previous section has concluded that electrochemical batteries are not the best powering options for wireless sensor nodes, the aim of this section is to shortly review and assess renewable power sources which could be deployed as alternatives to batteries. Table 3 summarizes commonly met renewable energy sources, outlaying their main advantages and disadvantages, while more insights on each source are given further.

Photovoltaic cells convert incoming photons into electricity and are the most popular and frequently used power sources for wireless sensor nodes after electrochemical batteries. They exhibit excellent power density and ease of integration. Besides, they may be installed in remote locations (e.g., deserts or ocean surfaces), yet are not efficient in dim or dirty environments (require often cleaning) and often become inadequate in terms of costs to efficiency ratio.

Thermal energy harvesters are based on the Seebeck effect – i.e., when two junctions, made of two dissimilar conductors, are kept at a different temperature an open circuit voltage develops between them. They are most efficient at locations where there is a steep temperature difference in close proximity (e.g., air and water interface) and so far were applied in industrial settings (e.g., utilizing heat flow between the engine body and surrounding ambient), as well as for human/animal monitoring (utilizing the temperature difference between body and environment). The main limitation of thermoelectric generator is its' low efficiency (between 0.1% and 8.0% [2]), which becomes even more pronounced in small areas (i.e., it is difficult to find greater than a 10° C thermal gradient in a volume of 1 cm^3).

Vibration induced energy can be found in instances where thermal or photonic energy is not available. Source of vibration energy can be a moving human body or a vibrating structure (examples of available vibration sources are presented in Table 4). Frequency of vibrations depends on the source: less than 10 Hz is typical for human movements while over 30 Hz to kHz for machinery vibrations [10].

Table 3. Summary of advantages and disadvantages of renewable energy sources

Energy	Advantages	Disadvantages
Solar energy	• Excellent power density in direct sunlight (solar radiation on the earth's surface is roughly 100 mW/cm^3); • Mature technology; • Efficiency of single crystal silicon cell is 12% - 25%, yet studies of multi junction solar cells report even 44.7%	• Inefficient in dim and dirty conditions (i.e., powering is available only at certain periods of time); • Relatively large surface areas may be required; • Require fine-tuning of cell design to the different composition of light; • Requires frequent cell cleaning;
Thermal energy	• Substantial enough, if thermal gradients are available; • Produced power - 10-15 µW/cm^3 from a 10 °C temperature gradient;	• Operating environment is limited; • Static temperature differences within ~1cm^3 are very rare;
Vibration induced energy	• Abundance and difference of sources; • Different conversion mechanisms;	• Complex systems may be employed; • Power densities are highly dependent on ambient frequency;
RF energy Fuel cells	• Ubiquitous in urban areas; • High energy density;	• Very low power density levels; • Require re-fuelling; • Limited lifetime;
Radioactive energy	• Long lifetime; • High constant power density;	• Hazards to health and environment;
Hydroelectric and wind energy	• Available in remote locations;	• Developed for macro-scale applications.

Table 4. Examples of vibration sources available in different environments

Human body	Industrial	Structures	Vehicles
Limb motion (arms, feet, fingers); Breathing; Blood pressure;	Cutting, turning & other vibrating machinery; Motors, compressors, fans;	Bridges, roads, tunnels, tall buildings;	Automobiles (tires, brakes); Aircrafts; Trains.

Energy of vibrations is transferred to electrical energy employing electromagnetic, electrostatic and piezoelectric mechanisms that will be discussed in more detail in subsequent sections of the thesis. Radio frequency (RF) energy available in the environment appears due to radio, wireless internet, cellular phone and other wireless devices operation. RF is an electromagnetic wave which is generated applying alternating voltage to an antenna. Since ambient RF energy is most abundant in urban areas, operation of RF powered wireless sensor nodes is most reliable at locations near cities, yet limited in remote locations (e.g., middle of the ocean).

Other power sources reported to generate small amounts of power yet not so commonly suggested for micro-applications include fuel cells, radioactive power sources, hydroelectric and wind power sources.

Traditional fuel cells use limited amount of fuel (e.g., hydrogen, hydrocarbons and alcohols) to generate electrical energy, thus refuelling (which may be as problematic as changing batteries) is still needed. However, one must note that it happens less frequent than battery replacement and lifetime of a node can be extended by several times. Meanwhile sediment microbial fuel cells (SMFC) generate electricity from microbial activity of native microorganisms present in sediment of natural water reservoirs. Reported powers of SMFCs are in the range of 3.4 to 36 mW and they may be utilized to power underwater and floating sensors [11]. The main advantage of this power source is everlasting fuel supply, as organic chemicals are renewed by natural sedimentation processes. However, disadvantages of low power generation and low voltage outputs must be noted as well.

Radioactive power sources, sometimes referred as nuclear batteries, are characterized by high power density and long lifetimes. Most of radioactive power sources are employed in space, as they proved to safely and reliably generate electricity for several decades in harsh environments with no health hazards to human beings.

Hydroelectric power and wind energy are historically employed in macro scale applications, yet some research papers report relatively efficient midi-scale hydroelectric and wind power systems, generating watt or kilowatt levels of power. Although both energy sources are available in remote locations (forests, mountains, ocean surfaces), scaling down of currently available technologies as well as reduction of costs and minimization of technical difficulties are necessary to use these sources for WSN nodes powering.

The above discussion on the alternative power sources may be summarized in Table 5 and visualized with Figure 5. As solar, vibration and thermal energy power outputs are not functions of lifetime, they are marked as boxes, defined by the average generated power bandwidth, which, of course, depends on environment conditions (e.g. maximum generated power is reached when solar cell, operates outdoors, at sunny day's midday, while minimum power is generated when solar cell operates in dim environment) [12]. Meanwhile all electromechanical batteries have limited lifetimes. However, it is important to note that batteries seem to be a viable solution to power devices in the range of one year, however, if one considers longer lifetimes of operating device, alternative energy sources are broadly cost-

comparable). Although reliability is at some concern for all alternative power sources, because harvested power depends on environmental conditions, which are inherently unreliable, this problem may be partially solved by using advanced power management circuits.
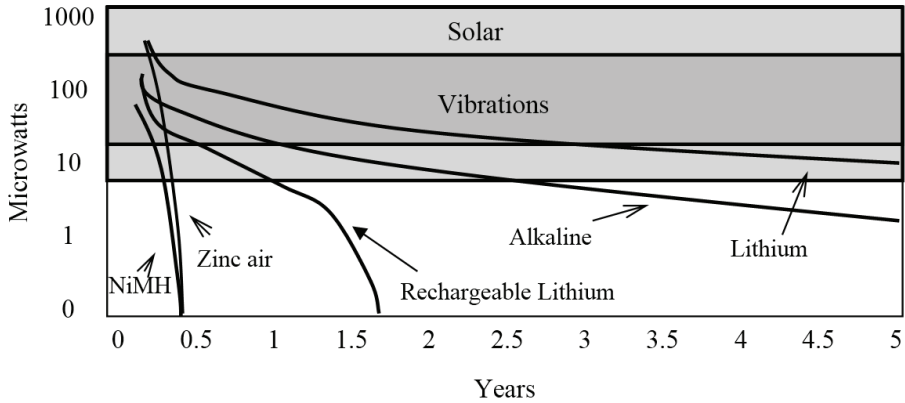
Figure 5. Power density versus lifetime for batteries, solar cells and vibration generators (after [12])

Table 5. Examples of batteries and alternative power sources that could be used to power wireless sensors [2]

Energy source	Type of sensor powered	Applications	Power / voltage
Batteries	Temperature, pressure, humidity, acceleration	Habitat monitoring, Environment monitoring, Military surveillance	1.2 – 12 V
Piezoelectric generators	Accelerometer, radio transceiver, strain gauge, temperature, humidity	Speed, leak test, environmental monitoring	3.5 mW
Hydroelectric generators	electrochemical	Agricultural	500 - 1000 mW
Wind energy generators	Temperature, wind speed, solar radiation	Agricultural	0.75 – 200 mW
Thermoelectric generators	Thermocouple	Environmental monitoring	32 mW
Ambient RF generators	Thermocouple, humidity	Environmental monitoring	0.0014 – 2.75mW
Solar cells	Thermocouple , optical, moisture	Environmental monitoring	0.4 mW – 85 W

It goes without saying that decision on alternative energy source choice is depend on environment conditions that harvester will be operating in. This makes designing of one type of energy harvester that can harvest energy from different environments and at different conditions impossible.

With this being said, the research presented in the thesis is directed towards designing a harvester driven by vibrations, since this source is most attractive due to its versatility and ubiquitousness.

As already discussed, vibration induced energy is attractive, renewable and, moreover, abundant, thus a number of studies [12- 14] were carried out to measure frequencies and accelerations of vibration sources suitable for energy harvesting applications, ranging from home appliances to industrial machines and structures. For example, Roundy et al. [14] analyzed environment vibrations, which emanate from domestic appliances (e.g., refrigerator, microwave oven, washing machine), transportation means (e.g., car) and industrial tools (e.g., HVAC vents). Measured vibrations were classified in two groups - low level vibrations (determined by 0-200 Hz range, dominating in household environment) and high level vibrations (appearing in the industrial environments, at frequencies above 200 Hz). Table 6 presents some examples of commonly encountered vibration sources (defined by their fundamental frequency and its acceleration magnitude) that could be employed in energy harvesting.

Table 6. Examples of vibration sources defined by the fundamental frequency and its acceleration magnitude [14]

Vibration sources in the environment	F, Hz	A, (m/s^2)
Refrigerator	240	0.1
Care engine compartment	200	12
Washing machine	109	0.5
Second floor of busy building	100	0.2
Base of a machine tool	70	10
HVAC vents	60	0.7
Car instrument panel	13	3
Nervous person tapping leg	1	3

It goes without saying, that it is highly important collecting all available information on vibrations prevalent in foreseen harvester's application environment, as most of vibration energy harvesters work efficiently only when excited at their resonant frequency (i.e., configuration of harvester is tuned to environmental conditions it will be operating in). Moreover, harvesters are often designed to be excited particularly at their first resonant frequency, since then devices exhibit highest displacement amplitudes which may be further converted to electricity employing different transduction mechanisms, which are detailed in the subsequent section.

1.4. Basic energy conversion principles

Williams and Yates [15] have created a general vibration to electricity conversion model, depicted in Figure 6. It is a spring-damper-mass system, which may be defined with the following equation for the motion:

$$m\ddot{z} + d\dot{z} + kz = -m\ddot{y},$$ (1.4.1)

where z is displacement of the device, y is the excitation, m is the proof mass, and d and k are the damping coefficient and the stiffness constants, respectively.

If ambient sinusoidal excitation vibration ($y(t) = Y_0 * \cos(\omega t)$) frequency matches resonant frequency of the device, its' power output is:

$$\left| P(j\omega) \right| = \frac{mY_0^2 \omega_n^3}{4\zeta}.$$ (1.4.2)

The main advantage of this particular model is that conversion mechanism does not need to be determined. System power outputs may be predicted knowing only frequency and magnitude of input vibrations and size (i.e., mass) of the overall system. Despite the fact that most of the actual energy harvesters are more intricate, it helps to define a few basic principles common for all vibration driven energy harvesters, namely: i) the smaller the harvester size, the less power may be extracted, as power is proportional to harvester mass; ii) power output may be optimized by equating electrically induced damping ratio to mechanical damping ratio; iii) harvester generated power is proportional to the square of the source vibration displacement magnitude; iv) harvester generated power (as well as its displacement magnitude) is inversely proportional to driving frequency; v) natural frequency of harvester should match source vibration resonant frequency.
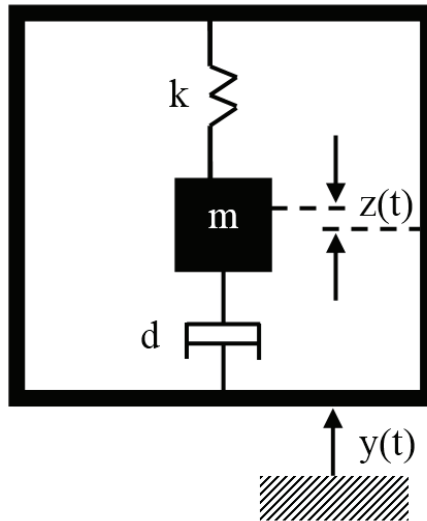
Figure 6. General model of vibration energy conversion (after [15])

Most common conversion mechanisms from vibrations to electricity rely on piezoelectric, electromagnetic, or electrostatic transduction.

Electromagnetic energy harvester converts vibrations into electrical energy using relative motion between wire coils and a magnetic field, i.e., coil is moved through a fixed magnetic field. A typical electromagnetic generator, described by Cao et. al. [16] is shown in Figure 7. As the scheme suggests, permanent magnet crosses coils due to base excitation, and vibration induced energy is converted to electrical energy per the Faraday's Law. Electromagnetic energy harvesters, used to power wristwatches [17], were actually one of the earliest commercial harvester products.
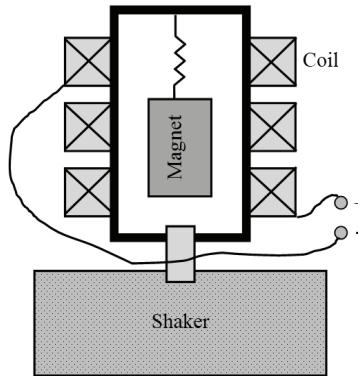
Figure 7. Electromagnetic generator model schematics

Electrostatic energy harvesters convert vibrations to electrical energy through relative motion of parallel capacitor plates. A typical variable capacitor, described by Chiu, Kuo, and Chu [18], is presented in Figure 8. In this case vibration caused relative motion between plates leads to capacitance changes between any two adjacent capacitors. MEMS-scale electrostatic energy harvesters were initially described by Chandrakasan et al. [19], with further investigations carried out by various authors [20].
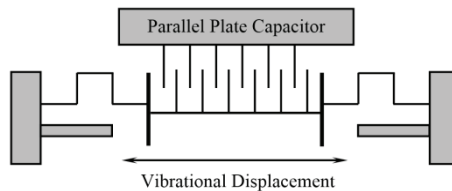
Figure 8. Variable capacitor schematics

Piezoelectric energy harvesters extract electrical energy from vibration induced deformations of piezoelectric material (they very often rely on configuration of piezoelectric material enveloped with electrodes and attached to a supporting beam). Ko et al. [21] were the first to describe and patent piezoelectric energy harvester in 1969. With the increase of low-power wireless devices applications,

26

attention to and research in this field increased dramatically, e.g., Glynne-Jones et al. [22] and White et al. [23] were the first to present piezoelectric energy harvester based on thick film piezoelectric technology.

Table 7. Summary of advantages and disadvantages of vibration induced energy conversion mechanisms

Conversion mechanism	Advantages	Disadvantages
Piezoelectric	• Direct conversion principle; • Highest energy density; • Relatively easy fabricated, Various configurations available; • No initial voltage source needed; • Combine most advantages of both electromagnetic and electrostatic converters;	• Integration with microelectronis is more complex (e.g., piezoelectric needs to be poled); • Most often requires tuning to ambient frequencies; • Require overload protection;
Electromagnetic	• No initial voltage source needed; • Mechanical contacts among the components are not required (reduced friction losses and improved reliability);	• Intricate fabrication process; • Difficulties with integration to other systems; • Greater constraints to miniaturization; • Lower levels of available voltage;
Electrostatic	• Ease of integration with other electronics;	• Initial voltage source needed; • Intricate fabrication process.

Main advantages and disadvantages of described conversion principles are summarized in Table 7. It is important to note that several review articles [24 - 25] are available on the conversion techniques and their peculiarities, thus reader may turn to them for more details. In order to summarize this section, electromagnetic induction is very convenient for harvesting vibration induced energy with large deflections as long as the geometric scale allows for sufficiently strong electromechanical coupling with a coil-magnet arrangement (it is always a challenge to develop and fabricate effective small scale electromagnetic harvesters due to poor transduction properties of planar magnets and limited number of induction loops). On the contrary, electrostatic energy harvesters are easily implemented via small scale device fabrication techniques. However, they require pre-charge (or priming) voltage in order to operate, which is considered as the main drawback of this conversion method. Meanwhile piezoelectric energy harvesting is most widely analyzed harvesting method due to its ease of application, high voltage output with no need of post-processing for voltage multiplication or bias input, high-power density, as well as relatively mature thin-film and thick-film manufacturing methods

that can be used for fabricating devices at different geometric scales. One may also refer to Figure 9 to visualize effectiveness of different energy harvesters versus device volume [26].

Piezoelectric transduction was chosen for this research as the means to convert vibrations to electricity due to the main advantages summarized above. Thus the subsequent sections will cover topics related to piezoelectric energy harvesters (PEHs) only.
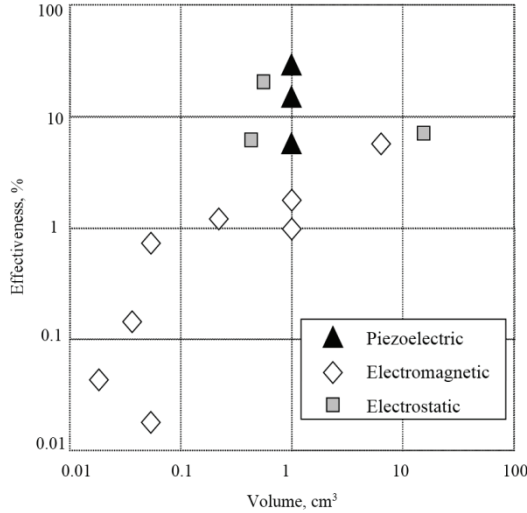
Figure 9. Effectiveness of reported harvesters versus device volume

1.5. Piezoelectric transduction

Transformation of ambient vibrations to electricity employing piezoelectric effect may be depicted by energy flow chart in Figure 10. Firstly ambient excitation energy is transformed to mechanical vibration energy E_m. Then mechanical vibration energy is transformed into electrical energy E_e, employing piezoelectric effect, i.e., charge distribution occurs within piezoelectric material due to material strains induced by mechanical vibrations – i.e., energy flow in piezoelectric energy harvester consists of two energy transformation steps.
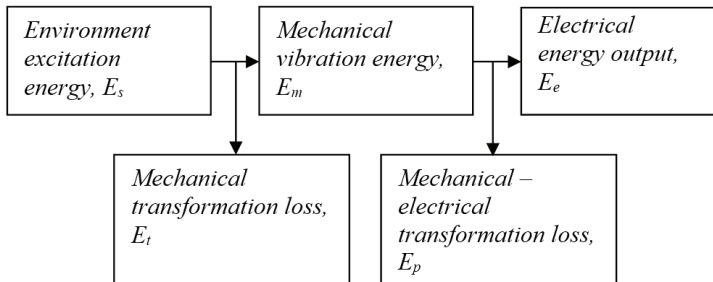
Figure 10. Energy flow chart of the piezoelectric energy harvester

Thus, stating in other words, piezoelectricity is a two-way coupling between mechanical and electrical behaviours of materials, i.e., if piezoelectric materials are mechanically strained, they generate electric field proportional to the strain (direct piezoelectric effect); conversely when electric field is applied the same material, it undergoes strain (converse piezoelectric effect). It goes without saying, that concept of energy harvesting primarily relies on direct piezoelectric effect to convert mechanically induced material strain into electricity. However, it is useful to note as well that the converse effect (often called as backward coupling) is still exhibited by piezoelectric material and manifests itself in the form damping for PEHs under operation [27]. Mechanical behaviour of material defines relationship between stress (σ) and strain (S) through modified Hooke's Law, while electrical behaviour defines relationship between electric field (E) and electric displacement (D) in a modified form of Gauss' law for electricity. Meanwhile piezoelectric coupling provides the medium for energy conversion [28]:

$$S_{ij} = s^E_{ijkl}\sigma_{kl} + d_{kij}E_k\,;$$

$$D_i = d_{ikl}\sigma_{kl} + \varepsilon^\sigma_{ik}E_{ik}\,, \qquad\qquad (1.5.1)$$

where subscripts i, j, k take values of 1, 2, and 3. S and σ are strain and stress tensors, respectively. σ [Nm^{-2}] represents stresses that are induced by mechanical and electrical effects. D [Cm^{-2}] and E [Vm^{-1}] are electric displacement and electric field vectors, s^E [m^2 N^{-1}] is elastic compliance matrix evaluated at a constant electric field. Piezoelectric strain constant, d, can be defined as ratio of electric charge density generated per unit area to applied force ([C/N] or [m/V]). Electrical permittivity of material, ε, is defined as dielectric displacement per unit electric field. Most commonly, relative dielectric constant (ε_r) is used, which is a ratio of permittivity of material to permittivity of free space.

It is important to note, that piezoelectric materials are anisotropic, i.e., their properties depend on the direction in which properties are evaluated (e.g., direction of polarization, stress, and applied electric field). Therefore, piezoelectric physical constants are defined by a system of symbols with superscript and subscript notations. The superscripts refer to quantities that are kept constant under boundary conditions. Subscripts describe direction of action and direction of response. The directions are denoted using numbers as shown in Figure 11. Positive direction of z-axis refers to the direction of polarisation. Positive directions of x, y and z are represented by 1, 2 and 3 respectively, and shear of these axes by 4, 5 and 6 respectively.

Some additional insights and more detailed information on the piezoelectric materials and their piezoelectric coefficients are presented in the subsequent section.
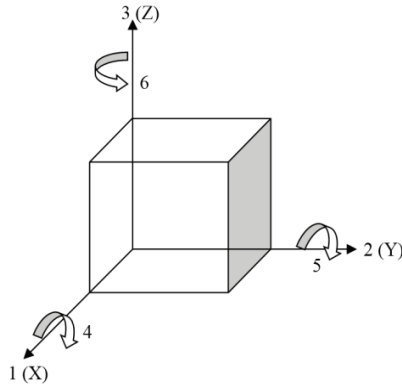
Figure 11. Notations for piezoelectric material coefficients

1.6. Piezoelectric materials and piezoelectric coefficients

There is a wide range of piezoelectric materials available for energy harvesting applications. They are usually categorized into three groups: i) crystals (e.g., quartz, PMN-PT (lead magnesium niobate-lead titanate)); ii) piezoelectric ceramics (e.g., barium titanate ($BaTiO_3$), lead zirconate titanate (PZT)); iii) semi-crystalline piezoelectric polymers (e.g., polyvinylidene fluoride (PVDF)).

When piezoelectric materials were discovered, piezoelectric effect was very poor and thus not promising for practical applications. Crystalline piezoelectric materials were firstly discovered and investigated, yet they could only be cut along certain crystallographic directions and this limited possible geometric configurations of energy harvesters. Meanwhile PZT (set alone or with various additives) become the dominant piezoelectric ceramic, developed and tailored for different energy harvesting applications. PZT is in nature brittle piezoceramic which has relatively high electro-mechanical coupling coefficient (up to 0.75) [29]. PVDF is piezoelectric polymer often produced in flexible sheets. On one hand, it is much more robust than PZT, yet on the other – it has much lower electro-mechanical coupling coefficient (0.120) [30]. Due to its greater stiffness and higher value of electro-mechanical coupling coefficient, PZT is often preferred for harmonically excited PEHs, while vibro-impacting devices may be produced either from PVDF or from PZT (depending on the foreseen PEH application). The type of selected piezoelectric material has a major influence on both performance and longevity of PEH.

Usually, the further described piezoelectric material coefficients are compared and evaluated when one is selecting suitable material for particular PEH. The three most critical parameters for selection of piezoelectric material for PEH operating in mechanical resonance are i) mechanical quality factor (Q); ii) electromechanical coupling factor (k); and iii) dielectric constant (ε). One should crave for high magnitudes of all these parameters. Quality factor is a system intrinsic feature, inversely proportional to its damping. A system with high quality factor value will not lose much energy to heat, thus more energy will be available for harvesting. Electromechanical coupling coefficient is an indication of material's ability to

convert mechanical energy to electrical energy or vice versa (clearly, the larger the strain and the coupling coefficients, the higher the potential for energy conversion). A higher dielectric constant is generally preferable because it lowers the source impedance of harvester.

The main coefficient to define piezoelectric material is piezoelectric strain coefficient d. It relates strain to electric field – i.e., it is defined as mechanical strain experienced by material per unit electric field applied to it (m/V). If one considers this coefficient for energy harvesting applications, the first subscript of this coefficient indicates the direction of polarisation and the second subscript indicates the direction of applied stress.

Figure 12 is a good illustration helping to distinguish between two different modes in which piezoelectric materials can be used for harvesting applications. If one employs piezoelectric in d_{33} mode, it means that both voltage and stress are acting in direction 3 (or, stating in other words, are parallel to one another), meanwhile applied mechanical stress is perpendicular to PEH electrodes. Typical examples of such PEH operation mode are piezoelectric stacks (which is not compatible with light-weight requirements of portable electronics and wireless sensor nodes). Yet if one employs piezoelectric in d_{31} mode, then voltage acts in direction 3 and mechanical stress acts in direction 1 (i.e. they are perpendicular to one another) and applied mechanical stress is parallel to PEH electrodes. Typical examples of such PEH operation mode are various beam configurations acting under base excitation. Judging on the fact that size of energy harvester is expected to be as small as possible, d_{31} piezoelectric operation mode should be used to produce larger strains of piezoelectric material with smaller vibration input and thus achieve higher efficiency of the harvester.
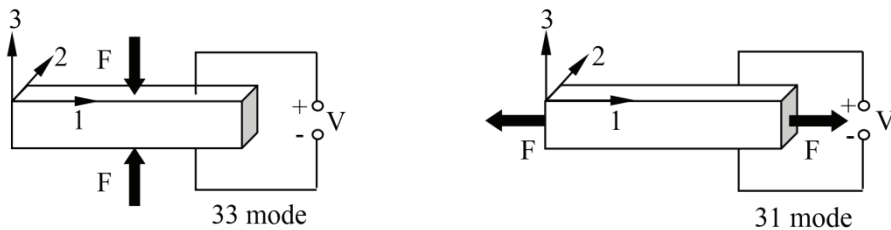
Figure 12. Illustration of d_{33} mode and d_{31} mode operation for piezoelectric materials

Another important properties defining performance of piezoelectric materials are elastic compliance constant (defined as the strain produced per unit of stress applied to the material), Young's modulus and tensile strength. Young's modulus primarily affects stiffness of the system, while the higher tensile strength should lead to higher voltage/power outputs, since the latter are dependent on average strain developed in piezoelectric.

Comparison of piezoelectric coefficients of different piezoelectric materials [30 - 33], representing piezoelectric crystal, piezoceramic and piezopolymer groups, is presented in Table 8. Moreover, this table is followed by the summary of advantages/disadvantages of different piezoelectric materials in Table 9.

Table 8. Comparison of PZT, PVDF and PMN-PT material properties [30-33]

Property	PZT	PVDF	PMN-PT
Strain coefficient (d_{31}), 10^{-12} m/v	320	20	420
Strain coefficient (d_{33}), 10^{-12} m/v	650	30	850
Coupling coefficient (k_{31}), CV/Nm	0.44	0.11	0.65
Coupling coefficient (k_{33}), CV/Nm	0.75	0.16	0.88
Dielectric constant, $\varepsilon/\varepsilon_0$	3800	12	3760
Elastic modulus, 10^{10} N/m^2	5.0	0.3	0.83
Tensile strength, 10^7 N/m^2	2.0	5.2	8.3

Table 9. Advantages and disadvantages of common piezoelectric materials

Piezoelectric material	Advantages	Disadvantages
PMN-PT - single crystal piezoelectric material	Excellent piezoelectric properties;	Became commercially available only recently; Very expensive;
PZT – piezoceramic material	Most commonly used; Good piezoelectric properties; Coefficients are usually pre-defined in modelling software; Often used for prototyping and experimental analysis	Brittle;
PVDF - piezoelectric polymer	Higher tensile strength and lower stiffness; Less brittle than ceramics;	Properties inferior to PZT.

Reviewing information presented in both tables one may conclude that PZT is widely used, yet brittle, which causes limitations in strain level that can be applied for energy harvester. PVDF has ability to withstand large amounts of strain leading to more mechanical energy available for conversion into electrical energy. Although, this material has low electromechanical coupling coefficient it is ideal for many applications because of its higher tensile strength, lower stiffness and its ease of integration in manufacturing processes. Although PMN-PT is demonstrating great piezoelectric properties, it is even more brittle than PZT and, moreover, highly expensive, thus not very suitable for vast practical applications. Following results of performed literature review and conclusions that can be drawn from piezoelectric materials' advantages/disadvantages presented Table 9, it was decided to choose PZT as a primary material for simulations, prototyping and experimental research described in the thesis. However, some harvester models had PMN-PT and PVDF piezoelectric layers in order to explore and compare performance of different configuration harvesters.

1.7. Different configurations of cantilever type PEHs

Cantilever beam with piezoelectric material attached to the top and/or bottom surfaces, operating in d_{31} mode (as depicted in Figure 13) is the most attractive and

mostly analyzed configuration for harvesting energy from vibrations. Cantilever type PEH configuration has proven to be easy to implement and adjusted. Resonant frequencies of this structure may be lowered by addition of concentrated mass at the tip of cantilever beam, which would result in higher levels of strain in attached piezoelectric layers. In order for PEH to operate at higher frequencies, one may decrease length or increasing thickness of the device.
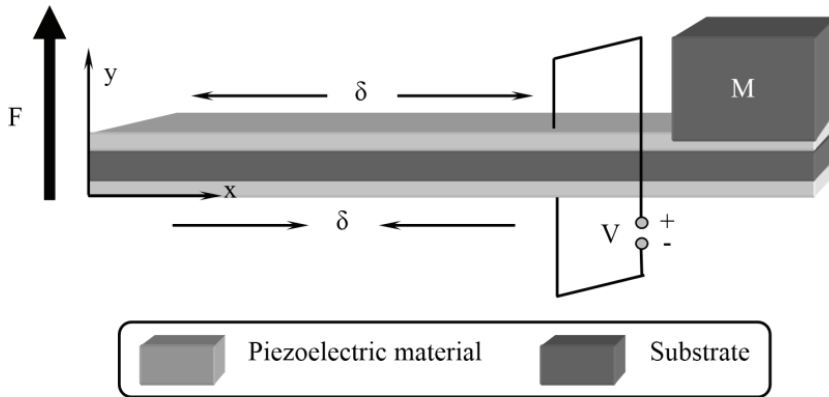
Figure 13. Typical PEH

If one considers PEH configuration with two piezoelectric layers, then one piezoelectric layer is in compression, while the other piezoelectric layer is in tension, as it is shown in Figure 13. Thus, elastic strain distribution of bimorph along x-axis indicates that top and bottom piezoelectric layers are in different strain conditions, however they have identical absolute values of strain. Therefore, if two piezoelectric layers are poled in the same direction with electrodes wired appropriately, their generated currents will double. Conversely, if two piezoelectric layers are poled in the opposite direction, their produced voltage will double.

Two combinations of multilayer structures are common: i) series type; and ii) parallel type, both shown in Figure 14. The series type triple layer bimorph is constructed of metallic layer, sandwiched between two piezoelectrics which are electrically connected in series. In the case of the parallel triple, which is also metallic layer sandwiched between two piezoelectric layers, piezoelectric materials are connected in parallel. The parallel triple layer bimorph has the highest power under medium excitation frequencies and load resistances, whereas the series triple layer bimorph produces highest power when excited under higher frequencies and load resistances. A series connection will increase impedance of device as well as improve generated powers at higher loads. Literature review results suggest that under low load resistances and excitation frequencies unimorph configuration would generate highest power, under medium load resistances and frequencies the parallel triple configuration would have highest power output, and under high load resistances and frequencies the series triple configuration would produce the greatest power output [34].
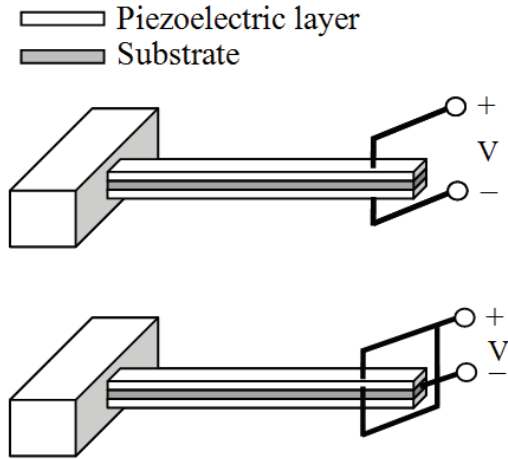
Figure 14. Series (top) and parallel (bottom) types of bimorph PEH

In order to enhance typical PEH configuration to better suit power harvesting applications, various modifications of PEH structure have been studied. Different authors have tried to address the following goals: i) maximize piezoelectric response for a given input (accomplished either by maximizing material's average strain for a given input or by changing the configuration to make use of direct coupling rather than transverse coupling); ii) improve harvester's robustness by reducing stress concentration; iii) minimize losses (damping) associated with mechanical structure; iv) improve harvester's manufacturability. Some examples of these modifications are presented further in the thesis.

Mateu and Moll [35] presented analytical comparison between rectangular and triangular (with the large end clamped and the small end free) cantilevers. It was proven mathematically that triangular cantilever with base and height dimensions equal to the base and length dimensions of rectangular beam would have higher strain and higher deflection for a given load. Higher strains and deflections in piezoelectric materials can be converted to higher power outputs; therefore triangular PEH would produce more power per unit area than rectangular PEH. Moreover, this was also confirmed by Glynne-Jones et al. [36] who developed a tapered cantilever type PEH profile of which ensures constant strain in piezoelectric film along its length for a given displacement.

Additionally, Roundy et al. [37] suggested that, with an increasingly trapezoidal shape of PEH substrate, strain can be more evenly distributed throughout the whole structure as opposed to rectangular PEH substrate that contains a non-uniform strain distribution. It was also stated that for the same volume of piezoelectric material, trapezoidal PEH can generate more than twice energy of rectangular PEH. It was concluded that, by using trapezoidal PEH substrate configuration, smaller and less expensive harvesters could be produced to satisfy given power requirements. Figure 15 illustrates bending energy curves of cantilevers of uniform width for three different substrate geometries.
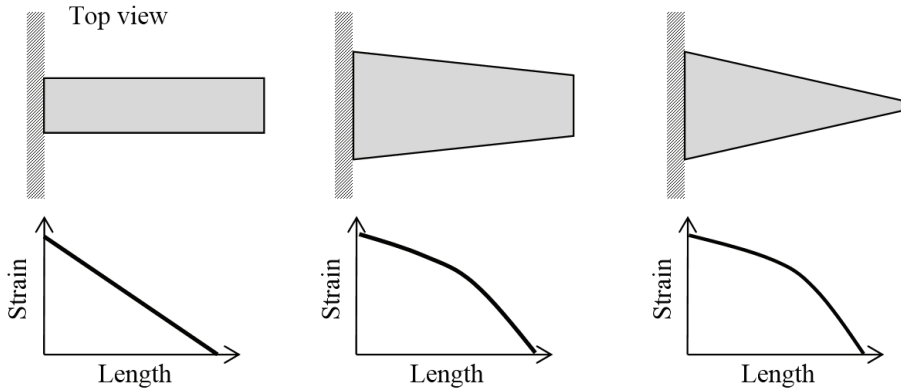
Figure 15. Bending energy curves of cantilever type PEH for three alternative beam geometries

Rather than altering profile of rectangular PEH substrate, Mossi et al. and Yoon et al. [38, 39] changed end constraints on PEH structure and created a so-called unimorph prestressed bender. This is an initially curved, arc shaped, rectangular piezoelectric device that elongates when force is applied to the top of the arc. The elongation causes strain in active material which produces voltage.

In studies performed by Lee et al. [40], novel fabrication technique was developed in order to create piezoelectric MEMS power harvesting device with interdigitated electrodes operating in d_{33} mode [41]. Although devices were successfully created, experimental testing was not performed.

Jiang et al. [42] also analyzed methods to increase efficiency of piezoelectric energy harvesters. Their study involved modelling of cantilever bimorph with concentrated mass attached to its tip and using the model to determine relationship between PEH performance and its physical as well as geometrical parameters. Results showed that, by reducing thickness of elastic layer of bimorph and by increasing concentrated mass attached to its tip, resonant frequency of the system may be substantially decreased. The maximum harvested power was shown to be greater for lower resonant frequencies.

Anderson and Sexton [43] arrived to a similar conclusion when optimizing physical and geometrical parameters of a similar bimorph. Varying the size of concentrated mass (attached at the tip of the beam) and other PEH dimensions, they discovered that changes in concentrated mass size had the greatest effect on power harvested by the system.

The work of Gurav et al. [44] focused on optimization of power outputs of micro-scale PEHs through modification of piezoelectric layers - altering their electrode pattern, changing their poling and stress direction, adding prestress to maximize coupling and applied strain of material - and tuning resonant frequencies of devices. The aim of their study was to determine the best possible design parameters for a micro-scale cantilever type PEHs. In order to avoid impossible PEH configurations, limits were set on each of the geometrical parameters to be optimized, examples of which are presented in Table 10.

Table 10. Optimization variables and constraints

Variables	Description	Constraints
l_m	Mass length	$h_m < 5$ mm
h_m	Mass height	$(l_m + l_b)w_m < 1$ cm^2
w_m	Mass width	$(l_m + l_b)w_b < 1$ cm^2
l_b	Beam length	$l_e - l_m < 0$
w_b	Beam width	$\delta_{max} < \delta_{yield}$
l_e	Electrode length	$\omega_n \approx 2\pi \times 120$
t_p	Piezo layer thickness	
t_{sh}	Shim thickness	
R_{load}	Load resistance	

Literature review presented on different configuration PEHs may be summarized in Table 11, which provides the names of authors of reviewed publications, PEH configurations they have suggested as well as the main advantages of the proposed designs.

Table 11. Summary of various piezoelectric geometries investigated

Author	Piezoelectric configuration	Advantages
Mateu and Moll [35]	Rectangular PEH & triangular PEH	Triangular configuration capable of higher strains and higher power;
Roundy et al. [37]	Trapezoidal PEH	Trapezoidal configuration allows strain to be evenly distributed for improved efficiency;
Glynne Jones et al. [36]	Tapered PEH	Tapered cantilever beam ensures a constant strain in piezoelectric layer;
Mossi et al. [38]	Unimorph prestressed bender	Initially curved shape can help improve harvesting capability;
Yoon et al. [39]	Initially curved unimorph	Initially curved shape can help improve harvesting capability;
Lee et al. [40]	Cantilever with interdigitated electrodes	Interdigitated electrodes configuration capable of higher power generation,
Jiang et al. [42]	Cantilever with concentrated mass	Capable of harvesting energy at lower frequencies
Anderson et al. [43]	Cantilever with concentrated mass	Optimization of cantilevers geometrical parameters

1.8. Issues associated with cantilever type PEHs and approaches to solve them

The most common issue associated with typical linear vibration energy harvesters is that they possess either high resonant frequency and/or require high acceleration levels. Besides, they are mainly configured to work efficiently only in resonance – i.e., at one defined frequency. In such case, the tighter resonance harvester possesses, the more beneficial it is from the performance point of view, yet, on the contrary, their practical implementation is limited due to significant drops of output power for relatively small fluctuations in the ambient vibration frequency.

Thus, a number of various techniques are sought for to overcome limitation of narrow operating PEH bandwidth and improve efficiency of piezoelectric energy harvesters. One of the most popular approaches is to divide these techniques into two main groups - one group aims to actively adjust resonance of harvester so that it constantly corresponds to source vibrations (so called continuous, or active, tuning), while the second group aims to widen harvester bandwidth, employing various structural configurations (intermittent, or passive, tuning). As the terms suggest, intermittent tuning operates periodically and requires no additional systems/energy sources to tune the system, which makes it more attractive approach compared to continuous tuning configurations. However, mismatch between ambient vibrations and system resonant frequencies may as well occur for in advance tuned harvesters due to un-constant nature of excitation frequency, environment temperature fluctuation, manufacturing tolerances, and other reasons.

Thus additional approaches and techniques - arrays of energy harvesters, re-imposition of system non-linear characteristics and advanced electric circuits - are as well investigated. These methods may be grouped employing Twiefel and Westermann [46] classification, presented in Figure 16.
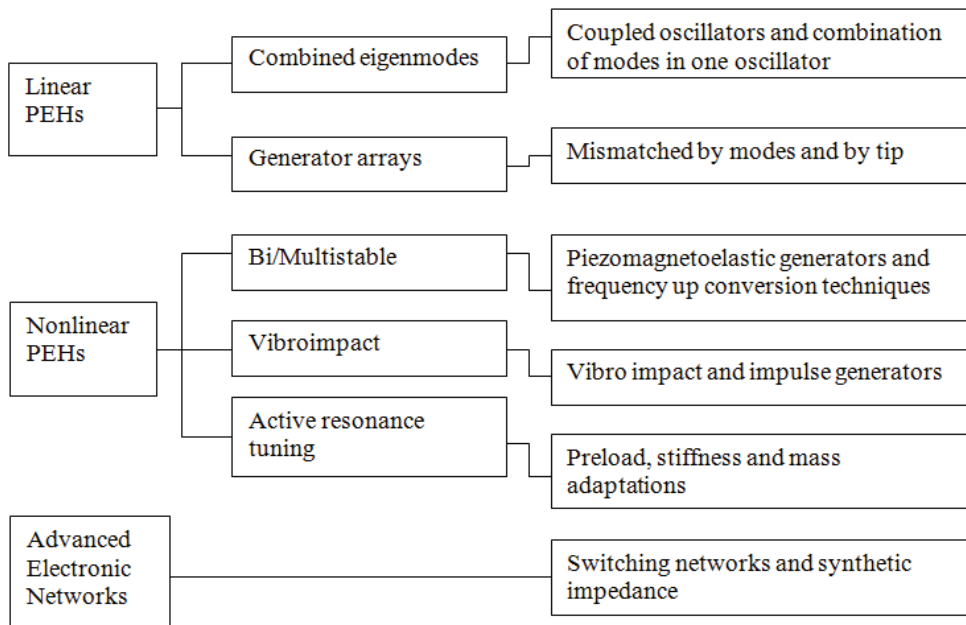
Figure 16. Twiefel and Westermann classification of methods to widen PEH bandwidth

They distinguish three main groups of PEH configurations: the first group covers liner energy harvesters, the second– nonlinear harvesters (i.e. employing nonlinear effects to increase system bandwidth); and the third one - advanced electronic networks and circuits. Most recent publications and methods aimed to widen operating PEH bandwidth are discussed below in detail, highlighting their operation principles, main advantages and disadvantages as well as application

areas. Nevertheless, one must note that PEH configurations presented below are suitable only for their specific applications, but none of them can be regarded as a universal solution. Or, stating in other words, it is not simple to choose PEH configuration, as it is extremely application specific.

Generator arrays [47] are the best example of combined linear systems. Each cantilever in generator array has its own resonant frequency, which is adjusted by tuning geometrical parameters of cantilever or adding concentrated mass to it. All beams within the array have similar resonant frequencies, thus if a vibration source, to which the array is mounted, has slightly varying dominant frequency, at least one of the array cantilevers operates in resonance. Increasing the number of cantilevers in the array would lead to its increased operation bandwidth. Example of such system and its broadened bandwidth is presented in Figure 17, a). Combined eigenmodes [48] method employs structures with two or more resonant frequencies that are very close to each other. Possible solutions are direct connected beams or coupling of multiple beams with springs (Figure 17, b)). Usually, the first two eigenmodes of single cantilever have a rather big frequency difference. Combination of two or more generators can shift those first eigenmodes closer to each other. The two-mass system has a higher bandwidth for a certain output level. Bistable/multistable harvesters [49] (example of which presented in Figure 17, c)) possess more than one stable equilibrium position. Analysis of the above methods revealed that, despite the fact that array of similar oscillating structures was reported to have wide operation range as well as an increased output power, drawback of increased system size exists. Moreover, design approaches with non-linear stiffness and non-linear springs are challenging to fabricate [46], as harvesters are usually multilayer structures and their cross sections may not be easily modified.

Meanwhile, mechanical supports (also known as amplitude limiters or stoppers) may be relatively easily implemented via micromachining technologies [50] or even emerge in the system due to space constraints. Supports are used to widen bandwidth of PEH employing non linear effects that occur during the impact (thus such PEHs are often called vibro-impacting systems (VIS)). For small PEH vibration amplitudes, system behaves like linear, yet at a certain frequency and certain excitation amplitude, PEH impacts on the incorporated support. As soon as this level is reached, frequency response remains on plateau even with increasing frequencies and a new stable region is added to the frequency spectrum [46].

Naturally, mechanical impacts may reduce lifetime of materials in the contact area, however overall reliability of PEH is increased as supports protect vibrating transducer from fracture when it operates at excessive loads. Thus, energy harvesters with incorporated supports may be subjected to vibrations of higher amplitude and non-linear effects induced during impact (e.g., frequency shifts), may be employed to modify their dynamical and electrical response.

As rigid support is implemented in PEH configuration considered further in this research, a more detailed literature review was performed on vibro-impacting PEH configurations, results of which are summarized below.
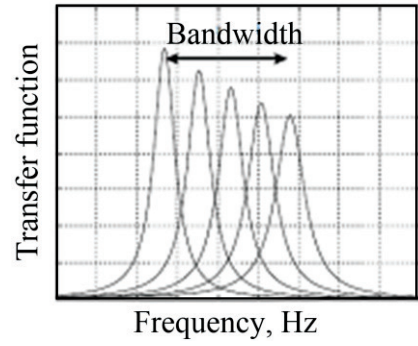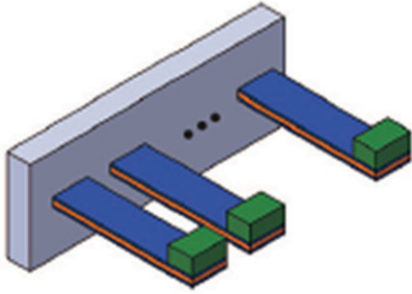
a)
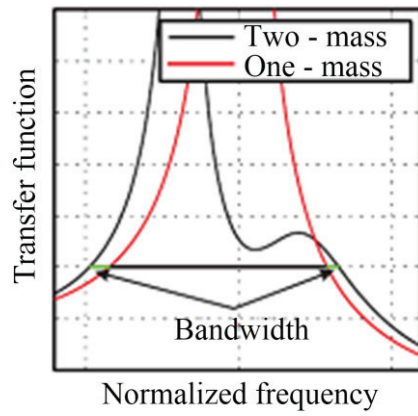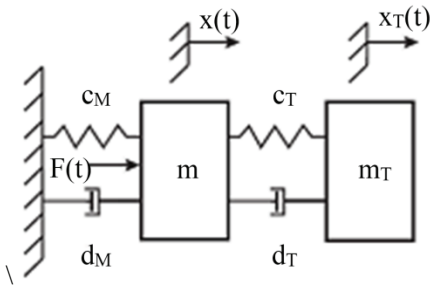
b)
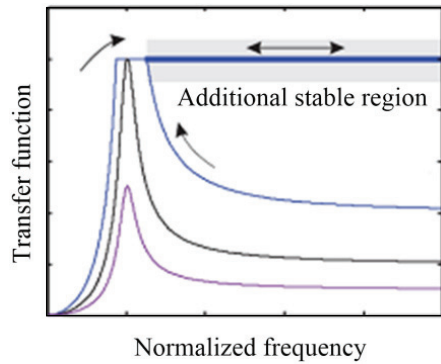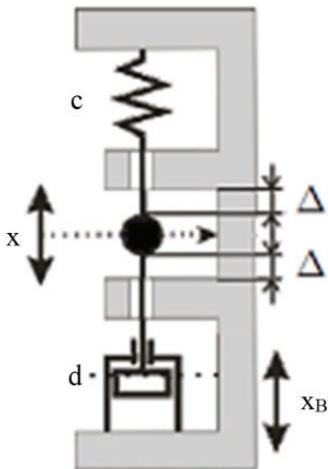
c)

Figure 17. Approaches to widen PEH bandwidth: a) generator arrays; b) combined eigenmodes, c) bistable/multistable devices (after [46])

Operation principles of the first vibro-impacting piezoelectric energy harvester (VIPEH) were described by Umeda et al. [**51**]. They studied piezoelectric disc, on which a steel ball, falling from a known height, was impacting. Once the ball bounced back off the disc, electrical energy was generated by piezoelectric disc vibrating at its resonance. Since then a number of PEH configurations were proposed, aiming to enlarge the bandwidth of harvesters (the most successful examples of which report up to 226 % bandwidth increase [52]).

However, one must note that a trade-off between increased bandwidth and reduced power output exists. On one hand, support acts as an amplitude limiter that reduces dynamic strains in the piezoelectric layer, leading to lower power output. On the other hand, power output may be increased if upon impacting higher vibration modes of PEH are excited and exploited.

Literature review revealed that VIPEH configurations may be classified into three main sets: i) configurations employing rigid supports only [53-56]; ii) more intricate frequency up-converting designs with primary and secondary vibrating systems [57 - 60]; iii) frequency up-converting configurations with moving masses hitting piezoelectric transducers [61-64].

Within the first category Mak et al. [53] proposed analytical VIPEH model that analyzed effects of geometric and material nonlinearities at the presence of support, which was used to reduce excessive bending of piezoelectric transducer. The authors have concluded that harvester performance was influenced by stopgap size - bending stresses were reduced leading to increased device lifetime, but limited power output. Blystad et al. [54] have also focused on nonlinearities induced by harvester impacting a support. It was demonstrated that overall output power is higher due to increasing spectral density of broadband vibrations once support is in effect. Moreover, the authors demonstrated that nonlinear power conditioning circuitry (both SSHI and SECE) performed better than simple passive circuitry for vibro-impacting configurations. Liu et al. [55] have considered several VIPEH configurations. In the first one, a traditional rectangular cantilever with large concentrated mass and deposited PZT layers was hitting base surface of casing resulting in bandwidth increase of 57 %. Later on [52], the shape of cantilever was refined by proposing S-shaped meandering beam, which led to bandwidth improvement of 226 %. Pozzi and Zhu [56] studied mechanical plucking as a frequency up-conversion strategy - piezoelectric bimorph was deflected via plectrum and then rapidly released to vibrate unhindered whilst electrical energy was collected from oscillatory cycles. Per authors' conclusions this technology should bridge between the low levels of excitation available from human motion to higher operating energy levels of piezoelectric devices.

. Within the second category Gu et al. [57] proposed VIPEH comprised of two cantilevers – low frequency (LF) driving cantilever, hitting high frequency (HF) generating cantilever. Authors have concluded that such configuration of VIPEH improved efficiency of energy conversion by reducing mechanical damping. Their harvester was reported to achieve 13 times greater power density as compared to the conventional linear systems.

40

Table 12. Examples and suitability of presented broadband techniques, their advantages and disadvantages

Methods/authors	Suitability	Advantages	Disadvantages
Generator arrays	For stochastic vibrations in a variable layout, large bandwidth;	Variable setup (ease to add or remove cantilevers); Not sensitive to mechanical disturbances (impacts, interrupts);	Large volume (less suitable for micro scale applications); More complex electric circuit is required to manage device power output;
Combined eigenmodes method	For stochastic vibrations in a variable layout, small bandwidth;	Optimized damping can achieve a broadband response; System is comparatively compact and not sensitive to disturbances.	Reduction of the response in each individual mode due to the mode coupling;
Bistable/multistable harvesters	For low frequencies in a small volume;	Demonstrate good performance for small frequencies have a large operating bandwidth as compared to the small size of the harvester	Need an auxiliary structure to implement the nonlinear stiffness;
Active tuning	For known slowly varying harmonic frequencies;	Harvester always operates at resonance frequency with a high power output;	Power supply needed for the active tuning need for a rather complex auxiliary structure to adopt the generators' mass and stiffness parameters;
Mechanical supports	For harmonic excitations in a small volume and high frequencies;	Robust and compact setup; Converter is theoretically always on the plateau with a huge bandwidth;	Very sensitive to disturbances that make the system jump to the low-level plateau.

Very similar configuration was introduced by Ferrari et al. [58], who have modelled energy harvesting system employing equivalent electro-mechanical lumped element circuits. Another common configuration in this category consists of driving LF cantilever (usually, non-piezoelectric) hitting piezoelectric HF cantilever

stops. Two similar designs of such systems were presented by Moss and Barry et al. [59, 60]. In one case concentrated mass was hitting two bimorph stops, while for the other case cantilever beam was hitting a number of double-sided, symmetrical piezoelectric bimorph stops. The array configuration was operating at higher frequencies with narrower operating bandwidth (increase of 13% available), while two bimorph configuration resulted in even 117 % widened operating bandwidth

Within the third category Jacquelin, Adhikari and Friswell [61] proposed analytical VIPEH model which was later studied by Renaud et al. [62]. Suggested configuration was based on two identical piezoelectric unimorphs impacted by sliding mass. Similar system was as well proposed by Manla [63], who explored non-resonant VIPEH, consisting of a ball bearing in tube impacting on piezoelectric beams mounted at each end of the tube. Only one trapezoidal piezoelectric cantilever was impacted by a steel ball in the configuration proposed by Minh et al. [64] – they have explored influence of ball-cantilever impact point on the overall performance of the harvester, with the maximum registered power of 44nW at acceleration of 4g.

Advanced electronic circuits are as well classified as one of the methods to improve PEH efficiency, since their application could lead to the increased harvester performance. However, they are not included in the scope of this research reader is directed to [65- 68] for more information.

To summarize, this section presents methods that are used to overcome main issues currently associated with PEHs - their low efficiency and narrow operational bandwidth. Reviewed methods are presented in Table 12 along with their main advantages and disadvantages. Since PEH with incorporated support is considered by the author as the best approach for PEH enhancement, recent publications related to this configuration were analyzed in greater detail. Analysis revealed that characteristics of vibro-impacting piezoelectric energy harvester are affected by incorporated support location and stopgap size, therefore aim of further research work is to analyze the influence of contact point location on mechanical and electrical characteristics of harvester with the ultimate goal to beneficially exploit nonlinear effects that are induced as a result of vibro-impact process.

1.9. Section Conclusions

This section presented a review of recent publications as well as main theoretical concepts and principles used in the field of energy harvesting. The reader was introduced to Internet of Things, wireless sensor nodes, their possible applications and typical powering requirements. These were followed by a brief review of electrochemical batteries, renewable energy sources, energy conversion principles and commonly met energy scavengers, with a particular emphasize on piezoelectric energy harvesters (PEHs). Most common configurations of PEHs with their capabilities, limitations as well as areas of design improvement were elaborated.

In general, this section introduced the reader to the field of energy harvesting, outlaying its basic principles, recent research achievements and commonly met issues or, in other words, presented a steady theoretical ground to understand

numerical and experimental research presented in the subsequent sections of the thesis.

The following conclusions were drawn from completed analysis:

- It was decided to designate developed PEH for powering of wireless sensors. Due to the ubiquitous presence of mechanical vibrations in industrialized and house hold environment, mechanical vibrations were chosen as energy source in this study;

- In terms of analyzed vibration - to - electricity conversion mechanisms, piezoelectric transduction was chosen for further research. It was selected due to high power densities, micro-scale integration ability, commercial availability of various piezoelectric materials and their ease of adaptation for different harvester configurations;

- As of different piezoelectric energy harvester configurations, cantilever type piezoelectric energy harvester operating in d_{31} mode was chosen for further research. It was selected due to ease of fabrication, ability to adapt resonant frequency of device and intrinsic dynamic response characteristics;

- It was as well decided to firstly implement finite element modelling technique in order to thoroughly understand performance of piezoelectric energy harvesters – i.e., the way performance of PEH is affected when one is changing dimensions and shape of PEH substrate, piezoelectric materials of PEH; introducing rigid support to PEH configuration, or connecting PEH to simple electric circuit.

- Moreover, vibrometry and holographic measurement systems were chosen as the main stands to perform experimental studies and verify numerical simulation results;

- As of different PEH performance enhancements discussed, it was decided to optimize geometric parameters and shape of PEH cantilever substrate as well as to incorporate mechanical supports to PEH configuration.

2. THEORETICAL INVESTIGATIONS OF PIEZOELECTRIC ENERGY HARVESTERS

Usually, piezoelectric energy harvesters cannot be cost effectively built and tested without prior modelling of its component, which may be performed with different software packages like Coventorware, ANSYS, or COMSOL Multiphysics. Preliminary design stage gives one the advantage to predict how developed PEH configuration will perform. Thus, one of the objectives of this research was to develop general and universal finite element (FE) model of PEH, parameters of which could be easily changed. This should help to analyse dynamic response of PEHs of various configurations and determine their possible electrical outputs.

The ultimate purpose of FE analysis is to mathematically recreate behaviour of an actual engineering system. In other words, we must obtain an accurate mathematical model of a physical prototype. Thus, FE model usually contains nodes, elements, material properties, real constants, boundary conditions and other features that are used to represent physical system. General steps for a FE model creation and simulations are:

- Geometry input,
- Material properties definition,
- Mesh generation,
- Application of loads and constrains,
- Simulations,
- Review of results and post processing.

For the purpose of this research, a 2D finite element (FE) model of vibro-impacting piezoelectric energy harvester (VIPEH) was developed with Comsol Multiphysics software. Figure 18 and Table 13 provide principal scheme and geometry data of developed unimorph transducer - cantilever beam of stainless steel covered by piezoelectric layer (of PZT, PVDF or PMN-PT), operating in transverse (d_{31}) mode. It was assumed that ideally conductive electrodes of negligible thickness cover the entire area of top and bottom surfaces of piezoelectric layer. Modelling was performed with Lagrange-quadratic elements using plane-strain approximation, since flexural vibration modes have greater influence on vibro-impact process in comparison to torsional modes. Boundary conditions were set to represent electrodes enveloping piezoelectric material and structure clamping, meanwhile simple electric circuit, comprised of a single resistive load, was introduced to electromechanically coupled system via SPICE circuit editor enabling closer-to-practice simulations of PEH.

Eigenfrequency solver function was used to determine resonant frequencies of harvester prototype, while transient solver function was employed to predict its displacement and voltage output. Simulated voltage output was exported as .txt data file and transferred for processing to MATLAB software. The below script was used to determine RMS voltage generated by PEH operating at certain conditions:

MATLAB script	Comments
text='1_PZT_290.txt';	% determines COMSOL Multiphysics data file;
[time,voltage]=textread (text, '%f%f', 'headerlines',100);	% reads data from file and trims off transient periods;
size(voltage)	% determines the number of rows and columns in matrix
x=voltage;	%defines variables
t=time;	%defines variables
n=size(x);	%determines trimmed voltage data quantity;
y=sqrt(1/n(1)*sum(x.^2))	%calculates and outputs RMS;
plot (t, x)	%plots time vs. voltage graph for trimmed data;
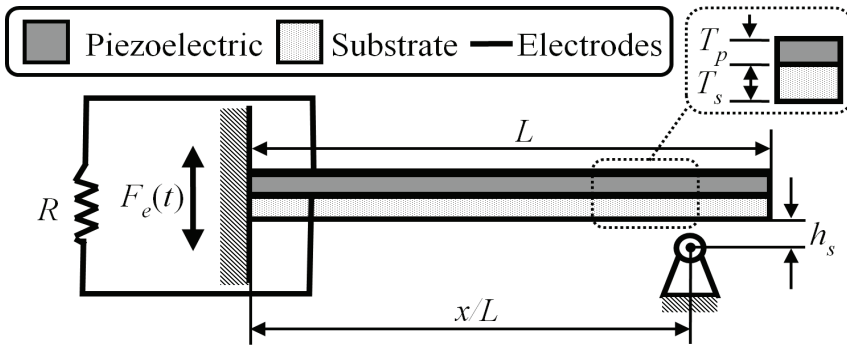
Figure 18. Principal scheme of developed FE model of PEH

Table 13. Main parameters of the developed model of PEH

Model parameters	Value	Description
L_s	100 mm	Substrate length
L_p	100 mm	Piezoelectric layer length
T_s	1 mm	Substrate thickness
T_p	0.2 mm	Piezoelectric layer thickness*
W_s	10 mm	Substrate width
W_p	10 mm	Piezoelectric layer width
A	1.0*g	Applied excitation acceleration
R_{sc}	100 Ω	Connected resistor load, corresponding to open circuit conditions
R_{oc}	1 MΩ	Connected resistor load, corresponding to open circuit conditions
F_e	*	Applied excitation frequency (corresponding to the first resonant frequency of the system)
h_s	2 μm	Stopgap size at the support location
C_{vdW}	1 x 10^{-32}	Adhesion constant

* numeric expression varied through the course of simulations

PEH dynamics is described by the following equation of motion presented in a general matrix form [69]:

$$[M]\{\ddot{z}\}+[C]\{\dot{z}\}+[K]\{z\}=\{Q(t,z,\dot{z},)\},\tag{2.1}$$

where [M], [C], [K] - mass, damping and stiffness matrices of the harvestert, respectively, $\{z\},\{\dot{z}\},\{\ddot{z}\}$ - displacement, velocity and acceleration vectors, while $\{Q(t,z,\dot{z},)\}$ vector represents the sum of external forces acting on the PEH.

To define piezoelectric effects, the following considerations and constitutive piezoelectric equations [28] were used in the FE model. As it was already discussed in the introductory section, when piezoelectric material is subjected to stress T, it produces polarization P, which is function of stress (direct piezoelectric effect):

$$P = dT.\tag{2.2}$$

In contrast, when electric field E is applied across electrodes of piezoelectric material, it produces strain S which is function of electric field (inverse piezoelectric effect):

$$S = dE.\tag{2.3}$$

For an elastic material, relationship between strain S and stress T is given by:

$$S = s^E T.\tag{2.4}$$

For a dielectric substance, relationship of electrical displacement D with electric field strength E is given by

$$D = \varepsilon_0 E + P,\tag{2.5}$$

with ε_0 being dielectric permittivity of vacuum and P being polarization of material due to applied field.

From these relationships, with electric field E and stress T as independent variables, the two constitutive piezoelectric equations can be written:

$$S = s^E T + dE$$
$$D = dT + \varepsilon^T E.\tag{2.6}$$

Since phenomenon of piezoelectricity is anisotropic, electric field E and electrical displacement D are represented in vector magnitudes, while stress T and stain S are given in symmetrical tensile magnitudes:

$$S_i = s_{ij}^E T_j + d_{mi} E_m$$
$$D_n = d_{nj} T_j + \varepsilon_{nm}^T E_m,\tag{2.7}$$

where $m, n = 1,2,3$; $i, j = 1,2,..,6$.

These equations can be as well represented in matrix form as:

$$
\begin{bmatrix} S_1 \\ S_2 \\ S_3 \\ S_4 \\ S_5 \\ S_6 \end{bmatrix} = \begin{bmatrix} s_{11}^E & s_{12}^E & s_{13}^E & 0 & 0 & 0 \\ s_{12}^E & s_{11}^E & s_{13}^E & 0 & 0 & 0 \\ s_{13}^E & s_{13}^E & s_{33}^E & 0 & 0 & 0 \\ 0 & 0 & 0 & s_{44}^E & 0 & 0 \\ 0 & 0 & 0 & 0 & s_{44}^E & 0 \\ 0 & 0 & 0 & 0 & 0 & 2(s_{11}^E - s_{12}^E) \end{bmatrix} \begin{bmatrix} T_1 \\ T_2 \\ T_3 \\ T_4 \\ T_5 \\ T_6 \end{bmatrix} + \begin{bmatrix} 0 & 0 & d_{31} \\ 0 & 0 & d_{31} \\ 0 & 0 & d_{31} \\ 0 & d_{31} & 0 \\ d_{31} & 0 & 0 \\ 0 & 0 & 0 \end{bmatrix} \begin{bmatrix} E_1 \\ E_2 \\ E_3 \end{bmatrix},
$$

$$
\begin{bmatrix} D_1 \\ D_2 \\ D_3 \end{bmatrix} = \begin{bmatrix} 0 & 0 & 0 & 0 & d_{15} & 0 \\ 0 & 0 & 0 & d_{15} & 0 & 0 \\ d_{31} & d_{31} & d_{33} & 0 & 0 & 0 \end{bmatrix} \begin{bmatrix} T_1 \\ T_2 \\ T_3 \\ T_4 \\ T_5 \\ T_6 \end{bmatrix} + \begin{bmatrix} \varepsilon_{11} & 0 & 0 \\ 0 & \varepsilon_{11} & 0 \\ 0 & 0 & \varepsilon_{33} \end{bmatrix} \begin{bmatrix} E_1 \\ E_2 \\ E_3 \end{bmatrix} \qquad (2.8)
$$

In order to simulate PEH operating in vibro-impacting mode, a viscoelastic - adhesive contact formulation was implemented into the FE model of PEH. This formulation is based on Kelvin-Voigt rheological model represented by linear spring connected in parallel with linear damper (this coupling element is defined by stiffness k_p and damping c_p). Additionally, adhesion-related parameter c_{vdW} is introduced, which allows taking into account Van der Waals forces acting at the micro-scale before mechanical contact actually occurs. Therefore, the proposed contact model may be used for simulations of both macro- and micro-scale energy harvesting devices. Dynamics of the VIPEH is defined by the matrix equation below:

$$
[M]\{\ddot{z}\} + [C]\{\dot{z}\} + [K]\{z\} = \begin{cases} \{F(t)\} + \{F_S(t)\}, & if \ z_{l_S}(t) < h_S - \xi_0 \vee p_{l_S}\left(\dot{z}_{l_S}, z_{l_S}, t\right) \geq 0; \\ \{F(t)\} + \{F_S(t)\} + \{P_C(\dot{z}, z, t)\}, & if \ z_{l_S}(t) \geq h_S - \xi_0 \wedge p_{l_S}\left(\dot{z}_{l_S}, z_{l_S}, t\right) < 0. \end{cases} \quad (2.9)
$$

$$
\{F_{ls}(t)\} = \begin{cases} \dfrac{C_{vdW}}{\left[h_S - z_{l_S}(t)\right]^3}, & if \ z_{l_S}(t) < h_S - \xi_0 \vee p_{l_S}\left(\dot{z}_{l_S}, z_{l_S}, t\right) \geq 0; \\ \dfrac{C_{vdW}}{\xi_0^3}, & if \ z_{l_S}(t) \geq h_S - \xi_0 \wedge p_{l_S}\left(\dot{z}_{l_S}, z_{l_S}, t\right) < 0. \end{cases} \quad (2.10)
$$

here $\{\dot{z}(0)\} = \{\dot{z}^0\}, \{z(0)\} = \{z^0\}$, [M], [C], [K] - mass, damping and stiffness matrices of PEH, $\{\dot{z}\}, \{\ddot{z}\}$ - velocity and acceleration vectors, $\{z^0\}$ - displacement at t=0, $\{\dot{z}^0\}$ - velocity at time point t = 0, $\{F(t)\}$ - vector of external forces acting on PEH (in this case this is base excitation), $\{F_s(t)\}$ - vector representing influence of Van der Waals forces, $\{P_c(\dot{z}, z, t)\}$ - vector of nonlinear interaction in the contact pair. The developed contact model is defined by the following two components:

$$C_{vdW} = \frac{A_H A_C}{6\pi} \tag{2.11}$$

$$p_{l_s}\left(\dot{z}_{l_s}, z_{l_s}, t\right) = -k_p\left[z_{l_s}(t) - \left(h_s - \xi_0\right)\right] - c_p\, \dot{z}_{l_s}(t), \tag{2.12}$$

where $z_{l_s}(t)$, $\dot{z}_{l_s}(t)$ - displacement and velocity of PEH surface point, h_s - stopgap, ξ_0- distance between surfaces when it is assumed that mechanical contact has occurred (~1 nm), k_p, c_p- stiffness and damping of the coupling element, respectively, A_H - Hamaker's constant, A_C - contact area, p_{ls} - contact pair's nonlinear interaction force at contact point (l_s- contact point position along longitudinal axis, measured from the clamped end, where $l=0$).

Developed contact model was introduced into the FE model of PEH as a transverse force acting on selected point located on the bottom edge of the PEH cantilever. The model allows variation of both vertical and horizontal position of the "virtual" support with respect to the transducer surface.

Thus, the above described developed PEH FE Model is universal (i.e. it takes into account a number of different constituents that can be easily adapted) and allows performing complex and integrated simulations, namely: i) evaluating dynamic and electric response of PEH and the way it is dependent on variation of geometric parameters of the device; ii) external electric circuit influence to dynamic and electric response of PEH; iii) analyzing nonlinear dynamic effects occurring as harvester is impacting on incorporated rigid support, location of which may be easily adjusted.

2.1. Evaluation of PEH response to harmonic and random excitation

The aim of this section's simulations is to ascertain the way electrical outputs of PEH change once it is subjected to harmonic and random base excitations. FE model of basic configuration with incorporated support, scheme of which is already depicted in Figure 18 and main characteristics presented in Table 14 is employed to perform subsequent simulations.

For the first round of simulations, harvester was subjected to sinusoidal base excitation, which was defined as vertically acting body load with magnitude controlled by imposed acceleration and excitation frequency. Meanwhile for the second round of simulations random base excitation signal was introduced to the model. In both cases a resistive load representing open circuit (1MΩ) was introduced to the electromechanically coupled system via SPICE circuit editor, keeping geometric parameters of the system constant.

Firstly, mechanical response of PEH was evaluated and resonant frequencies of system were determined. Determined first resonant frequency was further introduced into FE of PEH to define harmonic excitation signal. RMS voltage of impacting PEH was determined for a number of relative support positions and compared to the voltage output when the same harvester operates in the non-impacting mode.

Table 14. Geometric characteristics of FE model used to evaluate PEH electric response to harmonic and random base excitations

Parameters	Value
Stainless steel substrate dimensions (L_s x W_s x T_s), mm	100 x. 10 x 1
Piezoelectric PZT – 5H dimensions (L_p x W_p x T_p), mm	100 x 10 x 0.2
External electric circuit resistance, MΩ	1
Stopgap size at the support location, μm	2

For harmonic excitations of harvester, effect of support location on electrical outputs is demonstrated in Figure 19, which provides plot of impacting/non-impacting RMS voltage ratio as a function of relative support position. One may note that for harmonic excitation signal case, presence of support limits PEH displacements leading to the 50-90 % reduction of generated RMS voltages if compared to the RMS voltage when device is operating in non-impacting mode. However, magnified view in Figure 19 suggests that if relative support position is in the vicinity of the nodal points of the second and third transverse vibration mode ($0.78L$ and $0.87L$), PEH generated RMS voltages slightly increase. This implies that if support location coincides with the nodal points of the second and third transverse vibration modes, it enables improvement of the overall reliability of the considered system at the smallest expense of the generated voltage; however, the expense is still very high.
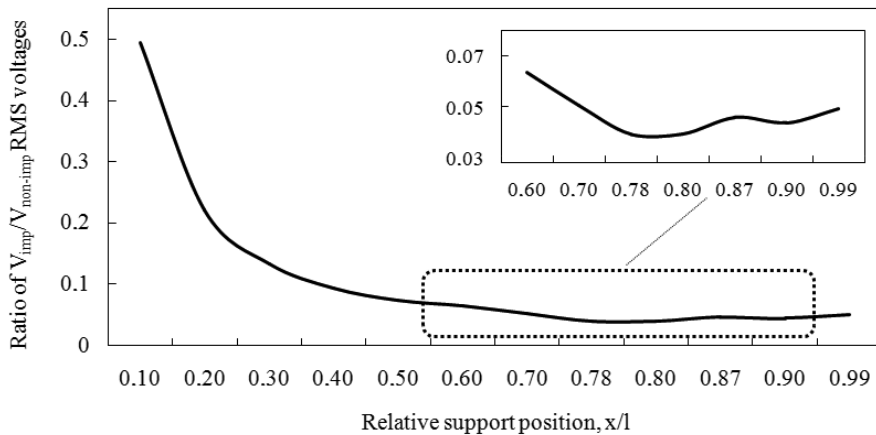
Figure 19. PEH generated impacting/non-impacting RMS voltage ratio as a function of relative support position (harmonic excitation signal)

For the second round of simulations random excitation signal was introduced into the FE model of the system, as it would represent more realistic case of vibro-impacting PEH utilization.
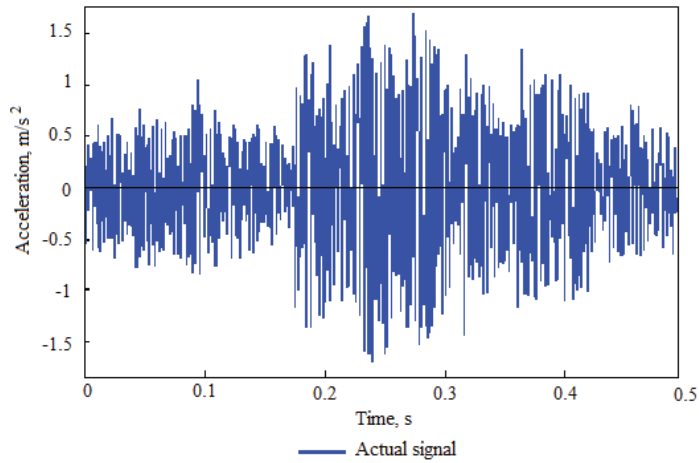
a)

b)

$$F=0.1322*\cos(2*pi*300*t-1.6153)+0.1164*\cos(2*pi*302*t+0.235)+0.2796*$$
$$*\cos(2*pi*320*t-.2856)+0.3476*\cos(2*pi*322*t+2.8952)+0.3383*\cos(2*pi*324*t--$$
$$0.9567)+0.344*\cos(2*pi*326*t+1.3189)+0.0898*\cos(2*pi*384*t-2.2426);$$

c)

Figure 20. Steps of random excitation signal mathematical approximation: a) measured real random signal; b) comparison or real (blue) and approximated (green) random excitation signal; $R^2 = 0.7869$; c) mathematical expression of approximated random excitation signal ($R^2 = 0.7869$)

In order to define random excitation signal the below described steps were taken: i) time-acceleration curve of operating industrial heating fan was registered employing accelerometer, oscilloscope and PicoLog software setup(measured real signal is presented in Figure 20, a)); ii) registered signal was mathematically processed with MATLAB software, which resulted in a few mathematical

50

expressions of excitation signal, qualitatively defined by the coefficient of determination R^2 (the more value of R^2 approaches 1, the more accurate random excitation signal mathematical approximation is (example of real excitation signal compared to approximated one is given in Figure 20, b)); iii) chosen random signal approximation was introduced in the FE as vertically acting body load (mathematical expression of approximated random excitation signal are presented in Figure 20, c).

PEH generated RMS voltages of impacting harvester, excited by random signal were determined for a number of relative support positions and compared to the RMS voltage output of harvester operating in non-impacting mode (Figure 21). As one may note from Figure 21, presence of support does not limit performance of the harvester, once it is excited by the random signal. Furthermore, if the support is located in the vicinity of nodes of the second and the third vibration mode, generated RMS voltages may increase up to 1.3 times for the analyzed PEH configuration.
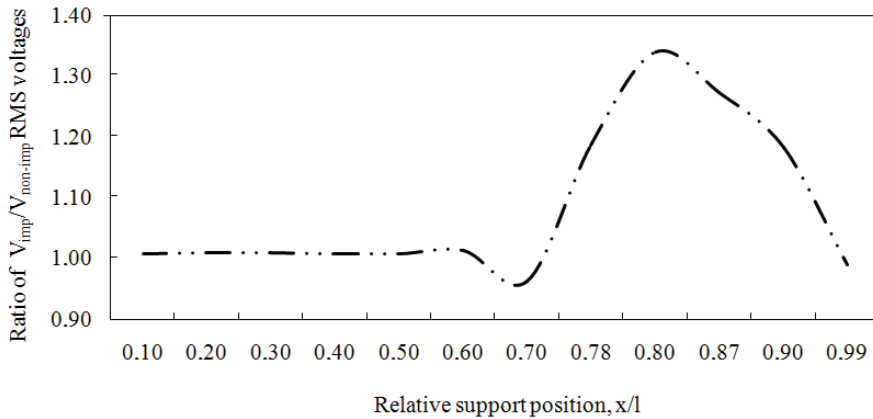
Figure 21. PEH generated impacting/non-impacting RMS voltage ratio as a function of relative support position (random excitation signal)

One should note as well that characteristics of generated voltage curve become quite different and have higher absolute voltage values as support is placed in the vicinity of nodal points, if compared to the generated voltage curve when support is placed elsewhere (example presented in Figure 22, a) time-voltage characteristics for support located at $0.1L$; b) time-voltage characteristics for support located at $0.87L$).

The advantages achieved when the support is positioned in the nodal point ($0.78L$) of the second or nodal point ($0.87L$) of the third vibration mode are related to the intensification of transverse vibrations of the respective modes. It should be noted that the amplification of the second and the third transverse modes (when the support is located at their nodal points) does not terminate the first mode of vibrations.
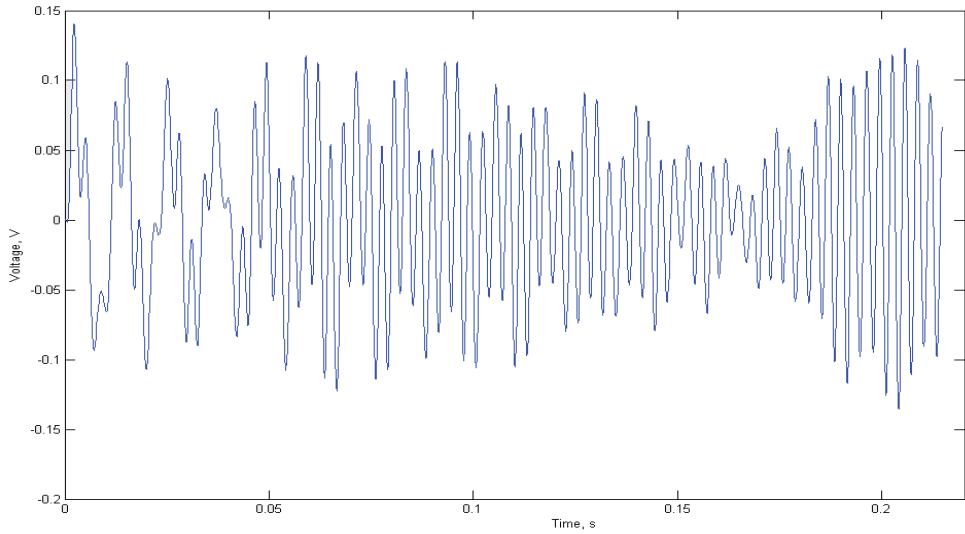
a)
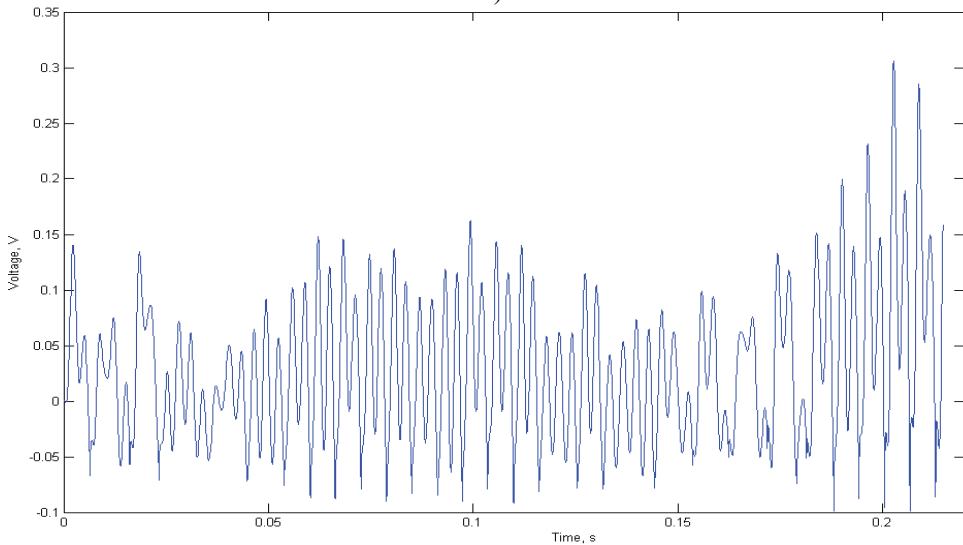
b)

Figure 22. Time – voltage characteristics of PEH generated voltage for different support locations: a) support is located at $0.1L$; b) support is located at $0.87L$

If one slightly increases the stopgap size between the support and PEH surface, the effect of support on PEH generated RMS voltage output becomes less pronounced (as may be seen in Figure 23, where stopgap size between the support and PEH surface is increased from 1 μm to 3 μm), yet increases in PEH generated RMS voltages may still be noted in the vicinity of nodal points.
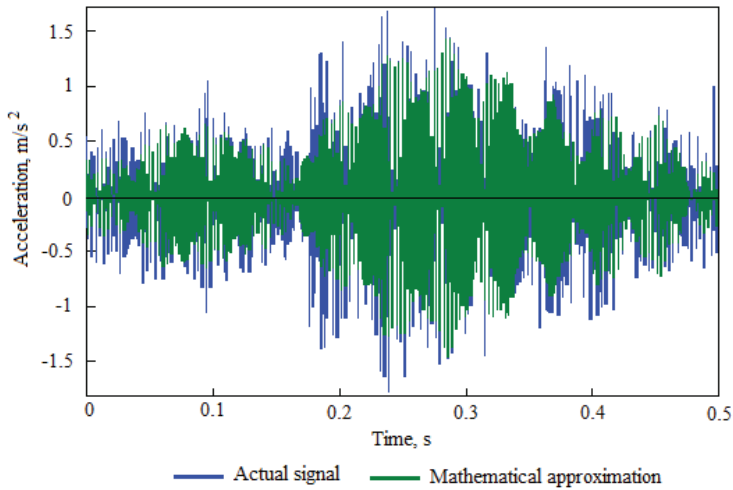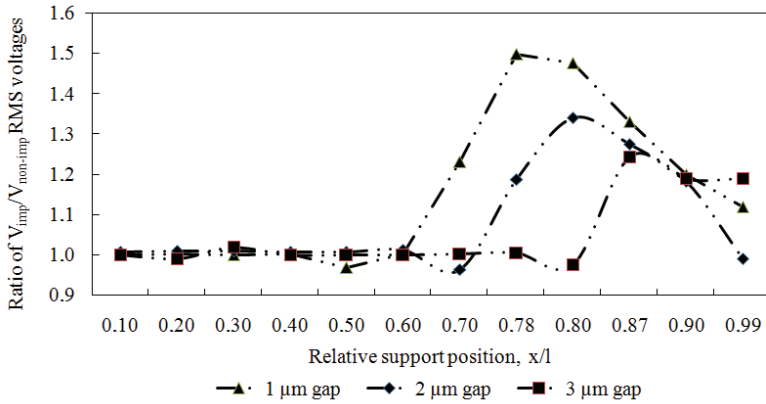
Figure 23. PEH generated impacting/non-impacting RMS voltage ratio as function of relative support position for different stop gap sizes (1 μm, 2 μm and 3 μm) in case of random excitation signal

Table 15. Comparison of PEH generated RMS voltages as it excited by harmonic and random excitation signal

Relative support position, x/l	Harmonic excitation signal		Random excitation signal	
	Generated RMS Voltage, V	$V_{imp}/V_{non-imp}$ ratio	Generated RMS Voltage, V	$V_{imp}/V_{non-imp}$ ratio
0.10	4.5589	0.4944	0.0522	1.0077
0.20	2.0375	0.2209	0.0523	1.0096
0.30	1.2273	0.1331	0.0523	1.0096
0.40	0.8557	0.0928	0.0522	1.0077
0.50	0.6687	0.0725	0.0522	1.0077
0.60	0.5844	0.0633	0.0525	1.0135
0.70	0.4695	0.0509	0.0499	0.9633
0.78	0.3650	0.0395	0.0615	1.1872
0.80	0.3662	0.0397	0.0694	1.3397
0.87	0.4249	0.0460	0.0660	1.2741
0.90	0.4063	0.0440	0.0613	1.1833
1.00	0.4564	0.0495	0.0513	0.9903
Generated RMS voltage in non-impacting mode, V				
-	9.22		0.0518	

To summarize this stage of simulations one may compare PEH generated RMS voltages as harvester is excited by harmonic or random signals (Table 15). One will be able to note that unsupported PEH, exited harmonically at its first resonance, generates significantly greater RMS voltages; generated RMS voltages drastically drop if support is introduced in such system. Meanwhile when PEH is excited by random signal, support positively influences PEH performance, especially if it is located in the vicinity of the nodal points of the second and the third vibration modes. This implies that if support location coincides with these nodal points, it enables improvement of overall reliability as well as performance of PEH as long as the system is excited by random signal.

2.2. Effects of piezoelectric material type on PEH generated voltages

Objectives of this research were to analyze effects of piezoelectric, elastic and dielectric piezoelectric material constants to PEH generated RMS voltages and to explore, if only large piezoelectric strain constants (especially d_{31}) account for substantially larger voltage generation. Or, stating in other words, to clarify if d_{31} constant alone is sufficient parameter to select piezoelectric material for PEH. While reviewing piezoelectric material properties it was noted that large piezoelectric constants are always followed by large elastic stiffness. Thus, it was assumed that for the latter reason, very large d_{31} constants may not necessarily lead to very large PEH generated voltages as stiffness of piezoelectric material affects PEH generated voltages via electromechanical coupling.

Three different piezoelectric materials - polymer PVDF (polyvinylidene fluoride), piezoceramic PZT-5H (lead zirconium titanate), single crystal PMN-28% PT (lead magnesium niobate) – were introduced one by one to the developed FE model of PEH (Figure 18) in order to explore the effect of piezoelectric material type to the magnitudes of PEH generated RMS voltages. The main geometric characteristics of FE model used for subsequent simulations are presented in Table 16.

Table 16. Characteristics of FE model used to evaluate how different piezoelectric materials influence PEH electric response

Parameters	Value
Stainless steel substrate dimensions (L_s x W_s x T_s), mm	100 x. 10 x 1
Piezoelectric dimensions (L_p x W_p x T_p), mm	100 x 10 x 0.2
External electric circuit resistance, MΩ	1
Stopgap size at the support location, μm	2
Piezoelectric materials introduced to the FE model	PMN-28%PT, PZT-5H, PVDF

Main material properties of PVDF, PZT-5H, and PMN-28% PT are listed in Table 17. There are quite many sources in literature and internet describing piezoelectric material properties, most of which are devoted to PZT ceramics. Meanwhile polymer and single-crystal material properties are more difficult to find, as this is a relatively new materials if compared to the PZT, which is most commonly met in energy harvesting applications. As one may note from Table 17, piezoelectric, elastic and dielectric properties of these active materials differ from each other considerably. For example, piezoelectric constants increase in the orders of magnitude if comparing PVDF and PMN-28% PT. One may note as well that large piezoelectric constants come with large elastic stiffness; meanwhile elastic compliance constants reduce comparing PVDF to PMN-28 % PT. As it was already stated above, it was assumed that large piezoelectric material stiffness may overweight the advantages of high piezoelectric strain constants and PEHs with PMN-PT layers may not necessarily generate higher RMS voltages

Table 17. Material properties of PVDF, PZT-5H, and PMN-28% PT [71-74]

	PVDF	PZT – 5H	PMN – 28 % PT
Elastic stiffness constants: c^E (10^{10} N/m^2)			
c_{11}^E	0.38	12.72	19.36
c_{12}^E	0.19	8.02	8.48
c_{13}^E	0.10	8.46	2.22
c_{22}^E	0.32	12.72	11.00
c_{23}^E	0.90	8.46	9.55
c_{33}^E	0.12	11.74	13.88
c_{44}^E	0.07	2.29	6.70
c_{55}^E	0.09	2.29	0.73
c_{66}^E	0.09	2.34	4.87
Elastic compliance constants: s^E (10^{-12} m^2/N)			
s_{11}^E	365	16.50	12.38
s_{12}^E	-192	-4.78	-19.44
s_{13}^E	-209	-8.45	11.38
s_{22}^E	424	16.50	53.09
s_{23}^E	-192	-8.45	-33.41
s_{33}^E	472	20.70	28.36
s_{44}^E	-	43.50	14.93
s_{55}^E	-	43.50	136.97
s_{66}^E	-	42,60	20,54
Piezoelectric constants: d (10^{-12} C/N)			
d_{15}	-23	741	2070
d_{24}	-27	741	150
d_{31}	21	-274	420
d_{32}	2.3	-274	-1140
d_{33}	-26	593	850
Dielectric constants: ε (ε_0)			
ε_{11}	12.50	1704.40	696
ε_{22}	11.98	1704.40	1090
ε_{33}	11.98	1433.60	716
Density, ρ (kg/m^3)			
ρ	1780	7500	8095

However, simulation results reveal that selection of material with highest piezoelectric constants (as well as highest stiffness), i.e., PMN-28%PT, results in greatest PEH generated RMS voltage values. FE model with PVDF as piezoelectric material displays smallest generated RMS voltages, meanwhile PEH performance with PZT-5H as active material is somewhat mediocre. This may be seen as well in Figure 24 and Figure 25, which depict generated RMS voltages of PEHs with piezoelectric material layers made of different materials versus relative support position when PEH is excited by harmonic (Figure 24) and random (Figure 25) excitation signals respectively.
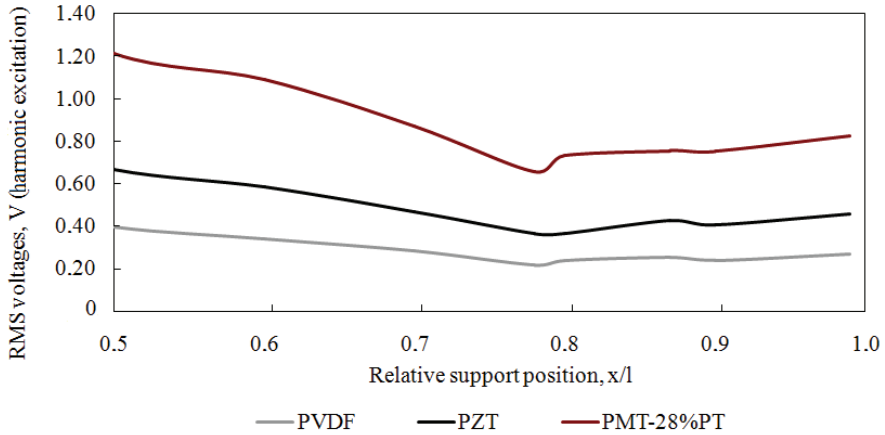
Figure 24. PEH generated RMS voltage as function of relative support position (harmonic excitation signal) for PEHs with piezoelectric layers of different material
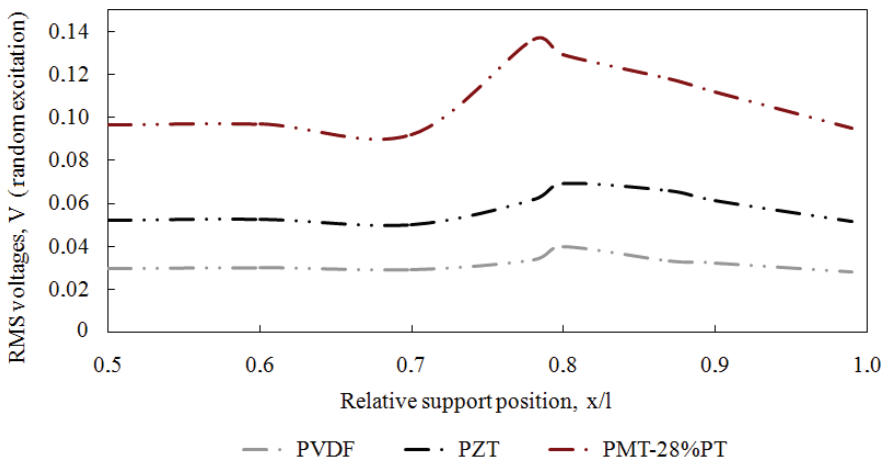
Figure 25. PEH generated RMS voltage as function of relative support position (random excitation signal) for PEHs with piezoelectric layers of different material

56

Summarizing this stage of simulations it is important to note that despite the superior performance of harvester with piezoactive PMN-28% PT material layers, it was decided to carry on most of the further investigations of PEHs with piezoactive layers of PZT-5H, since PMN-28%PT is extremely expensive, brittle and may not demonstrate longevity in actual PEH application environments, especially when PEH is operating in vibro-impacting mode. It may also be concluded, that despite the type of piezoelectric material, all generated RMS voltage curves display the same trend, which was already noted in the section before: if support is placed in the vicinity of nodal points ($0.78L$ and $0.87L$) of PEH vibration modes, one may note increase in PEH generated RMS voltages, which is especially prominent in case of random excitation signal.

2.3. Evaluation of effects of electric circuit connected to PEH

As already discussed in the literature review section, PEHs are usually connected to electric circuit that might consist of capacitors to store energy, rectifiers to convert from ac to dc, diodes, load resistors and etc. All these components should transform harvested energy to usable form. Nevertheless, most of current FE models of PEHs assume the vibration amplitude of the device is independent of the connected circuit. Erturk and Inman [75] prompted to incorporate external electric circuits in analytical PEH models, because ignoring backward piezoelectric coupling and using optimum load for the maximum power is incorrect. Moreover, it was discovered that increase of load resistance of connected circuit not only influences PEH electrical characteristics, but also dynamic response of the system changes. Voltage and current throughout load resistor and, therefore, generated power, as well as displacement of harvester are all coupled together, thus effects of external electric circuit must be determined and ongoing processes/phenomena explained.

Thus, this section places the greatest emphasis on incorporation of simplified electric circuit into the FE model of operating harvester. This, in turn, results in the development of electromechanically coupled system, which takes into account influence of external resistive load on electric and dynamic behaviour of PEH subjected to harmonic base excitation. Namely, effects of the external load resistance on resonant frequency and tip displacement of PEH and on electric outputs of current, voltage, and power are considered.

A very similar to in Figure 18 presented PEH configuration was used to evaluate effects of connected load resistance on mechanical and electrical characteristics of PEH. Developed FE model of PEH possesses geometrical characteristics listed in Table 18. As before, it is at one end clamped cantilever beam, comprised of piezoelectric PZT-5H layer (enveloped with electrodes) attached to the substrate (piezoceramic and substrate materials are assumed to be perfectly bonded to each other). Since continuous electrodes covering piezoceramic layers are assumed to be very thin if compared to the overall thicknesses of harvester, their contribution to the thickness dimension is assumed negligible. These electrodes are thought to be perfectly conductive, so that a single electric potential difference can be defined across them. Therefore, the instantaneous electric field

induced in the piezoceramic layer is assumed to be uniform throughout the length of the beam. For this research PEH is assumed to undergo bending vibrations due to harmonic base excitation only and no rigid supports are introduced in the system.

Table 18. Characteristics of FE model used to evaluate effects of external electric circuit to dynamic and electric response of PEH

Parameter	Value
Stainless steel substrate dimensions (L$_s$ x W$_s$ x T$_s$), µm	6000 x 10 x 1
Piezoelectric dimensions (L$_p$ x W$_p$ x T$_p$), µm	6000 x 10 x 0.5
External circuit electric load resistance, representing short circuit conditions, Ω	1
External circuit electric load resistance, representing open circuit conditions, MΩ	100

External electric load is introduced to electromechanically coupled system employing SPICE circuit editor. SPICE Circuit Import feature is commonly used to add circuit elements as variables to FE models created with COMSOL Multiphysics software, as this allows variables to be connected to a physical device model in order to perform co-simulations of circuits and multiphysics. For example, to introduce an external electric circuit with resistor of 50MΩ resistance to the operating PEH, the following command prompt should be used in SPICE:

```
R1 0 1 50Meg
X1 0 1 Piezo
.SUBCKT Piezo sens1 sens2 COMSOL: *
.ENDS
```

As mentioned before, piezoelectric harvester is subjected to harmonic base excitation, thus continuous electrical outputs can be extracted from the electromechanical system (only the fundamental resonant frequency and no higher modes of vibration are considered for these simulations).

Simulation results presented in Figure 26 - Figure 28 reveal the expected: increasing load resistance of the connected circuit not only influences electrical characteristics of PEH, but also dynamic response of the system changes.

Figure 26 depicts the shift of 15 Hz in resonant frequency as the resistance of connected electric circuit load increases from nearly short to nearly open circuit conditions. One may note that the structure becomes stiffer as higher resistance load is introduced to the external circuit. It is assumed that this frequency difference is resulting from backward coupling.

PEH generated voltage values increase increasing the resistance of connected load, meanwhile generated current values decrease, as load resistance increases from short to open circuit conditions (Figure 27).

Figure 28 combines PEH generated power and tip displacement plots as functions of connected load resistance at constant acceleration levels. Generated power plot is based on power calculations per equations below:

$$P = I^2 R_{load} \quad \text{or} \quad P = V^2 / R_{load} \tag{2.3.1}$$

58
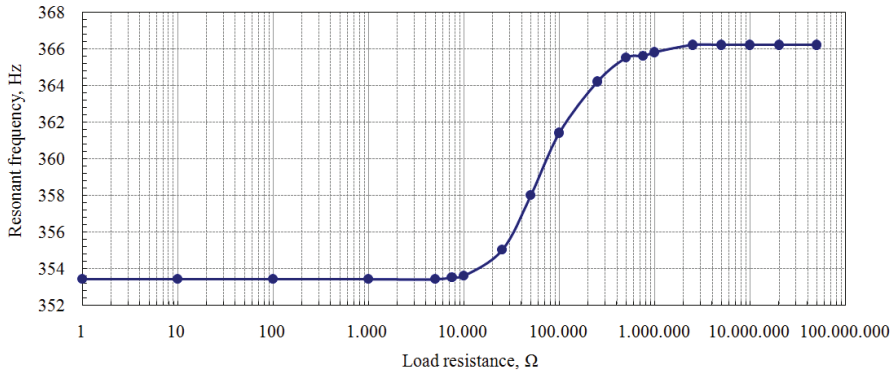
Figure 26. Resonant frequency of the device as a function of connected load resistance
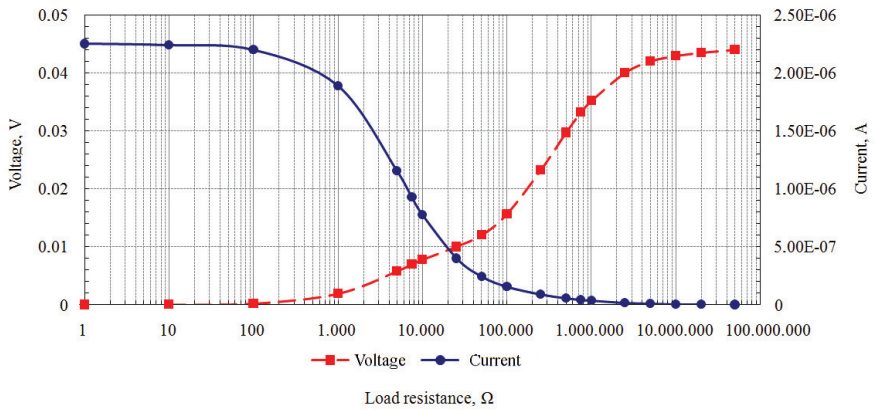
Figure 27. PEH generated voltage and current values as a function of connected load resistance.
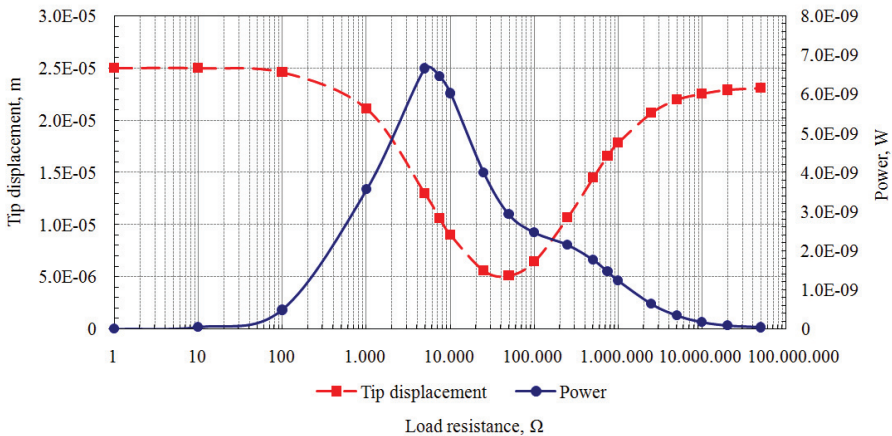
Figure 28. PEH generated power and PEH tip displacement as a function of load resistance

Figure 28 as well suggests that harvested energy can be visualized as decrease of PEH displacement due to electrical damping. When PEH operates at short or open circuit conditions, energy dissipation in the load is low. At the optimum load resistance maximum power is transferred from the harvester to the load, meanwhile displacement at the maximum power point is reduced (load resistance reduces PEH motion amplitude at the short-circuit conditions until so-called optimum load and enlarges the motion amplitude towards open circuit conditions). Energy harvesting may also be considered as electrical damping of PEH tip displacement. One may observe that both in the open and short circuit condition cases electrical damping is minimal and mass displacement is maximal. Vibrating PEH operating at a short circuit conditions is only mechanically damped as no electric power is consumed. As the connected load resistance approaches optimum load, mechanical energy is partly transferred to electrical energy. This harvested electrical energy is considered as electrical damping which adds to the still present mechanical damping. Eventually, the total damping (mechanical and electrical) leads to attenuation in PEH tip displacement.

Mechanical damping caused by air is a loss factor as well which reduces the output power and thus should be taken into the account. In order to prevent air damping one could use vacuum packaged devices. Furthermore, it is important to note that contribution of air damping to the total system damping is dependent on PEH substrate configuration and size. The bigger the surface area of the PEH, the greater the air damping contribution on total system damping will be.

Simulation results presented in this section reveal that it is very important to incorporate external electric circuits to FE models of piezoelectric energy harvesters, since PEH dynamic and electric performance is highly influenced by the magnitude of connected electric circuit resistance. One may note that with increasing external load resistance structures are getting stiffer (i.e. resonant frequency increases). Furthermore, PEH generated voltage values increase, meanwhile current values decrease, as resistance of connected circuit changes from nearly short to nearly open circuit conditions.

2.4. Evaluation of PEH piezoelectric layer segmentation on its electric outputs

The main principle of PEH operation relies on the fact, that dynamic strain field induced throughout piezoelectric material layers due to excitation results in alternating voltage output across electrodes covering piezoelectric material. As already mentioned in the literature review section, most of currently analyzed harvesters do not perform efficiently in real environments, since it is assumed that they are excited only by harmonic signal and at their fundamental frequency. However, if one analyses real environmental vibration energy source, it usually would not consist of one single harmonic and higher modes of harvester vibration may be excited. These higher vibration modes of cantilever beam have strain nodes – i.e., positions on the device, where bending strain distribution curve changes sign (examples of normalized strain distribution curves are presented in Figure 29, a)). Mathematically, curvature eigenfunction, which is a measure of bending strain, is the second derivative of displacement eigenfunction (examples of normalized

displacement curves are presented in Figure 29, b)). Authors of [76] suggested that if these strain nodes are covered by continuous electrodes, cancellation of electric outputs occurs, resulting in overall harvested energy reduction.
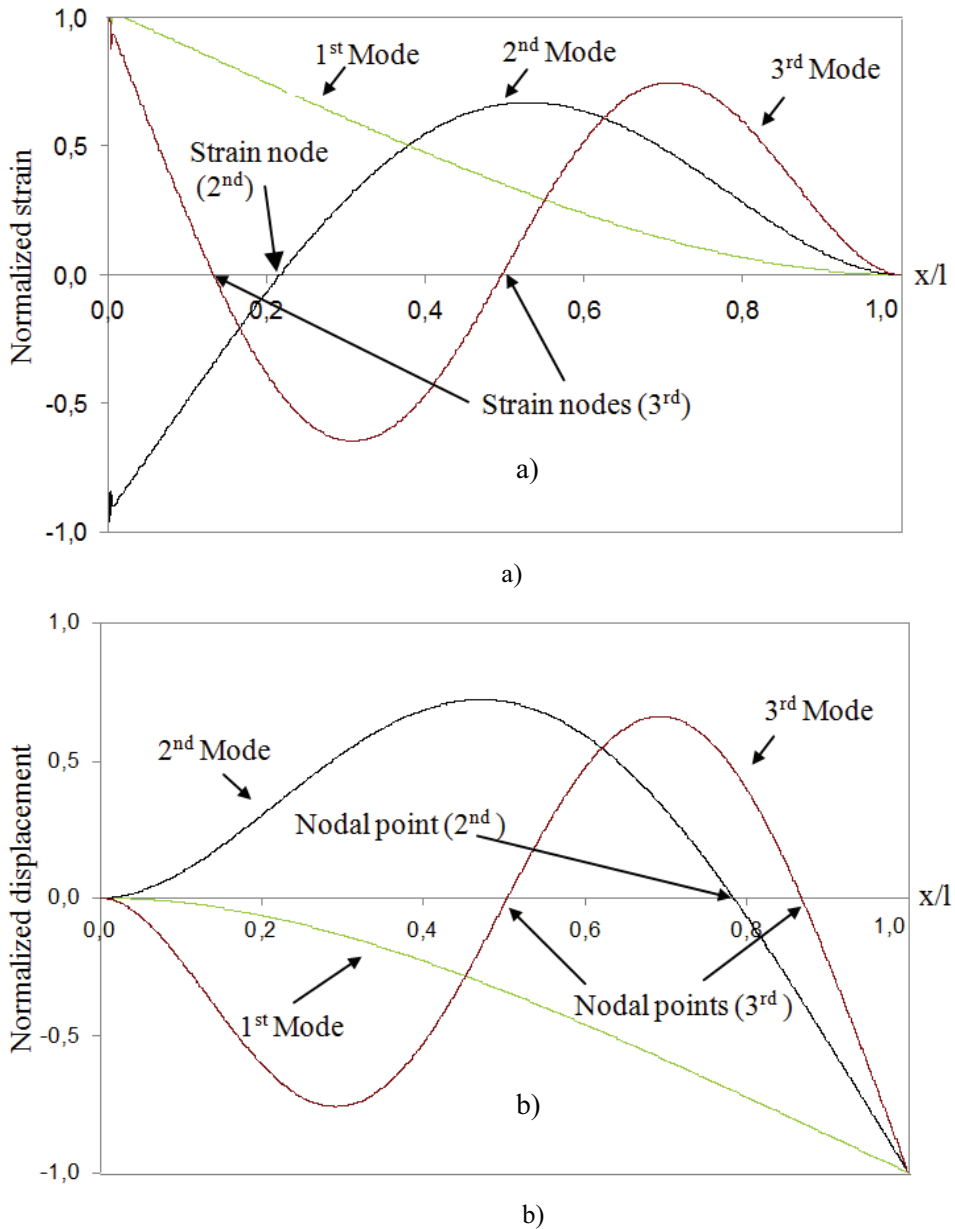
Figure 29. Examples for normalized strain (a), with highlighted 2nd and 3rd mode strain nodes) and displacement (b), with highlighted 2nd and 3rd mode nodal points) curves for the first, second and third vibration modes

Thus, the set of simulations presented in this section is aimed to clarify effects of PEH piezoelectric layer segmentation on electrical parameters of PEH. For this purpose FE model was slightly modified: one continuous piezoelectric (PZT) layer on stainless steel substrate was segmented either in two segments (location of segmentation coincided with the strain node of the second vibration mode) or in three segments (location of segmentation coincided with the strain nodes of the third vibration mode). In both cases, perfectly conductive electrodes of negligible thickness covered the entire area of the top and the bottom surfaces of piezoelectric material layers. They were directly connected to the resistive load, introduced to the electomecanically coupled system via COMSOL SPICE circuit editor (which is described in detail in the previous section). This circuit editor was used, as it would allow including additional and more complex circuit elements (e.g., diode bridges) in future research, aiming to develop complete energy harvesting system.

Locations of strain nodes were determined from bending strain distribution functions, as depicted in the Figure 29, a). Table 19 lists obtained dimensionless positions of nodal points and strain nodes of modelled PEH for the first three vibration modes.

Table 19. Dimensionless positions of nodal points and strain nodes of the PEH for the first three vibration modes

| Mode | Dimensionless positions (x/l) on x-axis of | | | |
	Nodal point		Strain node	
1	-	-	-	-
2	0.783	-	0.217	-
3	0.505	0.868	0.133	0.498

As already mentioned above, FE models were created for two PEH configurations – for the first one piezoelectric layer was segmented at the location of the second vibration mode strain node (presented in Figure 30, a) with the main characteristics presented in Table 20), meanwhile for the second one – segmentation occurred at the strain nodes of the third vibration mode (as depicted in Figure 30, b) with the main characteristics presented in Table 21). It was assumed that these configurations would allow one to avoid undesired charge cancellation effects in the piezoelectric material and, this, in turn, would increase PEH generated voltage.

Table 20. Characteristics of PEH model with piezoelectric layer segmented at the strain node of the second vibration mode (0.217L)

Parameter	Value
Stainless steel substrate (L_s x W_s x T_s), mm	100 x 10 x 1
1st piezoelectric segment (L_p x W_p x T_p), mm	21 x 10 x 0.2
2nd piezoelectric segment (L_p x W_p x T_p), mm	78 x 10 x 0.2
External circuit electric load resistance, MΩ	100
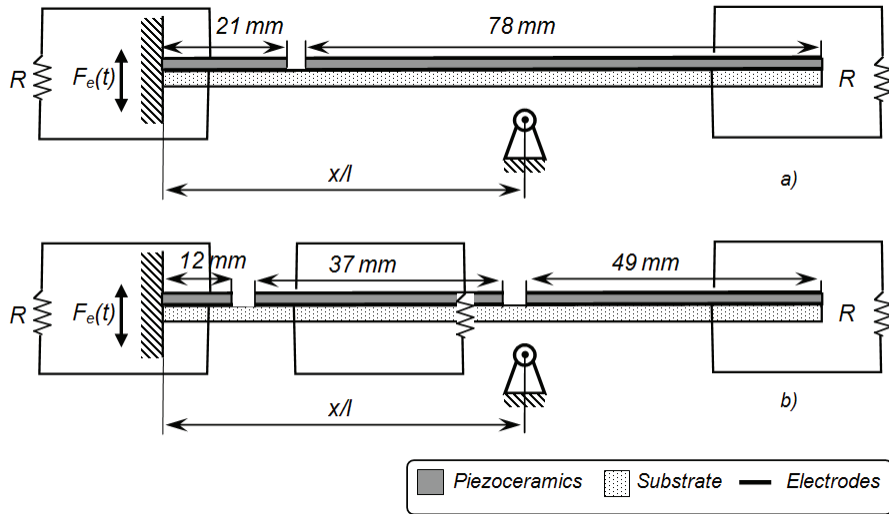
Figure 30. Principle schemes of segmented piezoelectric energy harvesters: a) PEH with piezoelectric layers segmented at the strain node of the second vibration mode; b) PEH with piezoelectric layers segmented at the strain nodes of the third vibration mode

Table 21. Characteristics of PEH model with piezoelectric layers segmented at the strain nodes of the third vibration mode ($0.133L$ and $0.498L$)

Parameter	Value
Stainless steel substrate (L_s x W_s x T_s), mm	100 x 10 x 1
1st piezoelectric segment (L_p x W_p x T_p), mm	12 x 10 x 0.2
2nd piezoelectric segment (L_p x W_p x T_p), mm	37 x 10 x 0.2
3rd piezoelectric segment (L_p x W_p x T_p), mm	49 x 10 x 0.2
External circuit electric load resistance, MΩ	100

RMS voltages generated by PEHs with segmented piezoelectric layers (calculated by adding RMS voltages generated by each piezoelectric segment) were plotted for relative support positions in the range of $0.5L$ to $1.0L$ in Figure 31 for harmonic and in Figure 32 for random excitation signals. As one may note from these graphs, PEHs with piezoelectric layers segmented at the location of second (Segmented, II mode) and third (Segmented, III mode) strain nodes generate much greater RMS voltages if compared to their counterpart with continuous piezoelectric layer OPT0 (when all are having the same geometric dimensions). All RMS voltage curves display the same trend, which was already revealed in the sections above: presence of the support limits PEH performance, when it is operating under harmonic excitation, yet improves its performance if it is excited by random excitation signal (especially, if support is placed in the vicinity of PEH nodal points). Comparing RMS voltage curves, generated by the two-segment (Segmented, II mode) and three-segment (Segmented, III mode) PEHs excited by harmonic signal, one may conclude that the two - segment PEH demonstrates better

performance – i.e. higher values of generated RMS voltages, when relative support position is ranging from 0.5L to 1.0L.
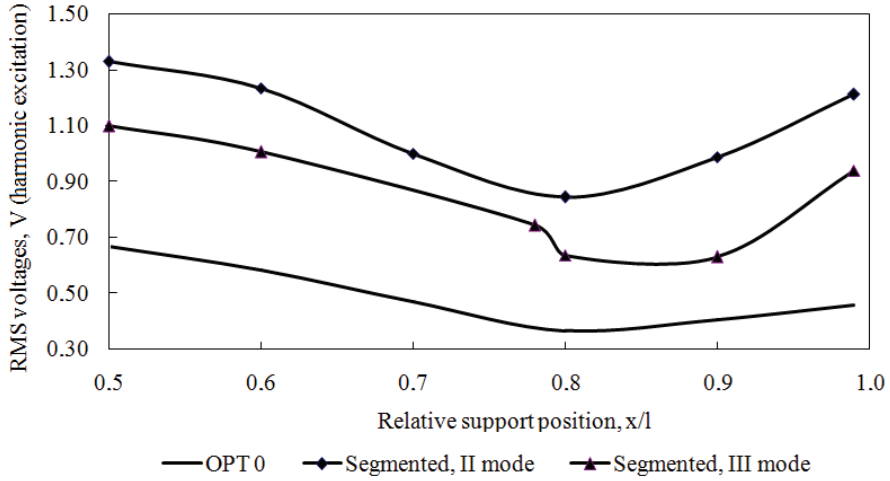
Figure 31. RMS voltages generated by different configuration PEHs as functions of relative support position (harmonic excitation signal)
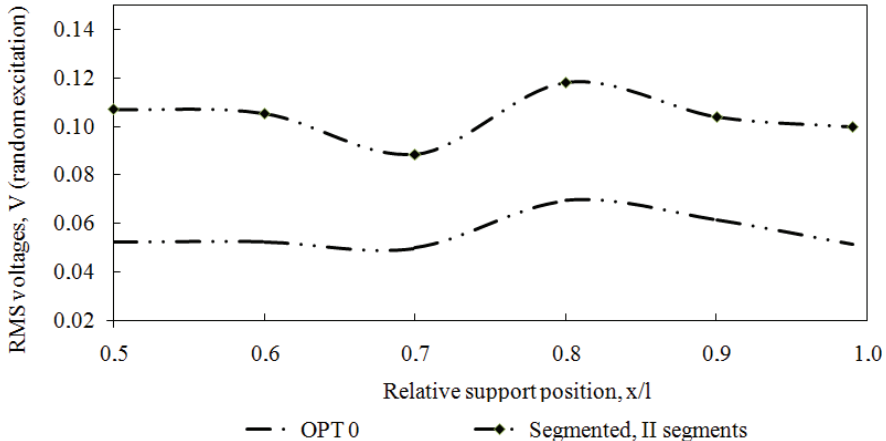
Figure 32. RMS voltages generated by different configuration PEHs as functions of relative support position (random excitation signal)

Although advanced electric circuits are not a part of this research, some considerations below are provided on relatively simple electric circuits that could be connected to PEHs operating at different environments (and thus excited by different frequencies).

If the first PEH vibration frequency is dominating in PEH operation environment, one may harvest energy with continuous piezoelectric layers, as then strain distribution over the length of device does not change sign. For the latter case, a fairly simple ad-dc conversion electric circuit (scheme of which is depicted in

Figure 33, a)) can be employed, where electrodes of piezoelectric are connected to diode bridge to eliminate electrical output sign alteration [76]. For the case when second resonant frequency is predominant, two separate piezoelectric segments could be used to cover substrate at regions 0-strain node, strain node-L and, in such way, cancellation in charge would be avoided, as voltage outputs from these segment pairs would be out of phase with each other. A relatively simple electric circuit could be used to collect harvested energy, where bottom electrodes of piezoelectric layers would be connected to each other and top electrodes of piezoelectric layers would be connected to diode bridge (as per Figure 33, b)) [76]. Yet the latter circuit configuration would be effective only for energy harvesting from the second PEH vibration mode, as it would result in charge cancellation for the first one. To harvest energy from both first and second vibration modes, more complex electric circuit, comprised of two separate diode bridges, connected in series (as per Figure 33, c)) is suggested to be used [76].
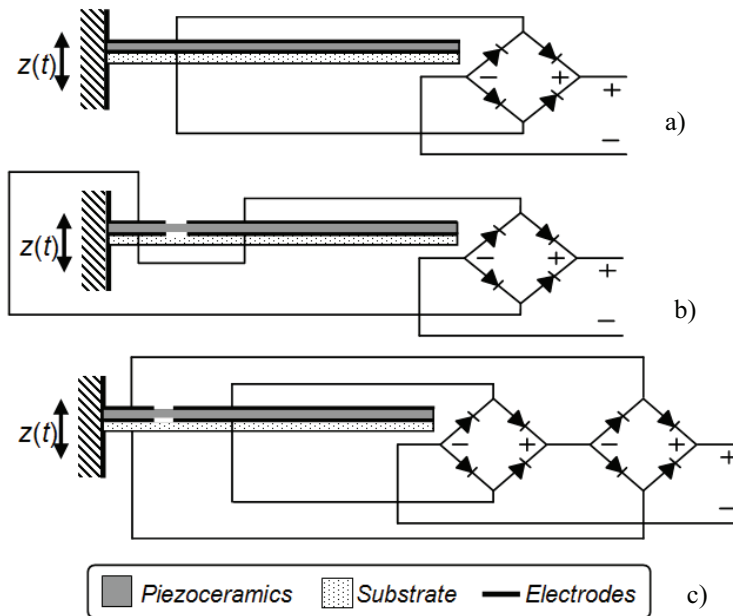
Figure 33. Electrode and electric circuit configurations, suitable for energy harvesting once (a) first vibration mode is predominant; (b) second vibration mode is predominant; (c) both vibration modes are excited

The other way to avoid charge cancellation using continuous piezoelectric layers is to apply "patterned polling" [77] to the piezoelectric material– i.e., change direction of polarization of pre-planned piezoelectric regions. This process involves etching electrodes of piezoelectric material at certain regions, corresponding to the strain nodes of vibrating harvester, applying strong electric fields at these desired portions (i.e., polling them), and reconstructing the electrodes back. The polled portions of piezoelectric material will have a sign of piezoelectric constant changed

and no charge cancellation should occur over restored continuous electrodes. However, it is important to note that practically patterned poling is only effective if harvester is excited at certain vibration mode for which the patterning is performed (e.g., if the harvester has patterned polling applied bearing in mind strain nodes of second vibration mode, a strong charge cancellation would occur once it operates at the first resonant frequency), which means that the approach is not flexible.

Thus summarizing this section one may come to the conclusion that use of segmented piezoelectric layers is more preferable than patterned polling, as it is practically easier to implement by combining the leads of electrodes accordingly and joining them to different electric circuits. Yet, whichever case is chosen, the main concern remains not to cover strain nodes of vibrating PEH with continuous piezoelectric layers in order to avoid charge cancellation problems. Simulation results reveal that PEHs with segmented piezoelectric layers are able to generate almost twice greater RMS voltages if compared to their counterparts with continuous piezoelectric layer.

2.5. Enhanced PEH configuration

Numerical studies of piezoelectric energy harvesters, that were described in the thesis so far, have concentrated on a few interrelated aspects of PEH dynamics (e.g., PEH response to harmonic and random excitations as well PEH operation in vibro-impacting regimes) and electrical outputs (e.g., effects of connected electric circuit and piezoelectric layer segmentation were explored). Consolidating all completed research aspects together, an enhanced PEH configuration was developed, analysis and numerical research of which will be presented in this section.

The initial step of PEH configuration enhancement was related to the optimization PEH cantilever beam substrate. PEH cantilever beam substrate optimization was performed following information in [69]. The aim of optimization of cantilever beam structure was to select such geometrical parameters that would correspond to the technical characteristics of the system and give a minimum value to a certain quality function (a very common example would be system mass minimization with the constraint of a prescribed vibration frequency). It was as well important to distinguish geometrical and structure performance constraints in order to avoid irrational structure configurations.

The target function of PEH cantilever substrate optimization per [69] is expressed as:

$$\Phi(A) = \min \rho \, a \, (A_1 + A_2 + ... + A_m), \tag{2.5.1}$$

where A_i- cross-sections of structure components, $i=1$, 2, m. If one employs the method of nonlinear programming, e.g., gradient projection, the following inequality-shaped constraints should be incorporated:

$$f_m(A) = 1 - A_m / A_i \le 0,$$

$$f_{m+1}(\omega) = 1 - \omega / \omega^* \le 0, \tag{2.5.2}$$

where ω^* is the prescribed frequency of structure vibrations.

Optimal PEH substrate configurations obtained with gradient projection method are presented in Figure 34. Figure 34, a) illustrates optimal structures obtained for the operation in prescribed (OPT I$^+$), second (OPT II$^+$) and third natural frequencies. These optimal cantilever structures would attain increased natural frequencies if compared to their counterparts with constant cross section. Should one like to use cantilevers with reduced natural frequencies (with respect to the constant cross-section versions), symmetrically inverted optimal structures would be obtained as depicted in Figure 34, b) for the operation in first (OPT I$^-$), second (OPT II$^-$), and third (OPT III$^-$) natural frequencies.

Examination of optimal PEH cantilever substrates in Figure 34 reveals that change of natural frequency leads to increase in the number of cross-sectional minima/maxima along the length of the structure. Moreover, distances from the minimum and maximum cross sections to the clamping site may be easily determined. For example, for the substrate structure that is optimal for operation in increased second frequency (OPT II$^+$) the minimum cross section is always located at the distance of 0.24L from the clamping site, while for the structure that is optimal for operation in increased third frequency (OPT III$^+$) – 0.15L and 0.5L, respectively (L is the cantilever length). More detailed analysis of optimal cantilever structures presented in Figure 34 reveals that the recurrence of maximum and minimum cross-sections corresponds to the positions of particular (maximum amplitude and nodal) points of vibration modes.

The second step of PEH configuration improvement is to adjust its configuration to have two separate piezoelectric material layers. As is it was already discussed in previuos section, PEHs with continous piezoelectric layes do not perform well if excited at greater than first resonant frequency. Therefore, active piezoelectric material layers must be segmented at the strain nodes of higher vibration modes to avoid undesired charge cancelation effects in piezoelectric material. Thus, integrating both assumptions described above, rational PEH configuration was developed, scheme of which is preseneted in Figure 35. Rational PEH configuration is based on a simplified optimal cantilver structure aimed for operation at decraesed second resonant frequency. Since one of research objectives was to suggest easily manufacturable PEH configuration, intricate optimal substrate shape (fabrication of which requires sophisticated automated cutting machinery) was replaced by a simplified design of PEH substarte with the hump at 0.24L. This configuration allows ease of piezoelectric material deposition/attachment and ensures natural segmentation of piezoelectric layer at the strain node of the second vibration mode.

A number of simulations were performed to compare performance of enhanced configuration PEH (OPT RAT) to its other counterparts (constant cross section cantilever OPT 0 and PEH with two segmented piezoelectric layers (Segmented, II segements)).

OPT I⁺ ... OPT I⁻

OPT II⁺ ... OPT II⁻

OPT III⁺ ... OPT III⁻

a) ... b)
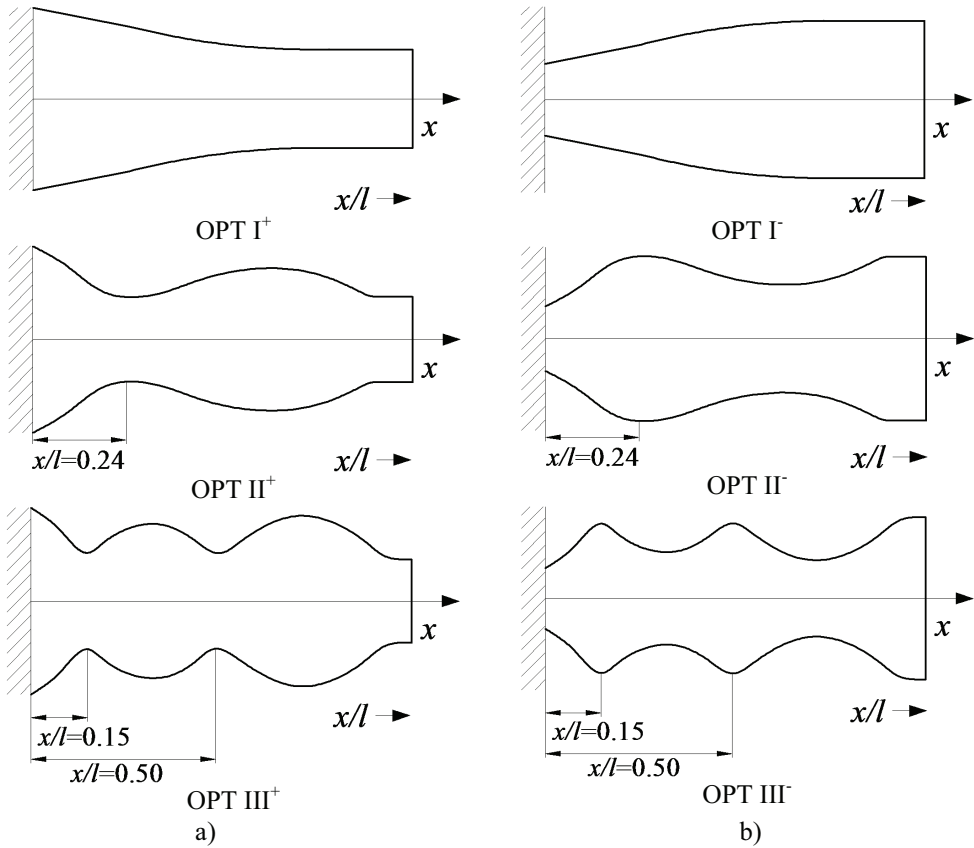
Figure 34. Optimal structures for operation in increased (a)) and decreased (b)) natural frequency of transverse vibrations (the first (OPT I), the second (OPT II) and the third (OPT III) from top to bottom)
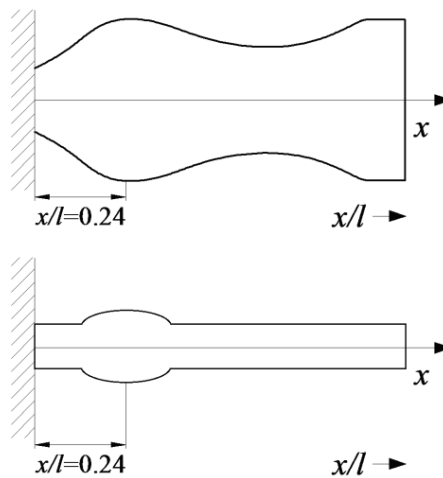
Figure 35. Optimal (top) versus rational (bottom) cantilever configuration
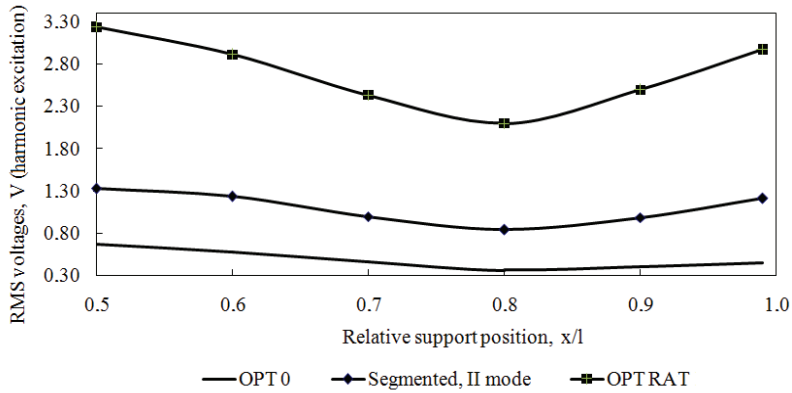
Figure 36. RMS voltages generated by PEHs of different configuration versus relative incorporated support location (harmonic excitation)
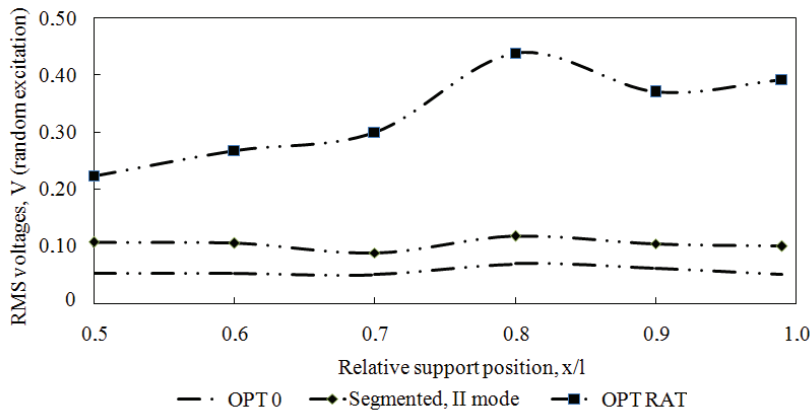
Figure 37. RMS voltages generated by PEHs of different configuration versus relative incorporated support location (random excitation)

Figure 36 presents generated RMS voltage versus relative support location graphs for contant crossection PEH with continous electrodes (OPT 0), constant cross-section PEH with segmented piezoelectric layer (Segmented, II mode) and rational configuration PEH (OPT RAT); all excited by harmonic signal, meanwhile Figure 37 presents generated RMS voltages for the same harvesters excited by random signal. As one may note from Figure 37, rational configuration PEH generates greater RMS voltages (especially prominent if support is located at the nodal point of the third vibration mode (0.87*L*)), if compared to the constant cross-section counterpart with continous piezoelectric layer. PEH with piezoelectric layer segmented at the strain node of the second vibration mode (yet constant cross-section) demonstrates higher generated RMS volatges than constant cross-section PEH with continous piezoelectric layer, yet a few times inferior if compared to the rational configuration PEH. The same trends are noted as PEHs are excited by

harmonic excitation signal, with the superior performance of rational configuration PEH, mediocre performance of PEH with segmented piezoelectric layers and worst performance of constant cross – section PEH with continous piezoelectric layer. As it was already discussed in previuos sections, incorportaed support limits PEH performance if excited by harmonic excitation signal, yet imporves the performance once PEHs are excited randomly.

2.6. Section Conclusions

As it was already discussed, piezoelectric energy harvesters cannot be easily and cost effectively built without prior modelling of its components. This preliminary design stage gives one the advantage to predict how elaborated configuration of PEH will perform.

Thus, meeting objectives of the research FE model of PEH was developed with COMSOL Multiphysics software. This FE model allows inter-related investigations of: i) PEH dynamic and electric response and the way it depends on geometric parameters of device as well as its excitation signal; ii) external electric circuits' influence on PEH generated voltages, iii) nonlinear dynamic effects occurring during the impact, i.e., once harvester is hitting on incorporated rigid support, location of which may be easily adjusted.

Numerical simulations performed throughout the research may be grouped in a few case studies: i) evaluation of response of PEH to harmonic and random excitation; ii) investigations of effects of the piezoelectric material type on the PEH generated voltage; iii) evaluation of effects of electric circuit connected to PEH generated voltage; iv) evaluation of PEH electrode segmentation on its electric outputs; v) considerations on enhanced PEH configuration.

Main conclusions drawn from numerical simulation results are the following:

- unsupported PEH of typical configuration, exited harmonically at its first resonance, generates greatest RMS voltages, yet generated RMS voltage drastically drop as support is introduced in such system. Meanwhile if PEH is excited by random signal, generated RMS voltages are significantly smaller. If support is introduced to the randomly excited model at the vicinity of nodal points of second and third vibration modes ($0.78L$ and $0.87L$) PEH generated RMS voltages may be significantly increased. This implies that if support location coincides with the mentioned nodal points it enables improvement of reliability and performance of the system (as long as the PEH excitation signal is random, which actually happens in most of practical utilization circumstances of PEHs);

- magnitudes of PEH generated RMS voltages highly depend on selection of material for piezoactive PEH layer. PEHs with the same geometric configuration, yet different piezoelectric materials – PVDF, PZT 5H and PMN - 28% PT - were modelled. Despite the fact that PEH with PMN – 28% PT piezoactive layers demonstrated greatest RMS voltages, it was decided to exclude this material from further investigations, since it is expensive and extremely brittle, thus could not be used in practical applications;

70

- resistance of connected electric circuit not only influences PEH electric, but also its dynamic response. As one increases resistance of connected electric circuit, shifts in PEH resonant frequency and tip displacement are noted. PEH generated voltage values increase with increasing resistance of connected electric circuit, meanwhile current values decreases;
- in order to avoid undesirable charge cancellation effects in piezoactive PEH layers once it is excited by random excitation signal or higher resonant frequencies, piezoelectric layers of PEH should be segmented at the location of structure's strain nodes. Numerical simulation results reveal that PEH with piezoelectric layers segmented at the location of strain nodes of second or third vibration modes outperform PEHs with typical continuous piezoelectric layer configuration;
- enhanced PEH configuration was suggested. It was based on rational PEH cantilever shape with piezoelectric layers segmented at the location of strain node of second vibration mode. Results of numerical simulations reveal that enhanced configuration PEH outperforms typical configuration PEH as well as PEH with segmented piezoelectric layer.

3. EXPERIMENTAL INVESTIGATIONS OF PROTOTYPES OF PIEZOELECTRIC ENERGY HARVESTER

The following section describes elaboration of PEH prototypes; customized equipment and stands used for experimental measurements as well as experimental studies with different configuration PEH prototypes performed throughout the research period. The aim of experimental studies was to evaluate dynamic and electric characteristics of harvester prototypes and verify adequacy of the developed FE model. This section is divided into two main parts – the first one describes main equipment and customized stands that were used to perform experiments/produce prototypes, while the second part presents performed experimental studies as well as their results.

Most of the experiments were performed with Laser Doppler Vibromery and Holographic Measurement systems (described 3.1.1 and 3.1.2 sections respectively), meanwhile water-jet cutting system was used in fabrication processes of different PEH prototypes. Experiments performed during the course of research may be grouped to the following cases: i) investigations of effects of connected electric circuit to dynamic and electric response of commercial PEH prototype; ii) investigations of PEH prototypes with non-segmented and segmented piezoelectric layers and effects of rigid support location to electrical outputs of PEH prototypes when they are operating in vibro-impacting mode; iii) investigations of dynamic response of optimal cantilever beam substrates intended for energy scavenging applications. The last chapter of this section is devoted to summarize experimental research and rehash main conclusions. Insights presented in this section may serve for development and fabrication of advanced PEHs, which would be able to harvest energy from various vibration sources (i.e., efficient not only in harmonic, but also random excitation cases).

3.1. Experimental research equipment and techniques

3.1.1. Holographic measurement system

Non contacting holographic measurement system PRISM (Precise Real-Time Instrument for Surface Measurement, Hytec, USA [78]) was used to evaluate dynamic response of different PEH prototypes – i.e., determine vibration forms of PEH prototypes and the way dynamic response of PEH prototype changes once it is impacting on rigid support. PRISM system was chosen since it is comprised of all components necessary to perform small lightweight system deformation and vibration measurements. Moreover, it allows completing and processing experimental measurements in less than 5 minutes as well as is capable of determining displacements of less than 20 nm (the main characteristics of the PRISM system are presented in Table 22).

Basic parts and operation scheme of holographic measurement stand are presented in Figure 38; a) and b) respectively. PRISM includes control block, light source, camera and computer with integrated state of the art software.
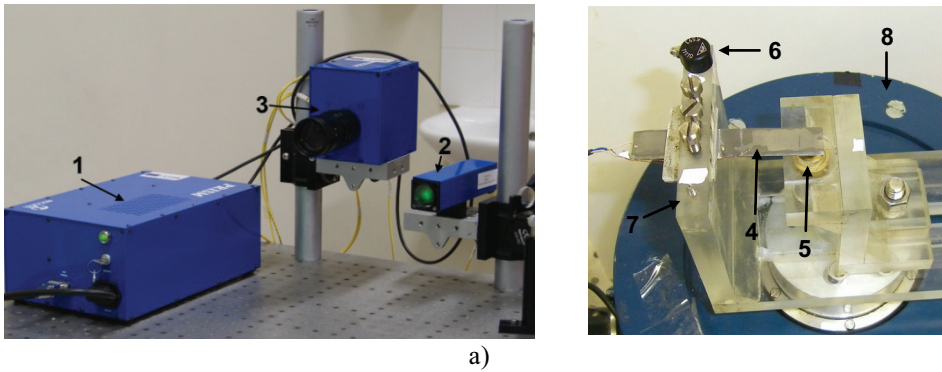
a)
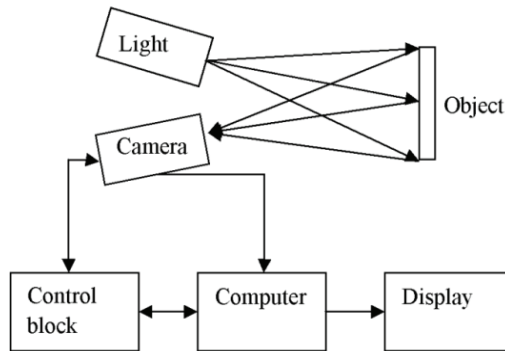
b)

Figure 38. a) Basic parts of holographic measurement stand: 1 - control block, 2 – light source illuminating the object, 3 – camera (1, 2, and 3 as the core of PRISM system); 4 – tested PEH prototype fixed in a custom built clamp, 5 – support, 6 – accelerometer, 7 – custom built clamp, 8 – electromagnetic shaker; b) Operation scheme of the PRISM

The main part of this holographic measurement system is control block, which splits green (532 nm, 20 mV) semiconductor laser beam into two beams – object and reference. Lenses are used to control object beam and light falling on the object. Light, reflected back from the object, is registered by means of camera, which combines object and reference beams, registering the interference pattern (ratio of the object and reference beams may be altered in order to achieve the best definition of interference bands). Interference pattern is transferred to computer, where it is processed with PRISMA-DAQ software, allowing to monitor real time dynamic processes occurring at the research object as well as deformations caused by internal and external forces. Once experiments are performed, tested PEH prototype (fixed in the custom-built clamp made of acrylic glass) is excited by an electromagnetic shaker and single-axis miniature piezoelectric charge-mode accelerometer METRA KS-93 (with sensitivity of k=0.35 mV/(m/s^2)) is attached at the top of the clamp for system acceleration measurements.

Once tested object is excited its shape changes. These shape changes produce fringes on top of the object image; all of which are displayed on the connected computer monitor. For the above system arrangement it is necessary to make an

assumption that time varying displacement occurs along z-axis – i.e., along the line of sight between the tested object and observer.

Table 22. Main characteristics of the PRISM system [79, 80]

Parameter	Characteristics
Measurement sensitivity	< 20 nm
Dynamic measurement boundary	100 μm
Measurement boundary	> 100 μm
Greatest measurement area	1 m diameter
Distance to the object	> ¼ m
Data registration frequency	30 Hz

3.1.2. Laser Doppler vibrometry system

Laser Doppler Vibrometry setup used for a number of further described measurements is schematically depicted in Figure 39. It consists of a tested PEH prototype (with connected electrical load) and three main systems – excitation, vibrometry and data acquisition.
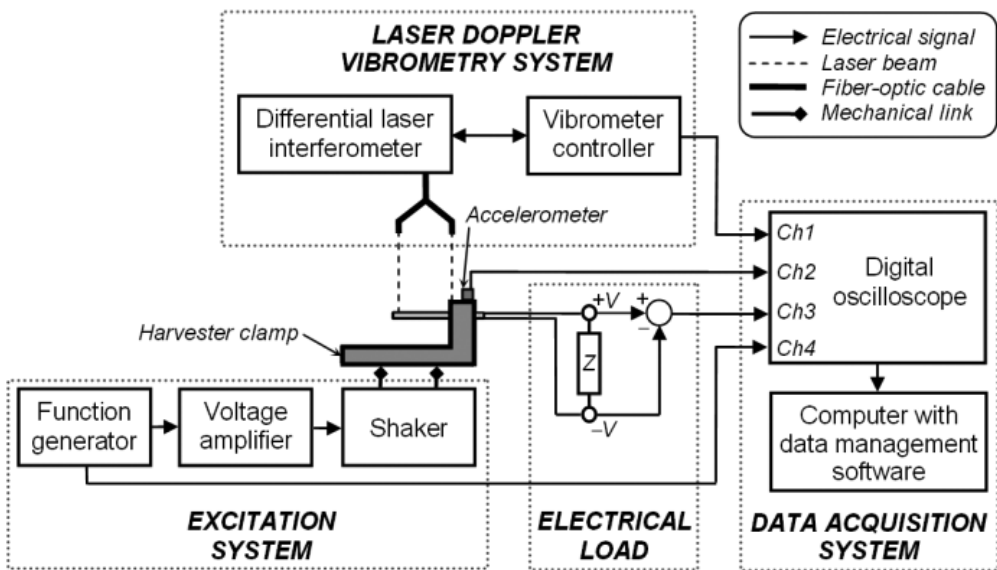
Figure 39. Scheme of experimental setup

The main part of excitation system is electromagnetic shaker, which is employed to excite PEH prototype that is fixed in the custom-built harvester clamp made of acrylic glass. It should be noted that actual overhang length of tested prototype may be different from the original length of this device. Function generator AGILENT 33220A and voltage amplifier KROHN-HITE 7500 are used to control harmonic excitation signal transmitted to electromagnetic shaker. Single-axis miniature piezoelectric charge-mode accelerometer METRA KS-93 (with sensitivity of $k=0.35$ mV/(m/s^2)) is attached at the top of the clamp for acceleration

measurements at the base of harvester prototype. In order to measure tip displacement (or velocity) of PEH prototype in the transverse direction, harvester tip and clamp top have small pieces of retro-reflective tape attached to enhance laser light collection back into the fibre-optic differential laser interferometer POLYTEC OFV-512, which is connected to vibrometer controller POLYTEC OFV-5000, both comprising the core of laser Doppler vibrometry system. The main advantage of this setup is that registration of relative motion between tip of harvester prototype and top of clamp allows measurement of actual tip displacement. Data acquisition system consists of a 4-channel USB oscilloscope (analog-to-digital converter) PICO 3424 that collects signals from function generator, laser vibrometer, base accelerometer and PEH prototype through connected resistive load. Signals from oscilloscope are forwarded to computer with data management software (PicoLog 5[®], Picoscope 6[®]).

3.1.3 Experimental setup used to determine stiffness of PEH prototypes

Experimental setup used to determine stiffness of PEH prototypes is presented in Figure 40. PEH prototype is fixed in the custom built clamp and weights of 20 and, later on, 30 grams are suspended at the free end of PEH prototype, 100 mm from the clamping point. Non-contact laser displacement sensor LK-82G (Keyence, USA) is used to measure deflection of PEH prototype and its stiffness is determined from equation below:

$$c = \frac{F}{y},$$
(3.1.3.1)

where F is force and y is deflection.
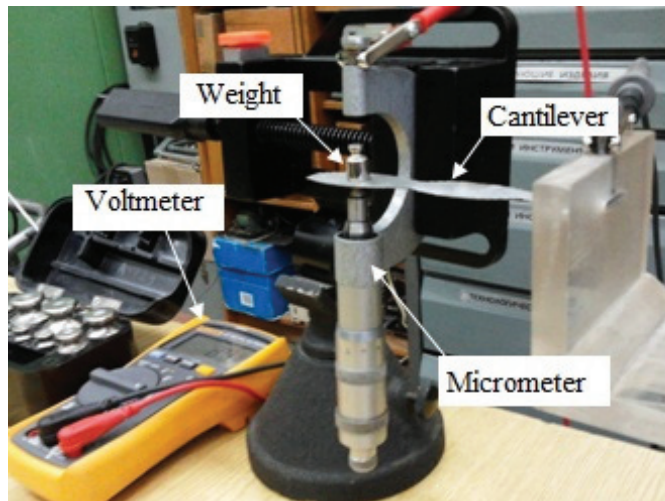
Figure 40. Experimental setup used to determine stiffness of PEH prototypes

3.1.4. Water jet cutting system

Some substrates for PEH prototypes were fabricated by means of water jet cutting system Resato ACM3060-2 (Resato International B.V., Holland) [81], general view and main features of which are presented in

Figure 41 and Table 23. This system was chosen as it allows cutting metal into intricate shapes without exposing workpiece to heat during cutting processes, thus no tension is created in the cutting area.
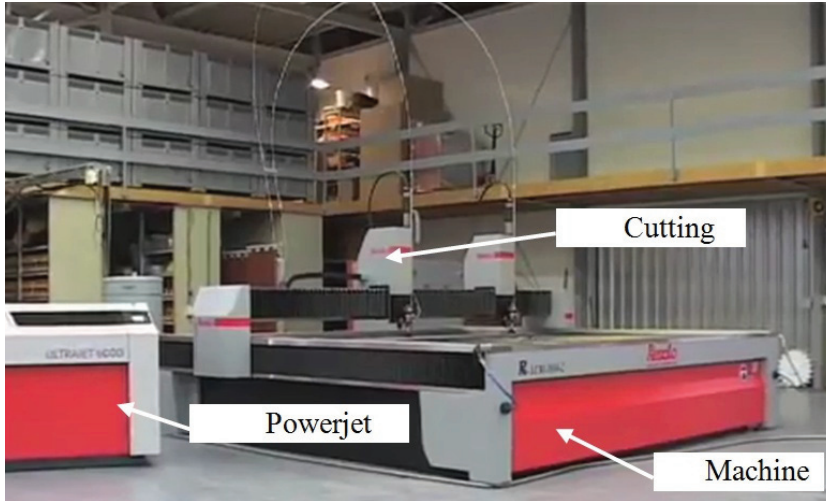
Figure 41. General view of the high pressure water jet cutting system

Table 23. Main technical features of water jet cutting system Resato ACM3060-2 [82]

Parameter	Characteristics
Positioning accuracy	± 50 μm / m (at 20°C)
Repeatability accuracy:	± 50 μm / m (at 20°C)
Cutting bed dimensions:	3020 × 6020 mm
Angle accuracy:	± 0.1°
Maximum angle adjustment:	55°
Cutting head rotating:	from -360° - to +360°

3.2. Evaluation of effects of connected electric circuit to dynamic and electric response of PEH prototype

Section below presents experimental study of dynamic and electric characteristics of commercial cantilever-type bimorph PEH at the presence of electric loads, resistance of which varies from nearly short circuit to nearly open circuit conditions. As it was already discussed in literature review and numerical simulation sections, when PEH is connected to electronic circuit (which should transform harvested energy into electrical energy) it may alter dynamic and electric response of PEH prototype. Moreover, this assumption was already verified via

numerical simulations (presented in 2.3 section) of PEH prototypes. Thus measurements of prototype frequency, tip displacements as well as voltage, current and power were performed by means of laser Doppler vibrometry system, described in 3.1.2 section.

It was important to clarify underlying physical mechanisms that govern coupled dynamic and electrical behaviour of harvester prototype when it delivers power to an electrical load (i.e. operates under real-life conditions). Influence of load resistance was considered for mechanical (resonant frequency, quality factor, displacement), and electrical (voltage, current, power) PEH prototype characteristics. It was demonstrated that resistance of connected electrical load significantly influences power generated by operating harvester as well as its other characteristics, thus it must be taken into account when predicting efficiency of PEHs. The trends in experimentally obtained data were analyzed and reasons behind them discussed. Conducted experimental study allowed characterizing coupled mechanical and electrical performance of standard PEH (with well-defined geometric and material properties) under variable electrical loading conditions. Moreover, performed measurements allowed extraction of damping and electromechanical coupling coefficients that might be used for numerical modelling of energy harvesters.

Laser Doppler Vibrometry experimental stand described in 3.1.2 section was used to evaluate performance of commercial PEH prototype - piezoceramic bimorph bending actuator T226-A4-503Y [83]. Its geometric and material properties are given in Table 24, while prototype itself is schematically depicted in Figure 42.
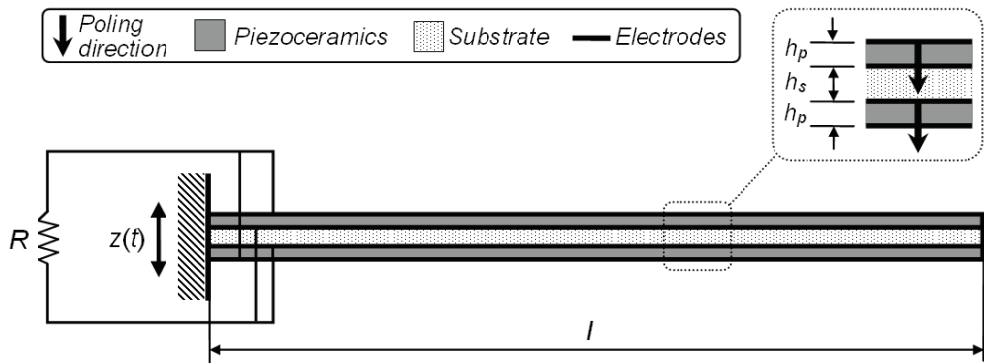
Figure 42. Configuration of the tested piezoelectric energy harvester

Tested commercial PEH prototype (produced by PiezoSystems, Inc.) picture of which is presented in Figure 43, is a brass-reinforced piezoelectric bimorph in quick-mount configuration – i.e., its' elements are wired for low voltage operation and bleed resistor mounted on board protects prototype and surrounding electronics from transient voltages. It may be seen from Figure 42 that piezoelectric layers of prototype are poled in the same direction. This configuration requires that each layer of the structure would be accessed individually, so two wires are connected to the outside nickel electrodes of relatively negligible thickness, while the others are

connected to the centre substrate layer. Once the harvester is under transverse mechanical excitation, one piezoceramic layer of structure is stretched, while the other one is compressed and charge is developed in each layer to oppose the imposed strains.
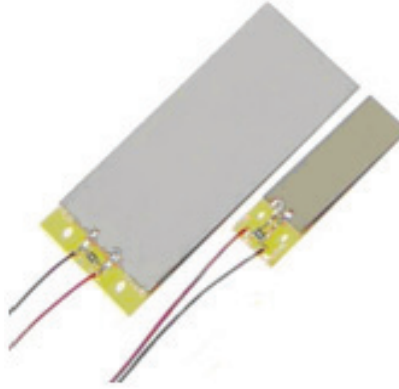
Figure 43. Commercially available PEH prototype T226-A4-503Y [83]

Table 24. Main characteristics of piezoceramic actuator T226-A4-503Y [83]

Dimensions	
Overhang cantilever length, *l*	40×10^{-3} m
Cantilever width, *w*	31.8×10^{-3} m
Thickness of substrate layer, h_s	0.14×10^{-3} m
Thickness of piezoelectric layer, h_p	0.27×10^{-3} m
Piezoelectric properties	
Piezoelectric strain coefficient d_{33}	390×10^{-12} m/V
Piezoelectric strain coefficient d_{31}	-190×10^{-12} m/V
Piezoelectric voltage coefficient g_{33}	24.0×10^{-3} Vm/N
Piezoelectric voltage coefficient g_{31}	-11.6×10^{-3} Vm/N
Coupling coefficient k_{33}	0.72
Coupling coefficient k_{31}	0.35
Mechanical properties	
Density	7800 kg/m^3
Elastic modulus Y^E_3	5.2×10^{10} N/m^2
Elastic modulus Y^E_1	6.6×10^{10} N/m^2

A set of resistors with different resistance magnitudes was used in order to create varying electrical loading conditions during frequency response measurements. Effective load resistance acting on harvester prototype was calculated bearing in mind that input channel of oscilloscope has impedance of 1 MΩ, which acts in parallel with the load resistor placed across piezoelectric layers. The effective load R_{eff} that is actually exerted on PEH prototype is influenced by this input impedance of oscilloscope and is defined as:

$$R_{eff} = \frac{1}{1/R_a + 1/R_{osc}} \qquad\qquad (3.2.1)$$

where R_a – actual resistance of a resistor, R_{osc} – input impedance of the oscilloscope.

Table 25 lists values of actual load resistances and their corresponding effective resistances. It should be noted that the maximum load resistance in this case cannot exceed 1 MΩ. Therefore load resistances used in this experimental study range from 47 Ω (close to short-circuit condition) to 1 MΩ (close to open-circuit conditions).

Frequency response measurements of tip displacement and voltage output of PEH prototype were performed with the function generator providing swept harmonic excitation within a frequency range of 140 - 230 Hz and sweep time of 500 s. It was aimed to maintain the same level of acceleration in the course of frequency response measurements, however acceleration magnitude fluctuated in the vicinity of 1*g* when sweeping.

The first resonant frequency of PEH prototype was analyzed in this experimental study.

Table 25. Conversion of actual resistance of connected resistors into effective resistance taking into account magnitude of input impedance of connected oscilloscope

Actual resistance of connected resistors (Ω)	Effective load resistance acting on the PEH (Ω)
47	47
390	390
1800	1797
3900	3885
4700	4678
6200	6162
15000	14778
56000	53030
100000	90909
510000	337748
3.90×10^6	795918
Open circuit	1.00×10^6

Figure 44 illustrates experimentally measured frequency responses of tip displacement and voltage output for varying electrical loading conditions ranging from nearly short circuit (s.c.) to nearly open circuit (o.c.).

It is observed that increase of load resistance leads to higher voltage output, which correlates with reduction in tip displacement amplitude at short-circuit resonant frequency (Figure 44). Yet at the o.c. resonant frequency tip displacement amplitude increases again and one may note that at o.c. resonant frequency both tip displacement amplitude and voltage output are amplified as external load resistance increases. Resonant frequency curves in Figure 44, a) corresponding to low

resistance values clearly reveal that the harvester exhibits nonlinear frequency responses with curves being shifted to the left-hand side of the frequency axis.
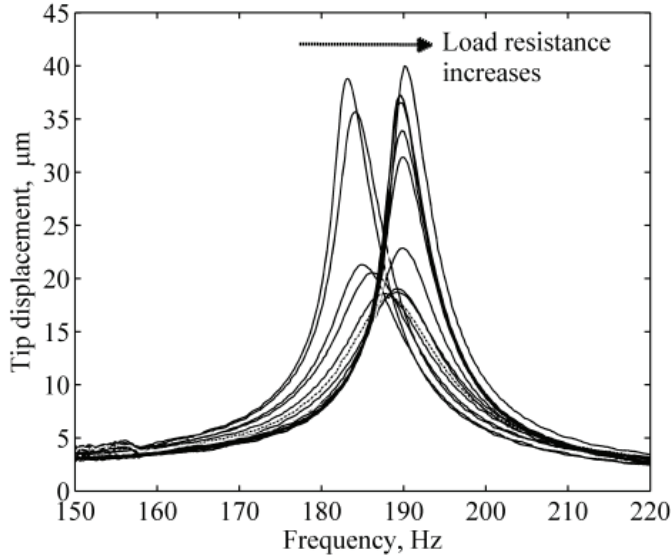
a)
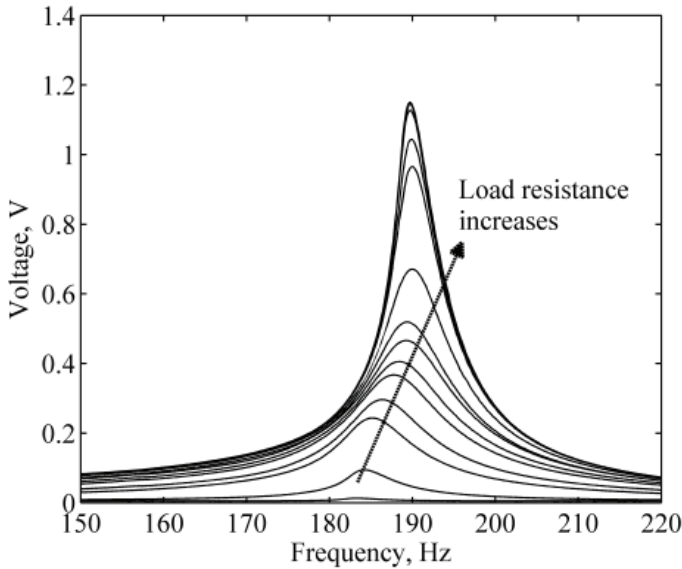
b)

Figure 44. Measured frequency responses of tip displacement (a)) and voltage output (b)) for different resistive loads spanning from nearly short circuit to open circuit

The reasons for the observed softening behaviour are diverse and are associated with complex interaction of various effects including but not limited to

nonlinear damping (due to air drag and material losses), viscoelectroelasticity, nonlinear electromechanical coupling, dielectric effects, and etc. Structural displacements were relatively small in these experiments (Figure 44, a)) therefore it is hardly possible that geometric nonlinearities were induced in this case. These experimental results also demonstrate that the observed nonlinear softening response diminishes with larger resistive loads (corresponding to larger electric fields generated inside piezoceramic layers). This, in turn, suggests that electromechanical coupling, which becomes more prominent with increased electrical loading, counteracts those effects that cause nonlinear softening behaviour at lower load resistances (i.e. at weaker electric fields).

Measured tip displacement and voltage output frequency responses in Figure 44 were subsequently used to derive graphs demonstrating variation of PEH prototype resonant frequency and quality factor (Figure 45), power output and tip displacement (Figure 46) as well as voltage and current (Figure 47) as functions of external load resistance.

One of the main characteristics of operating PEH is magnitude of generated power, which is directly related to dynamic response of piezoelectric transducer. Therefore it is important to examine variation of key mechanical characteristics such as resonant frequency, tip displacement and quality factor during process of power generation.

The resistive load of 47 Ω is very close to the short-circuit conditions for this experimental setup, therefore resonant frequency of 183.2 Hz derived from measured data may be considered as the fundamental short-circuit resonant frequency f^{sc} of tested piezoelectric energy harvester prototype. Fundamental open-circuit resonant f^{oc} is measured with resistive load of 1 MΩ and is equal to 189.9 Hz. The respective 3.7 % shift in resonant frequency is obvious in Figure 45. It should be mentioned that magnitude of the observed frequency shift is directly proportional to the square of the electromechanical coupling coefficient. This shift in resonant frequency is attributed to varying electrical boundary conditions: increase of load resistance from s.c. to o.c. condition leads to a change in harvester stiffness since elastic modulus of piezoelectric material increases.

Figure 45 reveals that quality factor, with the initial value of 33.6 at s.c. conditions reaches its minimum value of 18.4 at the electrical load of ca. 4670 Ω and then gradually increases up to 45.8 at the o.c. conditions. Quality factor is explained as a measure of dissipated mechanical energy of vibrating harvester.

Dissipated mechanical energy may be attributed to intrinsic characteristics of constituent materials and harvester design, thus it is difficult to separate individual damping factors. However, efforts are directed to distinguish between electrical damping and mechanical damping. Electrical damping is associated with conversion of strain induced energy into electricity. Amount of electrical damping is determined as power consumed in a resistive load, i.e. electrically induced damping is considered as power consumed in electrical domain, which is equal to power removed from mechanical system. Mechanical damping may be attributed to air and structural damping as well as material losses and thermoelastic effects.
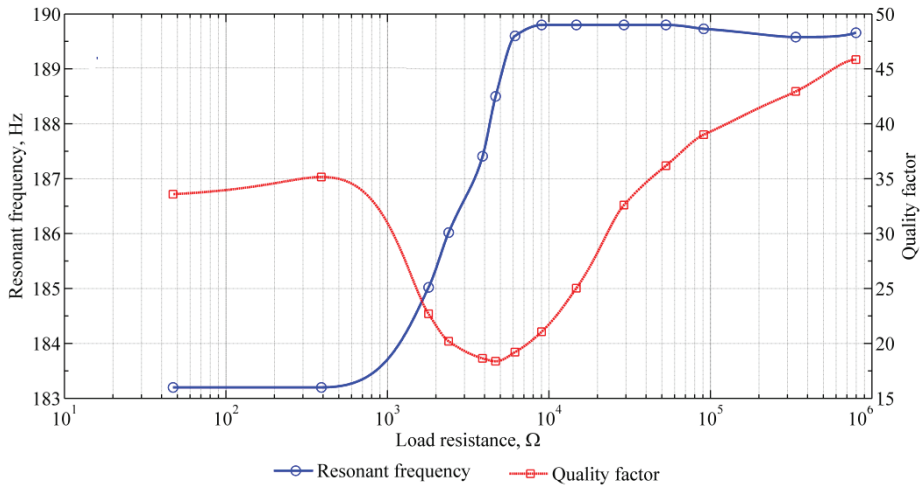
Figure 45. Resonant frequency and quality factor of the harvester as a function of load resistance
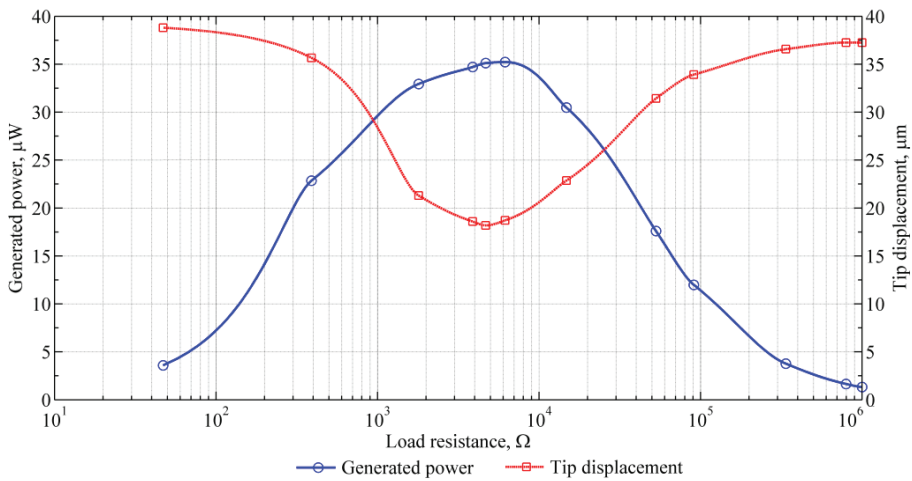
Figure 46. Variation of power output and tip displacement of the harvester as a function of load resistance

Figure 46 reveals that prototype vibration amplitude at s.c. resonant frequency is attenuated from value of 38.8 μm as load resistance is increased. It reaches its minimum point (18.2 μm) at the resistance of ca. 4670 Ω and then gradually increases again up to 37.2 μm at o.c. conditions. Attenuated structural response may be explained by electrically damped motion as in the case of quality factor reduction. A vibrating harvester prototype at s.c. conditions is under mechanical damping only since there is no electrical power consumed. As resistance is increased, mechanical energy is partially transferred to electrical energy. Harvested electrical energy is considered as electrical damping that sums up with mechanical damping, which finally leads to suppression of prototype displacement. It may be

concluded that electrical effect, called backward coupling, manifests in the harvester, i.e. the feedback is sent from the electrical domain to the mechanical one due to power generation, caused by converse piezoelectric effect. This phenomenon is explained by the theory of piezoelectrics, which are comprised of perovskite crystals with intrinsic dipole moment. Once these materials are strained, direction of polarization among neighbouring dipoles becomes unified, producing electric charge on the surface (direct piezoelectric effect). However, when feedback is sent from the electrical domain and electrical energy is applied to the poled piezoelectric material, it distorts orientation of dipole domains, and overall polarization becomes more random, resulting in mechanical strain (converse piezoelectric effect). Thus, it may be stated that the form of piezoelectric coupling is substantially different from conventional damping mechanisms.

Electrical outputs of harvester prototype are also analyzed in order to examine variations of generated electrical current, voltage and power, which subsequently must be considered in optimization process aiming for maximum power output when the harvester prototype is connected to complicated energy harvesting circuits.

Figure 46 provides a graph of harvested power as a function of load resistances. It is observed that the maximum power output of 36 µW is delivered at electrical load of ca. 6160 Ω, which may be considered as an optimal resistance for this PEH prototype. The resistive load of 47 Ω yields power output of 4 µW at s.c. conditions, whereas the resistive load of 1 MΩ yields 1 µW at the s.c. condition.

Results presented in Figure 46 reveal that electrical load resistance delivering the maximum power output (6160 Ω) does not coincide with the load resistance of minimum vibration amplitude (4670 Ω). This phenomenon is attributed to the nature of electromechanical coupling: vibration amplitude of the PEH prototype will not necessarily acquire its lowest value for the magnitude of electrical load corresponding to the maximum power generation. Thus, it is important to note here that harvested power is not considered to be directly influenced by displacement amplitude of PEH prototype, but is also affected by voltage and external load resistance.

Variations of electric current and voltage generated by PEH prototype for various resistive loads are plotted in Figure 47. Voltage amplitude increases monotonically with increasing load resistance from 0 V to 1.15 V, while current decreases monotonically from 275 µA to 0 µA. Electric current and voltage amplitude curves intersect close to load resistance of ca. 4650 Ω. It should also be noted that the asymptotic character of voltage and current output variation is observed when both curves approach extreme conditions of load resistance.

Measured frequency responses may be used to extract various damping parameters that might be subsequently employed for the development of FE model of PEH. Mechanical damping ratio ζ and Rayleigh damping parameter β are derived from the measured resonant frequency curves.
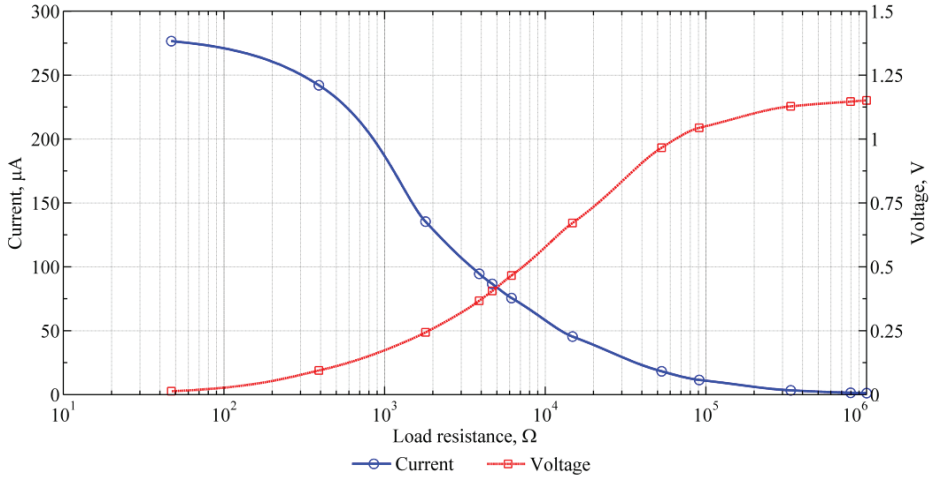
Figure 47. Voltage and current output of the harvester as a function of load resistance

Firstly, quality factor Q is calculated as:

$$Q = f_r / \Delta f,\tag{3.2.2}$$

where $\Delta f = f_2 - f_1$ is bandwidth, which represents distance between two points on frequency axis where the amplitude is equal to $1/\sqrt{2}$ of the maximum amplitude value.

Quality factor Q is used to derive damping ratio ζ:

$$\zeta = 1/2Q.\tag{3.2.3}$$

Finally, Rayleigh damping parameter β is calculated as:

$$\beta = \frac{1}{2\pi f_r Q}.\tag{3.2.4}$$

Following [84], coupling coefficient k of the system may be determined from the resonant frequencies under open-circuit and short-circuit conditions:

$$k^2 = \frac{(f^{oc})^2 - (f^{sc})^2}{(f^{oc})^2}.\tag{3.2.5}$$

Coupling coefficient k for this harvester prototype was determined to be 0.26. Material data listed in Table 24 indicates that coupling coefficient k_{33} of piezoelectric material PZT-5A is equal to 0.72, while the one measured for the tested harvester prototype is much lower. This reduction is explained by incorporation of substrate material in PEH configuration as it influences electromechanical coupling of the complete structure. Moreover, backward coupling discussed in the sections before is also thought to be mainly influenced by thickness and stiffness of PEH substrate material.

84

To conclude with, this section described experimental setup and measurement results characterizing coupled dynamic and electric performance of cantilever-type PEH prototype when it is connected to varying resistances, thereby providing electrical loading conditions that range from nearly short circuit to nearly open circuit. The examined parameters include prototype resonant frequency, tip displacement, quality factor, generated current, voltage and power. It was established that measured characteristics are significantly dependant on the magnitude of external load resistance. Major observations of this experimental study may be summarized as follows:

- Measured tip displacement frequency responses reveal nonlinear softening behaviour of harvester prototype for lower load resistances. The magnitude of the nonlinear response attenuates for larger resistive loads;

- Measured voltage frequency responses indicate monotonic growth trends with increasing load resistance, ultimately converging to a single o.c. voltage. The resulting frequency shift is equal to 3.7 % when passing from short to open circuit conditions;

- Non-monotonic variation trend of the PEH prototype structural response manifests with increasing load resistance: passing from s.c conditions it drops by 53.1 % at load resistance of 4670 Ω and increases again almost to the initial value at o.c. condition. These results are consistent with measurements of damping: magnitude of load resistance of minimum tip displacement is equal to the resistance that corresponds to the lowest quality factor (4670 Ω);

- Maximum harvested power is equal to 36 μW and is observed at 6160 Ω, which is considered to be the optimal load resistance for this PEH prototype. Power generated at this resistive load is 9 times higher with respect to power harvested at s.c. conditions;

- Mechanical coupling coefficient of harvester prototype calculated from measurement results is 2.8 times smaller than the one of the piezoelectric material of the commercial PEH prototype. This reduction is associated with introduction of substrate material to PEH structure and manifestation of effects of backward coupling.

These experimental results may be subsequently used for verification and improvement of developed FE model in order to enable accurate prediction of dynamic and electrical characteristics for different structural configurations of PEHs.

3.3. Investigation of effects of piezoelectric layer segmentation and incorporated support location to electric outputs of PEH prototype

As it was already mentioned in the literature review section, most of currently explored harvesters do not perform efficiently in real environments, since it is assumed that they are excited only by harmonic signal at their fundamental frequency. However, if one analyses real environment energy sources, they usually would not consist of single harmonic and higher modes of vibration may be excited. Moreover, these higher modes of vibration will be excited if rigid support is incorporated in PEH configuration and whole system starts operating in vibro-

impacting mode. These higher vibration modes of PEH prototype will have strain nodes – i.e., positions on the structure, where bending strain distribution changes sign. It was already demonstrated via numerical simulations that if these strain nodes are covered with continuous piezoelectric layers and PEH is excited by random excitation signal or higher fundamental frequencies, cancellation of PEE electric outputs occur, resulting in reduction of harvested energy.

Thus, this research is devoted to verify numerical simulation results described in 2.4 section and to ascertain that PEH prototype with piezoelectric layers segmented at the strain node of the second vibration mode would practically demonstrate higher electric outputs as compared to its counterpart with continuous piezoelectric layer. Moreover, the effects of rigid support location (on which PEH prototype is impacting) to the electrical outputs of prototype were analyzed in this study.
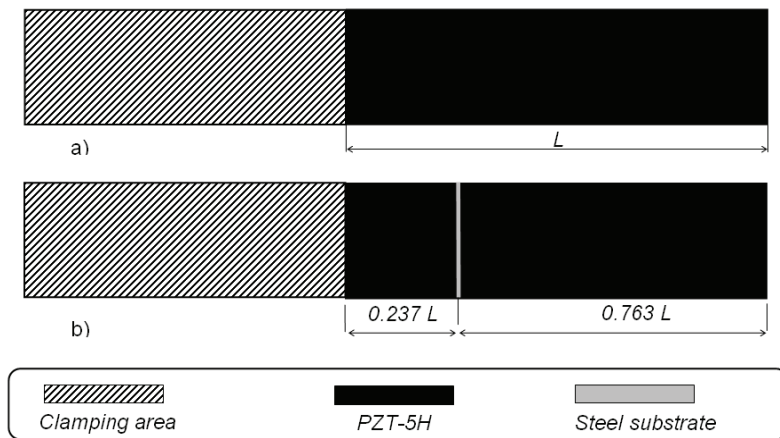
Figure 48. Schemes of fabricated PEH prototypes: a) non-segmented (i.e., with continuous piezoelectric layer); b) segmented at the strain node of the second vibration mode

For the purpose of this research two prototypes of PEH were fabricated. PZT-5H piezoceramic sheets (PiezoSystems, Inc.) [85], covered with nickel electrodes from both sides were cut to the dimensions of 36 x 10 x 0.2 mm by means of automatic dicing machine and were bonded with epoxy to stainless steel substrates with dimensions of 36 x 11 x 0.4 mm. Wire leads were soldered to PEH prototype electrodes to collect electrical output. The first PEH prototype (Figure 48, a) was designed to have continuous piezoelectric layer, meanwhile for the second PEH prototype (Figure 48, b) piezoelectric layer was segmented into two sections (which were confined by mechanically etching nickel electrodes) at the strain node of the second vibration mode.

All further described measurements were performed employing Laser Doppler vibrometry system described in 3.1.2 section.

Dynamic response of the vibro-impacting PEH was experimentally studied using PEH prototype with segmented piezoelectric layers (Figure 48, b). Firstly, frequency response function of voltage (Figure 49) was measured (at the arbitrarily

selected load resistance of 5000 Ω) in order to determine resonant frequencies of PEH prototype (ω_1 = 235 Hz, ω_2 = 1469 Hz) as well as to analyze resonant frequency bandwidth of operating PEH prototype. Its dependency on the stopgap size was explored: Figure 50 was constructed from a number of frequency response functions, outlaying frequency bandwidth, at which each piezoelectric segment of vibro-impacting PEH prototype generates voltage larger than 0.1 V. For this configuration optimal stopgap size is 30 μm since electrical voltage of more than 0.1 V may be extracted in 50 Hz frequency range. Once stopgap size is increased up to 110 μm (i.e., until no impact occurs), operating bandwidth decreases by 60 %, while maximum voltage increases by 68 %.

Measurements of maximum voltage that each PEH segment generates (Figure 51) verify the trade-off between increased PEH bandwidth and reduced voltage output – increasing stopgap size leads to higher PEH generated voltages at each segment since displacements of prototype are limited less. On the other hand, this trade-off could be less pronounced if support is located at the nodal point of the second vibration mode and higher vibration modes of harvester are excited during the impact.
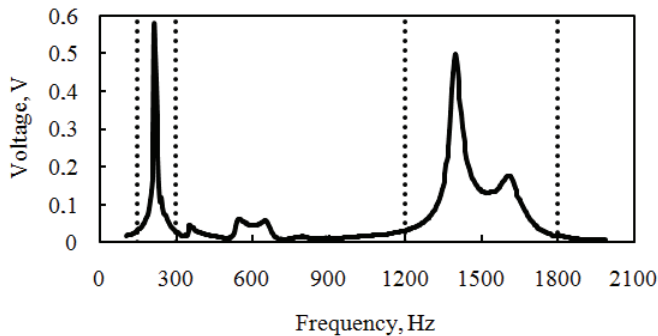
Figure 49. Frequency response function of voltage (ω_1 = 235 Hz, ω_2 = 1469 Hz)
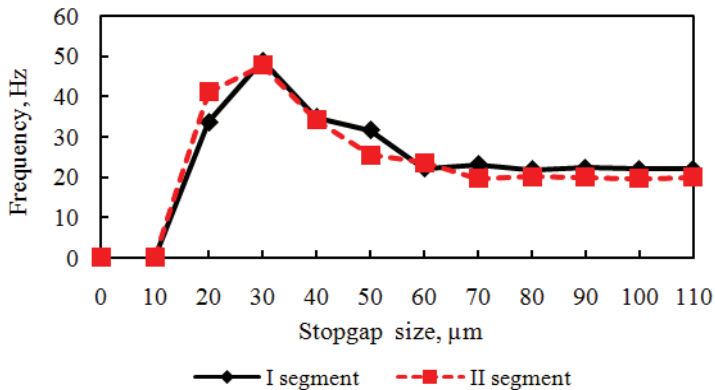
Figure 50. Bandwidth over which each vibro-impacting PEH prototype segment generates voltages larger than 0.1 V
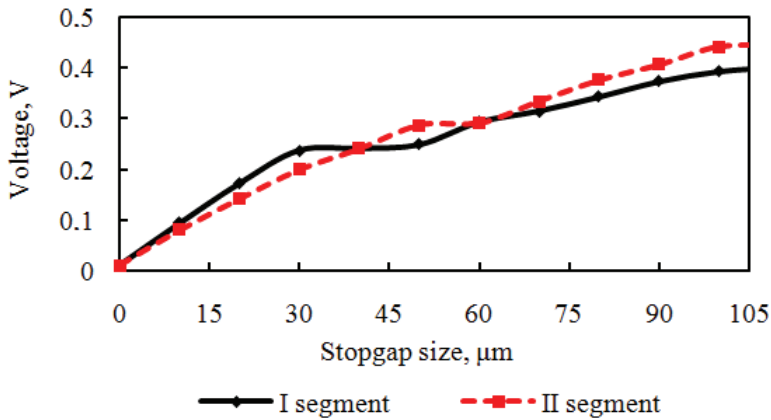
Figure 51. Maximum voltage output of each segment of PEH prototype as a function of stopgap size
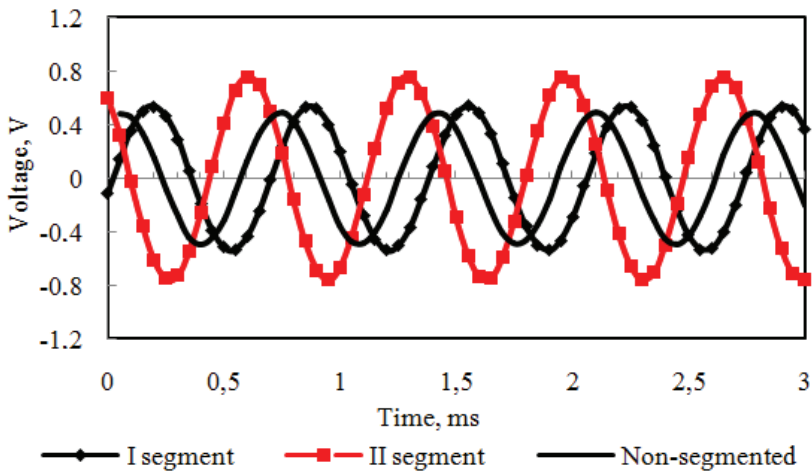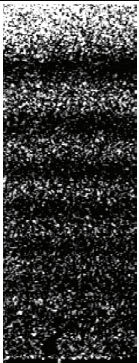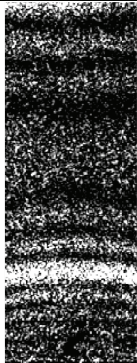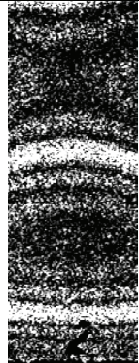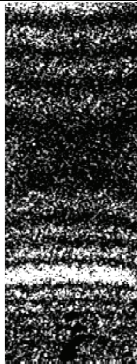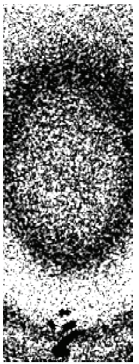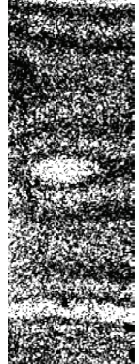
Figure 52. Comparison of the electrical outputs of segmented and non-segmented PEH prototypes

Finally, maximum voltage generated by segmented and non-segmented PEH prototypes were compared. Separate piezoelectric segments of segmented PEH prototype generate 0.54 V and 0.76 V respectively, while PEH prototype with continuous piezoelectric layer generates maximum voltage of 0.5 V (Figure 52). Implementing power conditioning circuit which could sum up voltages generated by each piezoelectric segment would result in up to 52% increase in voltage output as compared to PEH prototype with continuous piezoelectric layer.

Dynamic response of PEH prototype impacting on rigid support was as well evaluated by means of holographic measurement system PRISM (described in 3.1.1 section).

Table 26. Holograms of PEH

Support position	Excitation frequency		
	235 Hz	1469 Hz	4138 Hz
Not impacting			
Support located at 0.78*L*			
Support located at 0.87*L*			

Obtained holograms of PEH prototype are presented in Table 26: first row – PEH prototype is not impacting on incorporated support; second row – PEH prototype is impacting on rigid support incorporated 29 mm from the clamp (i.e., nodal point of vibration mode at 1469 Hz) and the third row – PEH prototype is impacting on the rigid support incorporated 32 mm from the clamp (i.e., nodal point of vibration mode at 4138 Hz). Holograms show, that support, placed 29 mm from clamping point (or 0.78 *L*, where *L* is length of energy harvester), has no influence for harvester vibrations at 1469 Hz resonant frequency, while support, placed 32 mm

from clamping point (or 0.87L, where L is length of energy harvester), has no influence for harvester vibrations at 4138 Hz resonant frequency. It could be noted that rigid support would limit vibration amplitudes at low frequencies (number of black fringes in the hologram decreases), however it could be used to protect PEH prototypes from rupture at excessive loads and ensure stability of PEH operation processes at higher frequencies.

To summarize, this section presented experimental analysis of vibro-impacting PEH prototype, which is intended both to prevent PEH prototype from excessive displacements as well as to increase its bandwidth and efficiency in actual excitation conditions. This is achieved by means of support incorporated in PEH configuration and segmentation of piezoelectric layers of PEH prototype. Conducted experimental study demonstrates that electrical outputs of vibro-impacting PEH prototype are dependent on incorporated support location. In order to achieve the most favourable trade-off between power output and bandwidth:

- support location should coincide with the nodal point of the second transverse mode or the second nodal point of the third transverse mode in order to intensify amplitudes of these vibration modes during impact and beneficially exploit them for energy harvesting;
- piezoelectric layer of PEH prototype should be segmented in such a way that it does not cover strain nodes of vibrating PEH prototype, thereby avoiding detrimental charge cancellation effects in piezoelectric material and, in turn, reduction in PEH generated voltages.

3.4. Dynamic research of optimized cantilever beams intended for energy harvesting applications

Literature review suggests that explicit studies of PEH substrate dynamics are being overlooked. Most of analyzed PEH configurations are based on cantilever beam substrate with a concentrated mass attached at its tip to lower the first resonant frequency of device. This configuration simplifies distributed parameter system to a single degree of freedom system with higher vibration modes being terminated. Meanwhile, this section introduces experimental research of optimal cantilever beam structures presented in 2.5 section. The main advantage of optimal cantilever substrates relies on the fact that resonant frequencies of structures are determined by cantilever shape rather than addition of concentrated masses. This allows minimizing the size of overall system and investigating structures as distributed parameter systems and, moreover, beneficially exploiting their higher vibration modes.

For the purpose of dynamic testing, cantilevers of three different configurations were fabricated: the first configuration (OPT 0) possesses constant cross-section; the second (OPT II) and third (OPT III) – optimal cross sections for the operation at the second and third natural frequencies of transverse vibrations, respectively. As described earlier, optimal cantilever configurations were obtained through optimization with the objective function of cantilever mass minimization in the presence of constraining equation system. The state of the cantilever was described by modal analysis equation with bounds (side constraints) imposing that

the second and the third natural frequencies of transverse vibrations of the optimal cantilevers must coincide with the corresponding frequencies of the initial cantilever with constant cross-section. Shapes of the optimal cantilevers are depicted in Figure 53. These cantilevers were fabricated from a thin steel sheet by means of water jet cutting machine RESATO ACM 3060-2 (described in 3.1.4 section). This machining method was chosen since it allows accurate cutting of intricate shapes without exposing work-piece to heat, thereby avoiding thermally induced stresses in the cutting area. Experimental setup and methods for cantilever stiffness determination is presented in 3.1.3 section.
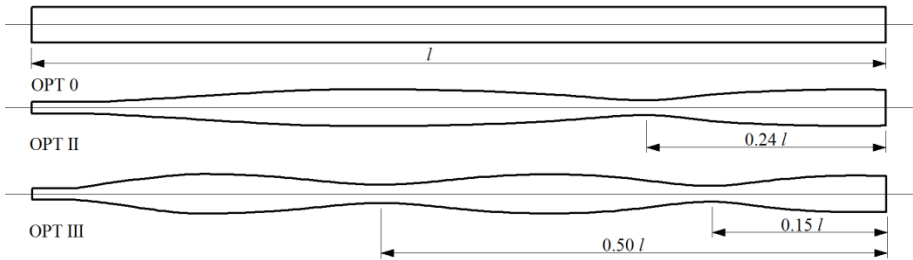
Figure 53. Magnified drawings (side view) of fabricated cantilevers

Average measured stiffness values for different configuration cantilevers are presented in Table 27 and graphically depicted in Figure 54. One may note that as cantilever configuration complexity increases, its average stiffness decreases (almost 2.7 times, if comparing OPT III and OPT 0 configurations).
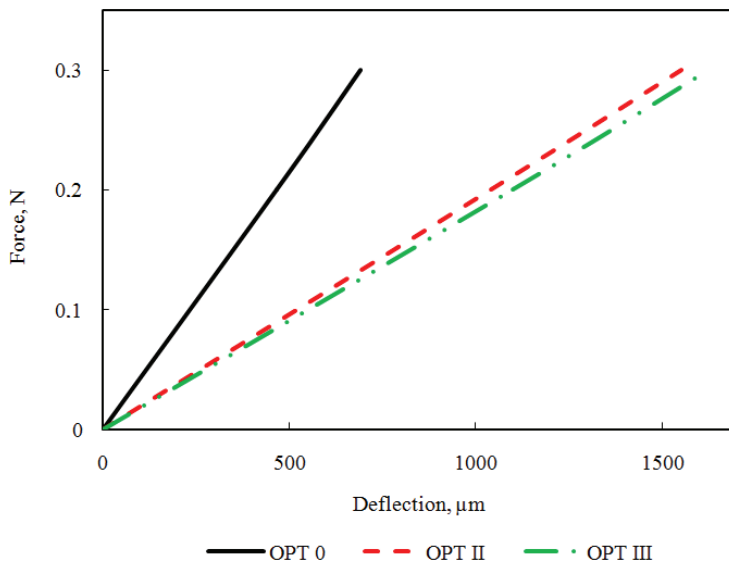
Figure 54. Stiffness graphs for different configuration cantilevers

Frequency response analysis was performed with Laser Doppler vibrometry system described in 3.1.2 section. Excitation frequency was swept in the range from 10 Hz to 1500 Hz and amplitudes of transverse vibrations were registered enabling determination of the first three natural frequencies of cantilevers. Measurements were performed for the unsupported cantilevers (non-impacting) as well as for cantilevers impacting against the support located at points approximately coinciding with the nodes of the second (0.8L) and third (0.9L) modes of transverse vibrations of the cantilever with constant cross section.

Table 27. Average measured stiffness values for different configuration cantilevers

Cantilever configuration	F, N	y, µm	c, N/m	$c_{avergae}$, N/m
OPT 0	0.2	467	428.3	430.9
	0.3	692	433.5	
OPT II	0.2	1040	192.3	192.9
	0.3	1550	193.5	
OPT III	0.2	1099	182.0	183.4
	0.3	1623	184.8	

For the unsupported cantilever configuration OPT 0 the first transverse vibration mode is registered at 75 Hz, the second – 470 Hz, while the third one was not registered in this case (Figure 55). It is obvious that the resonance peak of the first mode of the unsupported cantilever is significantly greater (up to 10 times) when compared to the corresponding peaks of the impacting cantilevers. As the rigid support is positioned at 0.8L, the second transverse mode is recorded at 469 Hz. It should be noted that once the support is placed at the node of the second mode, the amplitude of the corresponding vibration is magnified up to 10 times with respect to the case of unsupported cantilever. When the rigid support is shifted to the 0.9L, the first resonance is observed at 46 Hz, while the second one – 410 Hz (with both vibration amplitudes being smaller as compared to the case of 0.8L). For the latter two cases of impacting cantilever, one may note amplitude peaks at 135 Hz, which pertains to the fundamental mode of the cantilever clamp and is not considered here.
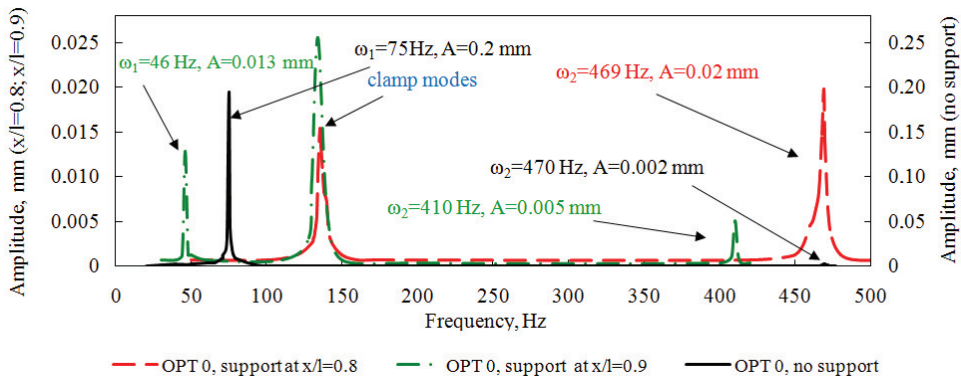
Figure 55. Amplitude-frequency characteristics for the cantilever configuration OPT 0

Frequency responses measured for the cantilever configuration OPT II (Figure 56)) reveal that the first natural frequency of the unsupported cantilever is excited at 64 Hz and the second one – 490 Hz. In the case of cantilever impacting the support placed at 0.8*L*, the second natural frequency is recorded at 492 Hz. For the case of support located at 0.9*L* the first mode is not registered in the considered frequency range, while the second mode shifts down to 430 Hz. For the configuration with support located at 0.8*L* the higher transverse vibration modes were registered as well, indicating that the free end of the cantilever vibrates more easily. As expected, the unsupported cantilever is characterized by the highest amplitudes of the first mode, meanwhile amplitudes of the second mode increase nearly 10 times (compared to the unsupported cantilever case) once the support position is juxtaposed with the node of the second transverse vibration mode.
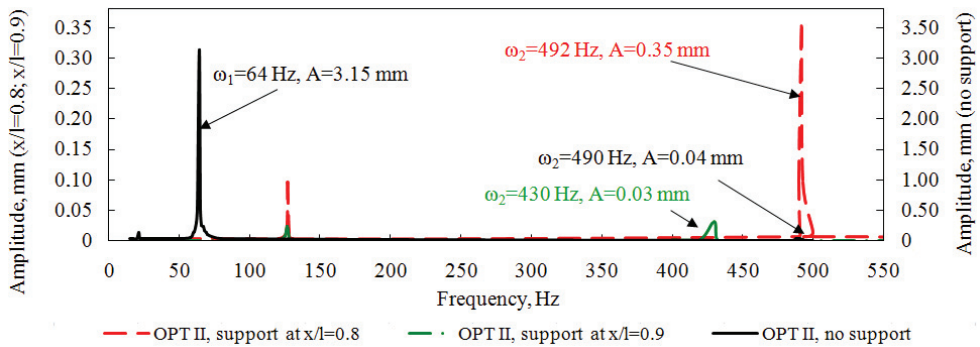
Figure 56. Amplitude – frequency characteristics for the cantilever configuration OPT II
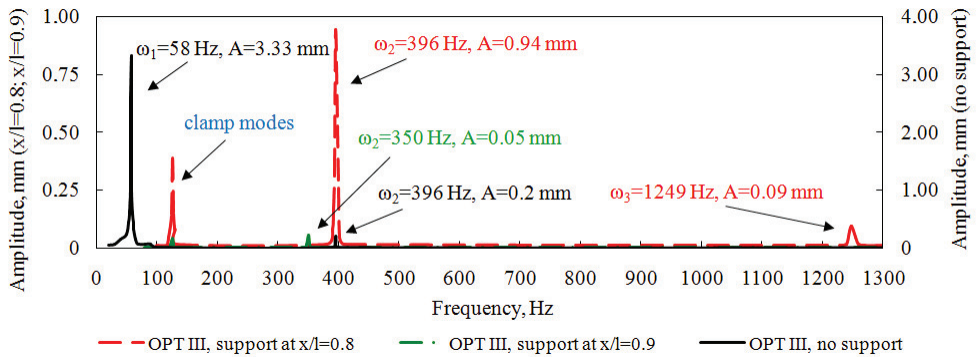
Figure 57. Amplitude – frequency characteristics for the cantilever configuration OPT III

Finally, Figure 57 provides frequency responses for the optimal cantilever configuration OPT III: for the unsupported cantilever the first natural frequency is registered at 58 Hz, the second and the third one – 396 Hz and 1336 Hz, respectively. As previously, the amplitude of the first mode is the highest for the unsupported cantilever. When the support is introduced at 0.8*L* the second mode is

observed at 395 Hz and the third one at 1249 Hz (the amplitude of the second mode reaches the highest value for this particular case as already noted for OPT 0 and OPT II cases). As the support is moved to 0.9L the second mode is reduced to 350 Hz, while the third one is observed at 1325 Hz with vibration amplitudes being considerably smaller when compared to the other cases.

a)

b)
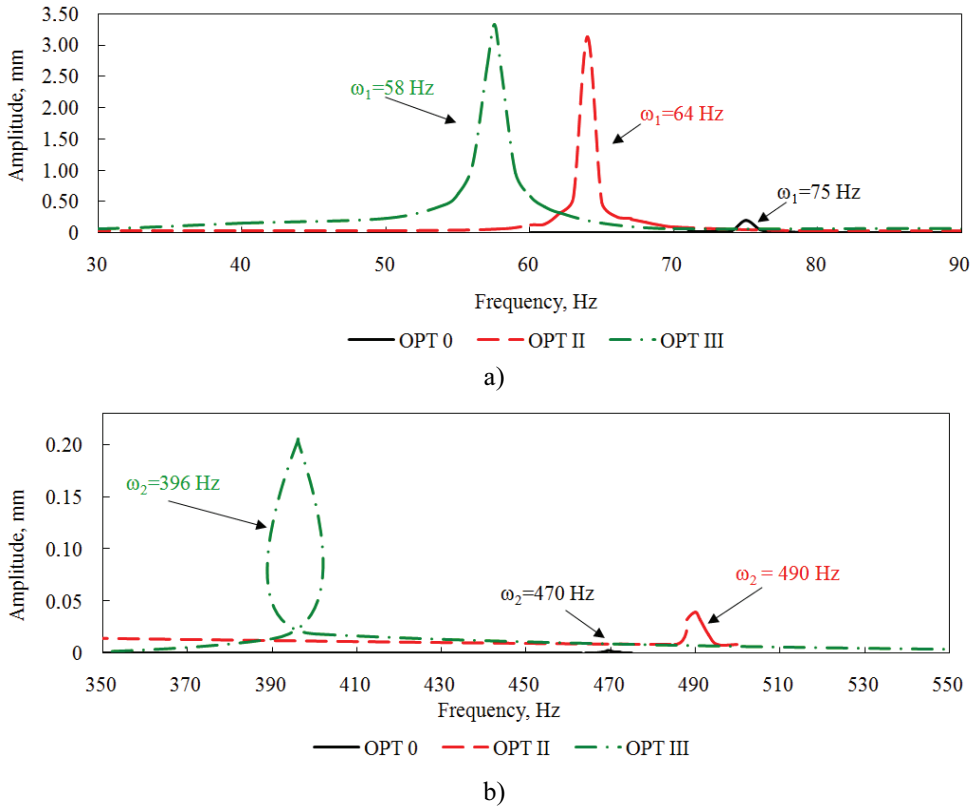
Figure 58. Shift of the first (a) and the second (b) natural frequency for different cantilever configurations

Figure 58 illustrates the shift of natural frequency for different unsupported cantilever configurations. The plots indicate that cantilever configuration OPT 0 is the stiffest one as it exhibits the highest first natural frequency (75 Hz) accompanied by the lowest amplitude peak. Optimal cantilever OPT III is characterized by the lowest first natural frequency of 58 Hz, which constitutes 23% reduction with respect to OPT 0, while the amplitude peak is higher more than 6 times. Cantilever OPT II is somewhat in the middle between the other configurations in terms of first natural frequency and modal amplitude. Analysis of the shift of the second natural frequency reveals that OPT II configuration possesses similar second natural frequency (490 Hz) as compared to its constant cross-section counterpart OPT 0 (470 Hz). The same trend is observed for the third natural frequency of cantilever OPT III (1368 Hz), which is very close to the corresponding natural frequency of OPT 0 (1335 Hz). These small discrepancies between the frequency values confirm

94

that the chosen cutting method with water jet was sufficiently accurate in realizing optimal cantilever structures with the second and third natural frequencies as close as possible to the corresponding frequencies of the cantilever with constant cross section.

Figure 59 combines frequency responses of different cantilever configurations for the case when the rigid support is located at 0.8L (node of the second transverse vibration mode). The plots reveal that cantilever OPT 0 exhibits the lowest amplitudes of the second mode, while OPT III is characterized by the highest vibration amplitudes for second and third vibration modes with the lowest second natural frequency and highest third natural frequency. Cantilever OPT II acquires frequency and amplitude values in-between other configurations.
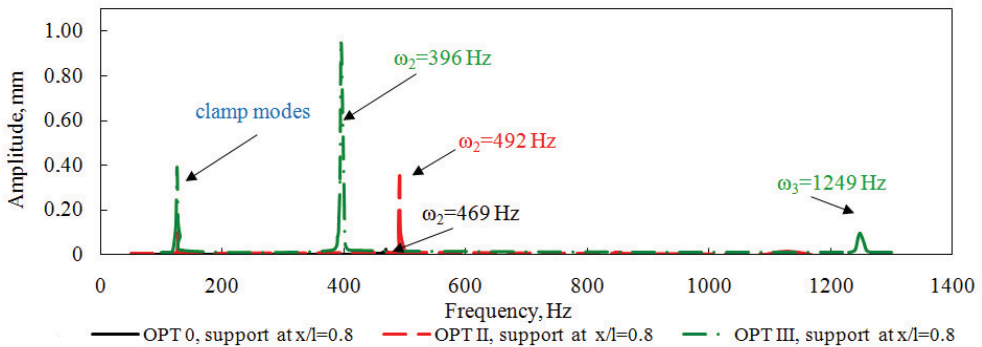
Figure 59. Amplitude – Frequency response characteristics for different configuration cantilevers with the support located at 0.8L

Similarly, Figure 60 provides frequency responses of different cantilever configurations for the case when support is located at 0.8L (second node of the third transverse vibration mode). Analogously to the preceding case, cantilever OPT III exhibits the highest vibration amplitudes of the second and third vibration modes, demonstrating the lowest second natural frequency and the highest third natural frequency.
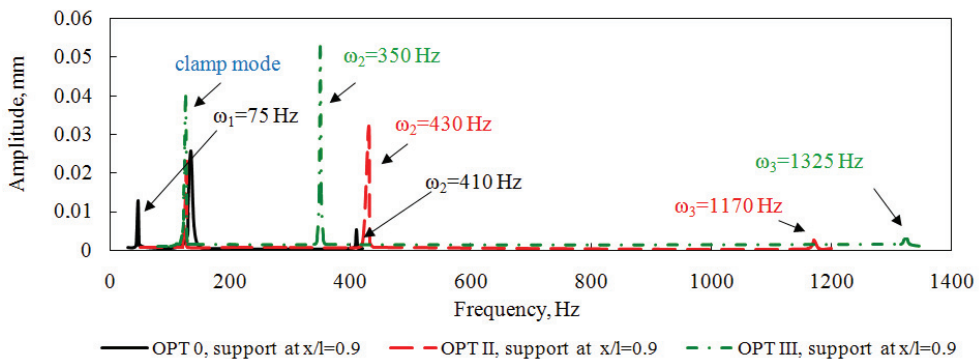
Figure 60. Amplitude – Frequency response characteristics for different configuration cantilevers with the support located at 0.9L

Further on, cantilever beams were analyzed employing holographic measurement system PRISM described in 3.1.1 section. Acoustic field was employed to excite the cantilevers by varying the harmonic driving signal from 10 Hz to 2000 Hz. Vibration mode shapes of the cantilevers with the corresponding displacement amplitudes and natural frequencies were determined via digital analysis of the registered interference patterns.

Figure 61 provides visualization of the measured vibration mode shapes of cantilever OPT 0 including schematic representation of tested configurations, both the unsupported and the impacting one with the support placed approximately at $0.8L$. Results for the unsupported cantilever indicate that the first transverse vibration mode is excited at 77 Hz, the second and third modes – 480 Hz and 1335 Hz, respectively. Both transverse and torsional displacements are observed for the third vibration mode. In the presence of rigid support the second transverse mode is detected at 465 Hz, while the third mode – 1186 Hz. Further increase of excitation frequency leads to a vibration mode at 1402 Hz, where both transverse and torsional components are visible.
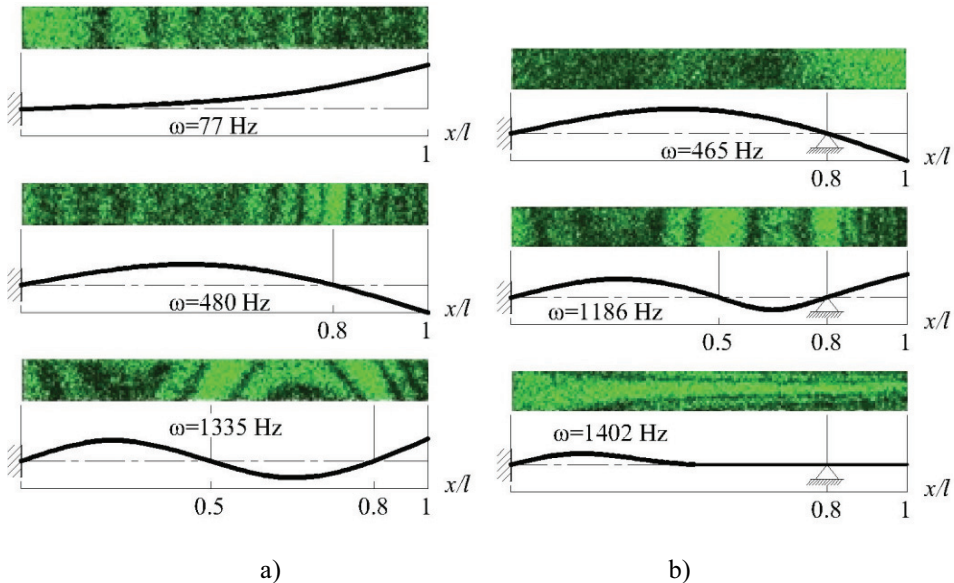
Figure 61. Measured natural vibration modes and frequencies for cantilever OPT 0: (a) unsupported, (b) rigid support located at $0.8L$ (mode number increases from top to bottom)

Similarly, Figure 62 visualizes vibration modes shapes for the optimal cantilever OPT II characterized both in the unsupported and impacting configurations. For the former, the first transverse mode is excited at 63 Hz, the second and third modes – 490 Hz and 1158 Hz, respectively. For the latter case, the second transverse mode is detected at 479 Hz, while the third mode – 1133 Hz. Further increase of excitation frequency induces flexural-torsional mode at 1660 Hz.
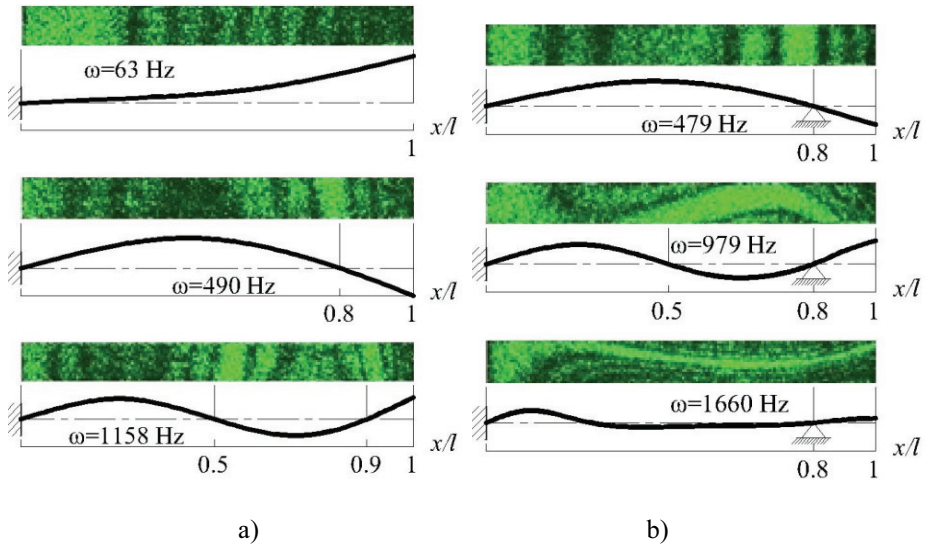
Figure 62. Measured natural vibration modes and frequencies for cantilever OPT II: (a) unsupported, (b) rigid support located at $\approx 0.8L$
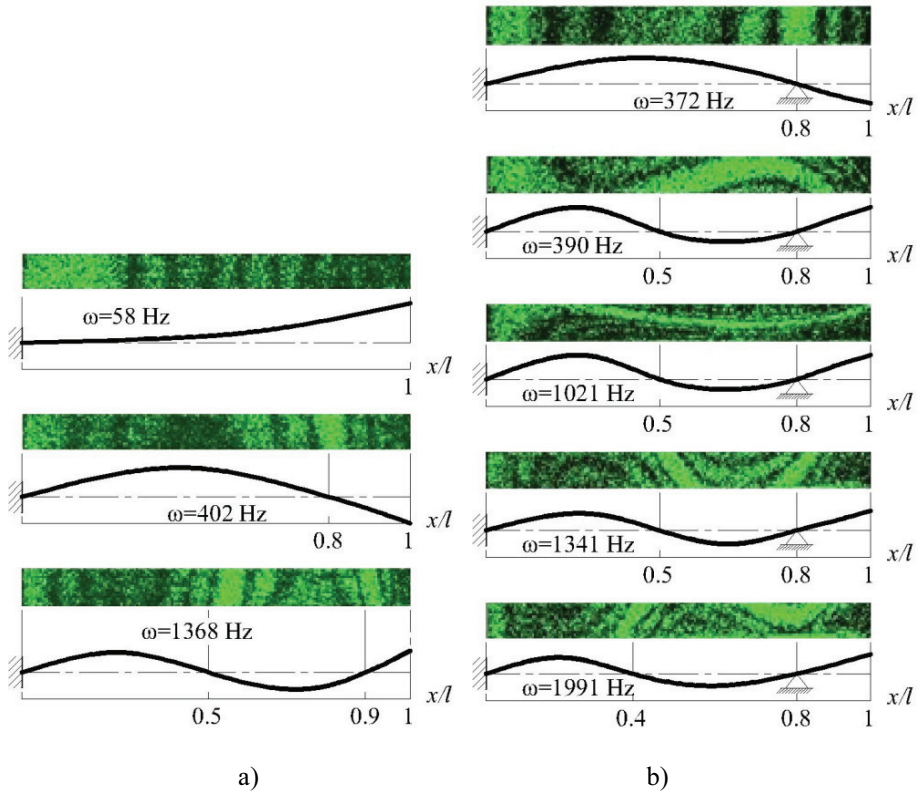
Figure 63. Measured natural vibration modes and frequencies for cantilever OPT III: (a) unsupported, (b) rigid support located at $\approx 0.8L$

Finally, Figure 63 presents measured vibration mode shapes for the optimal cantilever OPT III. For the unsupported case, the first transverse mode is excited at 58 Hz, the second and third modes − 402 Hz and 1386 Hz, respectively. In the presence of support at 0.8L the second vibration mode is observed at 372 Hz. Further increase of excitation frequency yields a number of higher vibration modes at 390 Hz, 1021 Hz, 1341 Hz and 1992 Hz, which are characterized by both transverse and torsional displacement components. Holographic image of the mode shape at 1341 Hz reveals that the cantilever undergoes torsional oscillations in one direction, while at 1991 Hz the torsion is observed in another direction. One may assume, that the third cantilever resonance occurs at 1341 Hz frequency, while higher vibration modes are excited at 1991 Hz.

Table 28 summarizes natural frequencies for different cantilever configurations tested in the laser vibrometry setup, while Table 29 lists natural frequencies derived from holographic interferometry measurements. The values of natural frequencies obtained using different optical measurement techniques are in a close agreement (discrepancies are in the range of 2-3%). Moreover, it could be reiterated that this study attempted to optimize and then fabricate optimally-shaped cantilevers (OPT II and OPT III) so as their second and third natural frequencies of transverse vibrations would be equal to the corresponding frequencies of cantilever with constant cross section OPT 0 (ω_2 = 480 Hz and ω_3 = 1335 Hz). Presented experimental results indicate that for the cantilever OPT II the second natural frequency is equal to 490 Hz, while for OPT III the third natural frequency is 1368 Hz, which amounts to 2% error with respect to the values of corresponding frequencies obtained for cantilever OPT 0.

Table 28. Summary of natural frequencies for different cantilever configurations measured with Laser Doppler Vibrometry System

Cantilever configuration		Support location					
		Unsupported		x/l=0.78		x/l=0.87	
		ω, Hz	A, mm	ω, Hz	A, mm	ω, Hz	A, mm
OPT 0	ω_1	75	0.2	-	-	46	0.013
	ω_2	470	0.002	469	0.02	410	0.005
	ω_3	-	-	-	-	-	-
OPT II	ω_1	64	3.15	-	-	-	-
	ω_2	490	0.04	492	0.35	395	0.99
	ω_3	-	-	1128	0.01	1249	0.141
OPT III	ω_1	58	3.33	-	-	-	-
	ω_2	396	0.2	396	0.94	350	0.05
	ω_3	-	-	-	-	-	-

Table 29. Summary of natural frequencies for different cantilever configurations determined with holographic measurement system

Cantilever configurations		Natural Frequencies, Hz	
		Rigid support location	
		Unsupported	x/l=0.8
OPT 0	ω_1	77	-
	ω_2	480	465
	ω_n	1335	1186, 1402
OPT II	ω_1	63	-
	ω_2	490	479
	ω_n	1158	1133, 1160
OPT III	ω_1	58	-
	ω_2	402	372
	ω_n	1368	1341, 1991

To conclude with, this section presented experimental study of optimal cantilever beam structures. Dynamic responses were analyzed for cantilevers of non-optimized (i.e., constant cross-section, OPT 0), optimal for operation at increased second resonant frequency (OPT II) and optimal for operation at increased third resonant frequency (OPT III). Comparing study results one may note, that shape of the cantilever highly influences its dynamic response, namely:

- first resonant frequency shifts by 22% if one compares OPT 0 and OPT III configurations, besides tip displacement amplitudes at the first natural frequency are 16 times higher for OPT III;
- cantilever, optimal for operation at its increased second resonant frequency (OPT II), posses the highest second resonant frequency amongst others; second resonant frequency for this structure remains highest as all structures are operating in vibro-impacting mode. Moreover, as this structure is operating in vibro-impacting mode, it posses highest cantilever tip displacement amplitudes at second resonant frequency (e.g., OPT II tip displacement amplitudes are 17 times higher if compared to the OPT 0 tip displacement amplitudes).
- cantilever optimal for operation at its increased third resonant frequency (OPT III) posses the highest second third frequency amongst others;

Insights on dynamic response of optimized cantilever beam structures presented in this section may serve as a basis for enhanced PEH designs, allowing controlling resonant frequencies as well as device amplitudes without addition of concentrated masses at the tip of cantilever. In such a way the device still possesses all features of distributed parameter system and higher vibration modes may as well be exploited for energy harvesting as opposed to the typical single degree of freedom systems (cantilevers with concentrated masses at the tip), which utilizes only its first resonant frequency.

3.5. Section conclusions

This section presented the reader with equipment, customized experimental stands, fabrication of PEH prototypes as well as experimental studies performed during the course of research.

Most of experimental studies were performed exploiting Laser Doppler Vibromery and Holographic Measurement systems, thus a significant part of the section is devoted to their description and operation principles. Experiments performed during the course of the research were grouped into three case analysis studies: i) investigations of effects of connected electric circuit to dynamic and electric characteristics of PEH prototype; ii) investigations of PEH prototypes with non-segmented and segmented piezoelectric layers and effects of incorporated support location to electric outputs of PEH prototypes, operating in vibro-impacting regime; iii) investigations of dynamic response of optimal cantilever beams intended for energy scavenging applications.

The main conclusions of the first case analysis study devoted for analysis of effects of connected electric circuit to performance of PEH prototype may be summarized to:

- dynamic and electric response of PEH prototype is influenced by resistance of connected electric circuit;
- if one increases resistance of connected electric circuit, changes in structure's resonant frequency, tip displacement, generated voltage, current and power may be noted;
- one may experimentally determine such value of resistance (so called optimal load) of connected electric circuit at which PEH prototype would generate maximum power.

The main conclusions of the second case analysis study devoted for investigations of PEH prototypes with segmented and non-segmented piezoelectric layers and effects of rigid support location state that for achieving the most favourable trade-off between PEH power output and bandwidth:

- incorporated support location should coincide with the nodal point of the second transverse mode or the second nodal point of the third transverse mode in order to intensify amplitudes of these vibration modes during impact;
- piezoelectric layer should be segmented in such a way that it does not cover strain nodes of the vibrating harvester, thereby avoiding detrimental charge cancellation effects in piezoelectric material when PEH is operating at higher frequencies or is excited by random signal.

The main conclusions of the third case analysis study devoted for optimal cantilever structures state that cantilever shape highly influences its dynamic response, namely

- one may note shifts in the first, second and third resonant frequency of optimal cantilever beams if compared to the constant cross-section counterpart;
- cantilever beams tip displacement amplitude in resonances is much greater for optimal cantilevers (e.g., cantilever, optimal for operation at its increased second

resonant frequency posses the highest second resonant frequency tip displacement amplitudes amongst others;

Insights of the experimental research presented in the section verified the adequacy of developed FE model of PEH (i.e., experimental results follow the same laws and patterns as numerical simulation results) and led to the development, fabrication and analysis of enhanced piezoelectric energy harvester, which is described in section 4.

4. ANALYSIS OF PIEZOELECTRIC ENERGY PROTOTYPE BASED ON RATIONAL CANTILEVER BEAM STRUCTURE

Literature review presented in the first section reveals that relatively little research work has been performed on structural optimization of cantilever-type vibro-impacting PEHs with thorough dynamic response studies being scarce. Investigation of dynamics-related performance parameters of vibro-impact systems (VIS) such as operation speed, stability, reliability, longevity is a high priority topic among the other research work [86], as designing a commercially viable device is possible only through in-depth understanding and accurate prediction of its vibrational behaviour.

Dynamic characteristics of vibro-impact systems are influenced by various structural parameters. Theoretical model of a cantilever-type VIS was analyzed by Wang and Wu [87]. They have employed numerical methods to determine the influence of clearance, damping and cubic nonlinearities on dynamic characteristics of the system and reported results found practical applications by exploiting the nonlinear phenomena and the instability mechanism. Previous research work on VIS dynamics is also concerned with: methodology to automatically choose measurement locations of a nonlinear structure that needs to be monitored while operating [88]; deriving piecewise-linear models with a single degree of freedom for a driven vertical cantilever with localized mass and symmetric stops [89]; introducing modelling framework that is suitable to resolve singularities of impact phenomena encountered in practical applications [90]; or developing novel optimized cantilevers with enhanced travel ranges [91].

Researchers working in the field of vibration energy harvesters proposed a number of different designs and approaches to improve power generation efficiency. Patel [92] developed a versatile linear model that accurately predicts the performance of cantilever-type PEH. An integral part of this model used a transfer matrix method to accommodate the difference in structural dynamics for both uniform and non-uniform structures. The developed linear model was used to carry out parametric studies on geometry of three distinct energy harvester configurations, thus revealing key variables and geometrical changes which can improve harvester performance up to 200%. Barton and Burrow [93] performed experiments with nonlinear PEHS using control-based continuation method, which resulted in a number of different device configurations. Khovanova and Khovanov [94] conducted a comparative analysis of linear and nonlinear piezoelectric PEHs subjected to random impulsive excitations modelled by white Poisson noise. They showed that harvester performance depends on both nonlinearity and properties of ambient energy, while nonlinearity should be optimized for a given type of ambient vibration in order to achieve efficient energy harvesting. Multiphysics finite element model of a vibro-impacting PEH was reported in [95] demonstrating the coupling of mechanical, piezoelectric and fluidic domains. The model was used to run various dynamic simulations that revealed influence of structural, excitation and ambient pressure parameters on dynamic and electric performance of the device. Jacquelin et al. [96] studied piezoelectric impact type energy harvesting device consisting of two

piezoelectric beams and seismic mass with the final aim to optimize its performance. Dynamic simulations were used to study influence of various mechanical design parameters (seismic mass, beam length, stopgap, gliding length, impact location) on performance of the system. It was shown that impact location is an important parameter and may be optimized only through simulation. Li et al. [97] and Lv et al. [98] adopted design approaches different from common cantilever-based configuration. Authors in [97] presented practical acoustic energy harvesting mechanism for relatively low audible frequency using the quarter-wavelength straight tube resonator with multiple PZT cantilever plates, while [98] reported PEH based on solid-solid phononic crystal and piezoelectric material. Zhang [99] proposed design optimization of a single piezoelectric bimorph generator using genetic algorithm. It was based on the notion that optimized solutions for an equation can be approached by iteratively combining an initial pool of solutions and varying successive iterations in a fashion similar to the process of "genetic evolution". Vullers et al. [100] generalized energy harvesting components and their power management circuits. They have concluded that management circuits for micro-power sources have received comparatively little attention and progress is required in order to decrease the percentage of generated power used for power management. Roundy and Wright [101] considered modelling, design and optimization of PEHs. They proposed model of the cantilever-type PEH with end mass aimed to lower the first natural frequency. This allowed simplification of the distributed parameter system to a single degree of freedom system and higher vibration modes were excluded from the study.

Meanwhile, this research aims to reduce the first natural frequency of cantilever-type PEH by treating its structure as distributed parameter system that is characterized by variable cross sections, which are distributed along the length of the cantilever using dynamic optimization procedure. It is expected that pre-defined modes of settled transverse vibrations can be excited employing optimal structures, which could lead to improved power generation in energy harvesting applications.

Moreover, this section describes steps that were taken to implement the final aim of the research - development of enhanced configuration PEH prototype. The knowledge obtained through numerical simulations presented in section 2 as well as experimental research sections provided in section 3 enabled one to introduce enhanced PEH prototype based on rational cantilever beam substrate with segmented piezoelectric material layers. The section will cover numerical and experimental research of rational PEH as well as comparison of electrical outputs of enhanced configuration PEH to electrical outputs of typical configuration PEH.

As already mentioned in 2.5 section, initial step of PEH configuration enhancement was related to the optimization of PEH prototype substrate. Cantilever beam structure optimization was based on information provided in [69]. The aim of structure optimization was to select such geometrical parameters that would correspond to technical characteristics of the system and give a minimum value to its mass at a predetermined vibration frequency. Optimization target function and constrains as well as optimal configurations of cantilevers for operation at prescribed increased and decreased second and third resonant frequencies were already

described in 2.5 section. However, it is obvious that large-scale accurate fabrication of such intricate structure with smooth variation of cross section would be relatively complex from technological point of view leading to prohibitively high manufacturing costs. In addition, straightforward covering of the curved surface of the optimal cantilever with brittle piezoceramic layers would not be possible, requiring application of special techniques for deposition of the active layers, which would further raise the costs. Therefore, simple-to-fabricate rational cantilever structure (OPT RAT) was designed on the basis of optimal cantilever OPT II⁻ (the second cantilever from top in Figure 34, b), intended for operation at the reduced second natural frequency.

In order to determine structural parameters of the rational cantilever, a 2D finite element model was created and analyzed in Comsol Multiphysics (Figure 64). The objective of the conducted simulations was to determine such geometric configuration of the OPT RAT cantilever that would allow it to be excited at the predetermined second natural frequency.
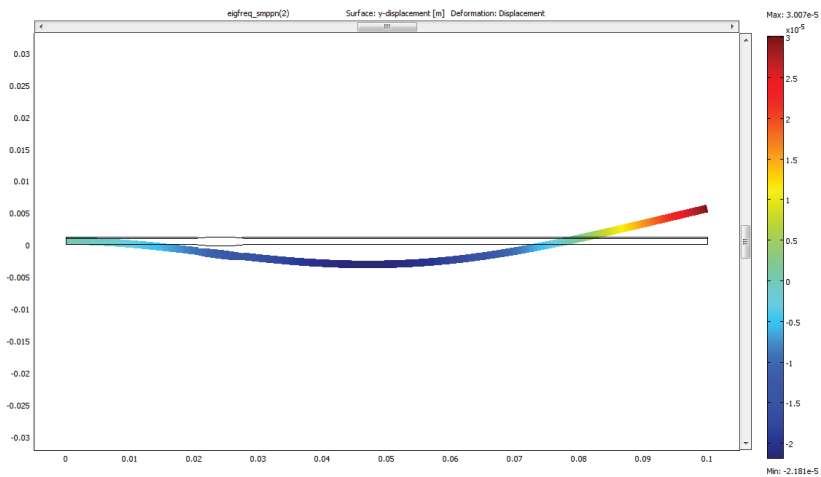
Figure 64. Visualization of FE model of OPT RAT PEH prototype developed in Comsol Multiphysics

Figure 65 provides structural configuration of the modelled PEH prototype that is intended for operation in transversal (d_{31}) mode. The prototype consists of the rationally-shaped cantilever of stainless steel (UNS S30100) covered with piezoelectric PVDF layers. A rational design approach that is adopted here implies that an optimally-shaped zone of increased cross section (with centre located at 0.24L) in the optimal cantilever OPT II⁻ (Figure 34, b)) is replaced by a hump-like zone, length of which varies from 1 to 7 mm, while sections of the structure outside the hump retain constant cross section (overall length and width of the cantilever do not change with respect to the initial cantilever of constant cross section). Flexible PVDF patches with electrical leads were used for PEH prototype fabrication, therefore three separate PVDF segments were introduced in the FE model as depicted in Figure 65. It was assumed that ideally conductive electrodes of

104

negligible thickness cover the entire area of the top and bottom surfaces of the piezoelectric layers. Modelling was performed by applying Lagrange-quadratic elements using plane-strain approximation since transverse vibration modes have more significant influence on vibro-impact process in comparison to the torsional modes. Appropriate mechanical and electrical boundary conditions were set to represent cantilever clamping and electrodes on piezoelectric layers. In addition, FE model of PEH based on cantilever of constant cross section OPT 0 was realized (Figure 65). Both OPT RAT and OPT 0 models were subjected to harmonic and random base excitations, which were defined as vertically acting body load. In order to introduce random excitation signal to the FE model, the following steps were taken: i) transient acceleration characteristics of operating industrial heating fan were registered; ii) registered signal was approximated using Matlab code, which resulted in several mathematical expressions of excitation signal, qualitatively defined by the coefficient of determination R^{2}; iii) random signal approximation with the greatest value of coefficient of determination was introduced in the FE as a vertically acting body load. Resistive load was introduced to the electromechanically coupled system via SPICE circuit editor enabling prediction of the generated voltage. Simulations were performed for both freely vibrating (i.e. unsupported) and vibro-impacting cantilevers (support located at $1.0L$). Results of numerical modal analysis indicate that natural frequencies of OPT RAT and OPT 0 models are as follows: $\omega_1 = 58$ Hz, $\omega_2 = 348$ Hz, $\omega_3 = 988$ Hz and $\omega_1 = 87$ Hz, $\omega_2 = 536$ Hz, $\omega_3 = 1493$ Hz, respectively.
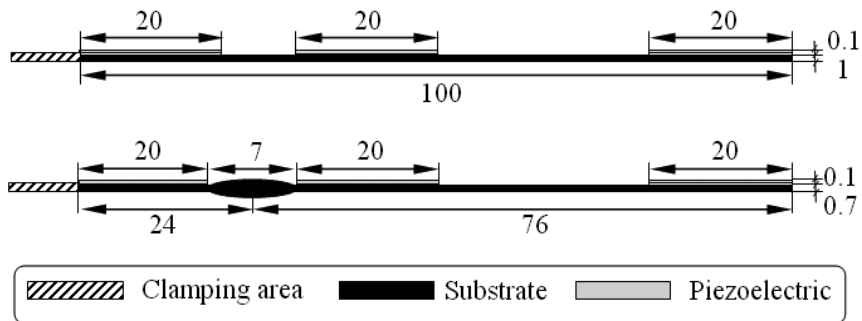
Figure 65. Technical drawings of modelled and fabricated energy harvesting prototypes: a) OPT 0; b) OPT RAT

Geometric parameters of the OPT RAT model were used to fabricate a prototype of the piezoelectric energy harvester (depicted in Figure 66) by employing rationally-shaped cantilever structure as a substrate and attaching atop three separate laminated PVDF segments with leads LDT1-028K/L (Measurement Specialties, Inc.) Natural frequencies of transverse vibrations of the fabricated OPR RAT harvester were measured to be $\omega_1 = 48$ Hz, $\omega_2 = 271$ Hz, $\omega_3 = 746$ Hz. Discrepancy between the measured and simulated frequency values is attributed to added mass of electrical leads (neglected in the model) and non-ideal clamping of the prototype, both contributing to the decrease of the natural frequencies. PEH prototype OPT 0

was also fabricated following the same procedure but using steel cantilever of constant cross section as a substrate.
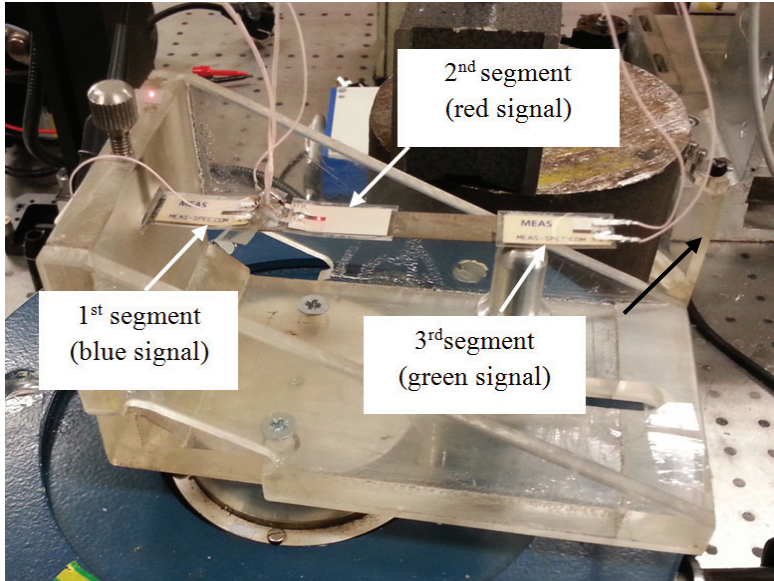
Figure 66. Picture of actual fabricated prototype OPT RAT.

Both PEH prototypes were subjected to electrical characterization in the laser vibrometry setu in order to compare their energy harvesting performance. Generated open-circuit voltages were measured for two cases: i) unsupported cantilever; ii) vibro-impacting cantilever with support located at the free end (1.0L). Figure 67 presents plots of voltage signals collected by three PVDF segments of OPT 0 prototype, which is subjected to harmonic excitation at its first natural frequency of 71 Hz when the cantilever of constant cross section is vibrating without impacts (Figure 67, a)) and with impacts (Figure 67, b)). Meanwhile, Figure 68 provides analogous plots for the case of OPT RAT prototype (excitation signal frequency – 45 Hz). Comparison of shapes of voltage signals generated by both prototypes operating in vibro-impact mode indicates markedly larger content of higher-order harmonics in the case of OPT RAT signals. Consequently, it demonstrates that OPT RAT prototype undergoes self-excitation at higher modes with the predominant second mode of transverse vibrations. Thus, excitation of the proposed rationally-shaped vibro-impacting PEH at low first natural frequency (48 Hz) induces vigorous vibrations at much higher frequencies (>270 Hz), which results in improved energy harvesting efficiency under variable-magnitude excitation conditions since it is known that generated power in vibration energy harvesters is strongly dependent on the frequency of oscillation: higher operational frequency ω_{op} of the piezoelectric transducer (characterized by capacitance C_h) leads to stronger electrical damping due to reduced optimal load resistance ($R_{opt} = 1/\omega_{op} \cdot C_h$), thereby increasing power flow into the electrical load.
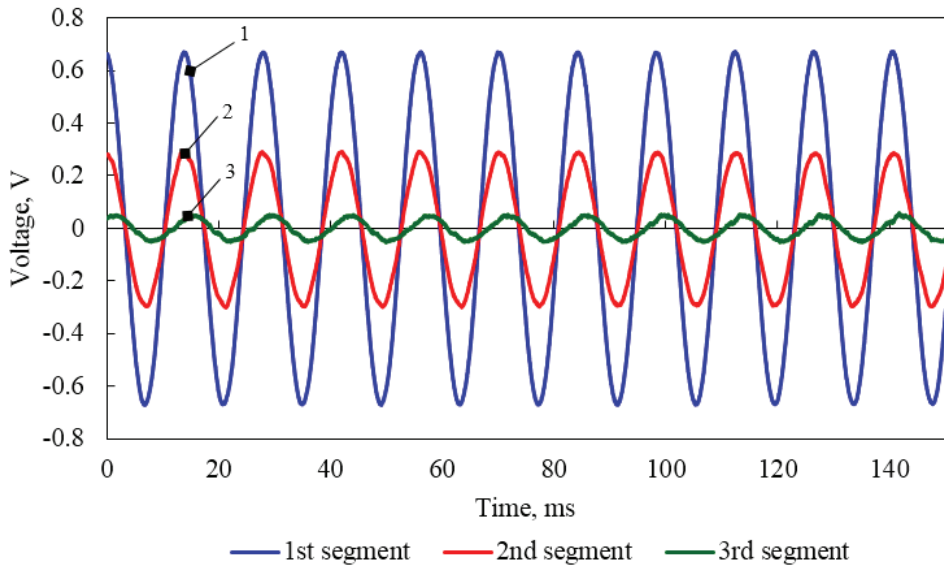
a)
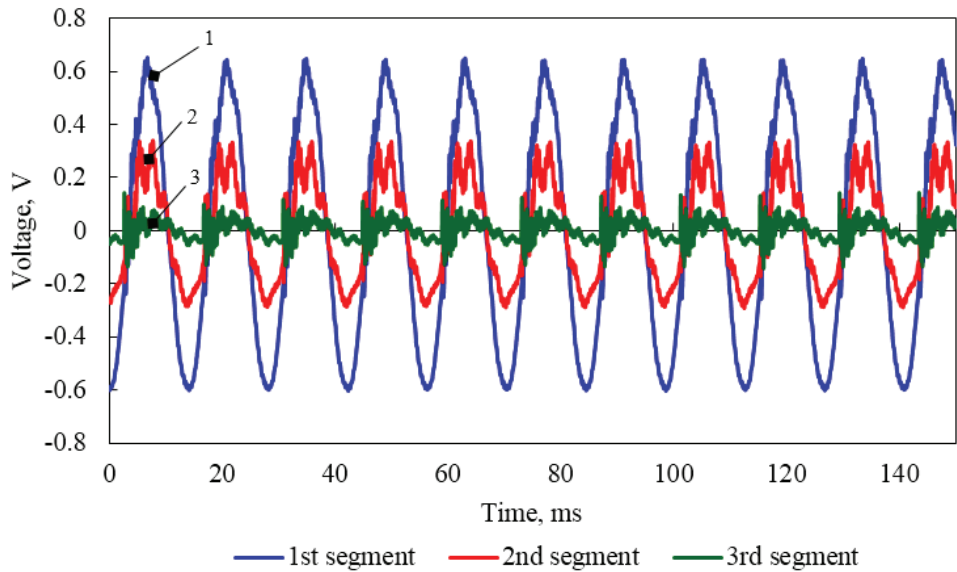
b)

Figure 67. Experimentally determined electrical outputs of OPT 0 prototype (1st PVDF segment – blue, 2nd – red, 3rd – green lines), operating a) unsupported; b) in vibro-impacting mode (support located at 1.0*L*)

a)

b)

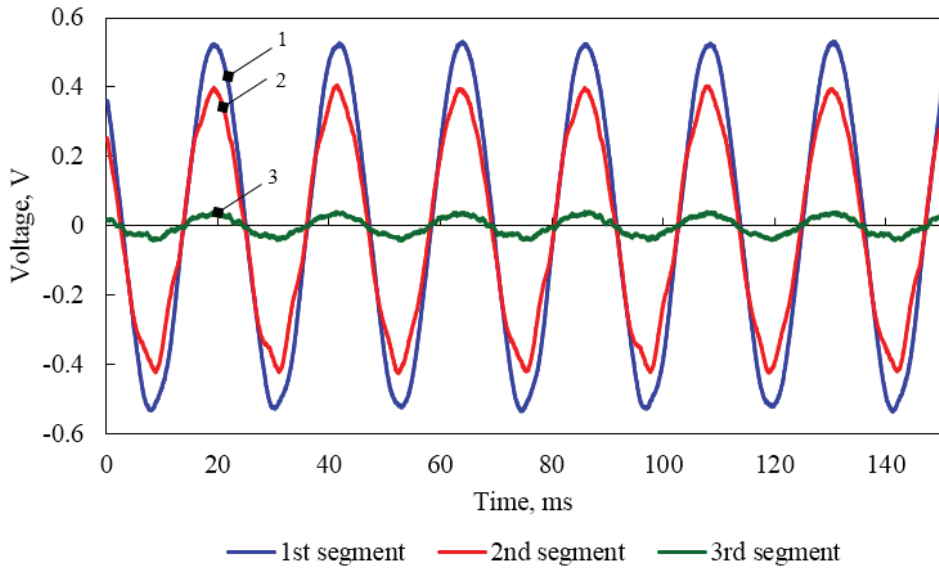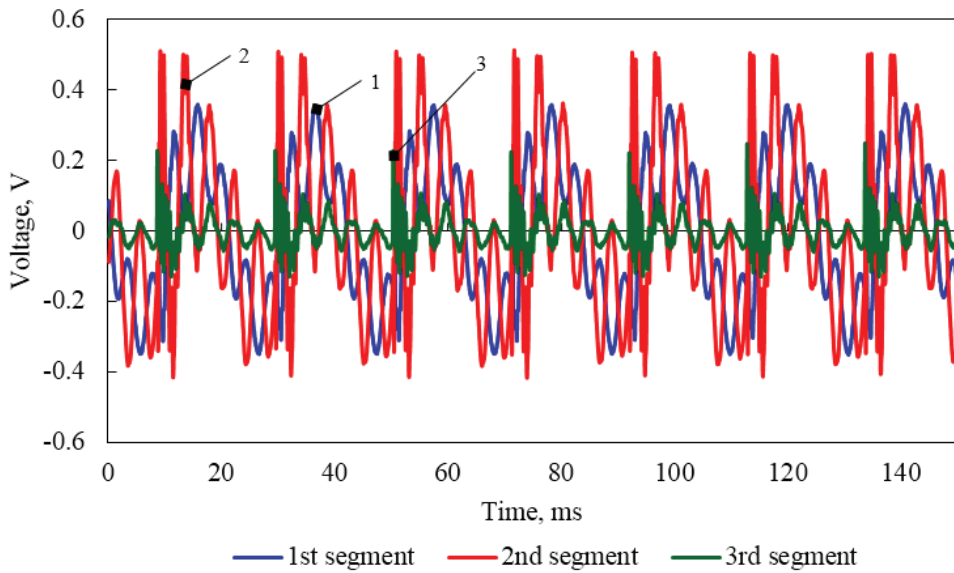**Figure 68.** Experimentally determined electrical outputs of OPT RAT prototype (1st PVDF segment – blue, 2nd – red, 3rd – green lines), operating a) unsupported; b) in vibro-impacting mode (support located at 1.0*L*).

Table 30. V_{RMS} voltages generated by OPT0 and OPT RAT energy harvester prototypes

Energy harvester prototype configuration	V^1_{RMS}, mV	V^2_{RMS}, mV	V^3_{RMS}, mV	ΣV_{RMS}, mV
OPT 0, unsupported	472.10	206.10	32.38	710.58
OPT RAT, unsupported	373.30	279.90	24.99	678.19
OPT 0, supported at x/l=1	243.60	128.70	45.14	417.44
OPT RAT, supported at x/l=1	195.50	232.50	46.67	474.67

The aim of this study was to validate an approach based on effective exploitation of intrinsic modal characteristics of elastic structures for increasing power generation efficiency of cantilever-type piezoelectric energy harvester configured as a vibro-impact system with targeted applications in vibratory environments that are characterized by highly variable excitation amplitudes (i.e. vibration sources for which implementation of amplitude limiters (supports) in a harvesting device is inevitable in order to retain structural integrity of the components). The proposed VIPEH would be able to not only accommodate wide variations in excitation magnitude, but would also deliver improved energy harvesting performance due to amplified higher-order mode responses resulting in better energy conversion efficiency attributed to increased electrical damping. The adopted design approach is referred here as rational since shape of the piezoelectric cantilever is derived on the basis of optimal structures, i.e. the rationally-designed PEH substrate effectively reproduces modal behaviour that is characteristic to the cantilever structures with distribution of cross-sectional areas determined through dynamic optimization. The proposed vibration energy harvester constitutes an adaptive device that could provide enhanced harvesting performance under varying real-life excitation conditions. In addition, due to rational design modifications the device is amenable to conventional machining and thus represents a cost-effective alternative to the energy harvesters that are based on complex-shaped optimal structures.

CONCLUSIONS

1. Literature review presented and summarized recent research ongoing in the field of energy harvesting. It was determined that the main issue hindering practical application of piezoelectric energy harvesters is their low efficiency (5-20 %), especially prominent when harvesters are excited by random signals. To resolve the low efficiency issue, configuration of piezoelectric energy harvester with incorporated support was suggested, which allows to take benefit of self-excitation of higher vibration modes when harvester is operating in vibro-impacting mode.
2. A universal finite element model of piezoelectric energy harvester was developed, allowing integrated investigations of dynamic and electric response of harvester to harmonic and random excitation signal, interference of external electric circuit with electromechanical coupling of harvester and nonlinear dynamic effects occurring as harvester is impacting on incorporated rigid support.
3. Developed FE model was used to evaluate effects of harmonic and random excitation signal, variation of shape and geometric configuration of harvester, segmentation of its piezoelectric layers, support location and connected electric circuit to dynamic and electric response of harvester. Numerical simulation results revealed that:
    i)   piezoelectric energy harvester models operating in vibro-impacting regime and excited by random excitation signal may generate up to 1.3 greater RMS voltages, when rigid support location coincides with the nodal points of vibration modes ($0.78L$ or $0.87L$), if compared to harvesters impacting on rigid support at other locations;
    ii) harvester prototypes with piezoelectric layers segmented at strain nodal points of higher vibration modes ($0.22L$, or $0.13L$ and $0.5L$) may generate up to 2 times greater RMS voltages, if compared to the harvesters with continuous piezoelectric material layers;
    iii) rational piezoelectric energy harvester configuration (with the cross section thickened at $0.24L$) may outperform typical configuration piezoelectric energy harvester in terms of generated RMS voltages by 6 times (if both are excited by random signal, with the support placed at $0.78L$).
4. Laser Doppler Vibrometry and Holographic measurement stands were adapted to perform experimental studies of piezoelectric energy harvester prototypes. Experimental tests verified:
    i)   influence of external electric circuit on electric (increase in generated voltage, decrease in generated current and change in generated power) and mechanical (increase in resonant frequency and change in tip displacement) response of piezoelectric energy harvester;
    ii) beneficial effect (increase in generated voltages) of segmentation of piezoelectric layers of harvester at the strain nodal point of higher vibration mode ($0.22L$);

iii) previously only theoretically described dynamic behaviour of optimal shape cantilever substrates (changes in resonant frequency and displacement amplitude);

iv) adequacy of developed FE model (experimentally determined harvester characteristics follow the same laws as determined via numerical simulations).

5. Piezoelectric energy harvester design that would ensure effective electrical energy generation under varying mechanical excitation conditions was developed. Developed harvester concept based on incorporation of rigid support, location of which coincides with the nodal points of vibration modes ($0.78L$ or $0.87L$), and rational substrate shape - simplified optimal cantilever configuration, which is obtained by thickening the cantilever at particular point of cross section ($0.24L$). This allows self-excitation of higher harvester vibration modes when it is operating in vibro-impacting mode and, thus, increase in harvester generated voltages.

REFERENCES

1. J. Yick, B. Mukherjee, D. Ghosal, Wireless sensor network survey, *Computer Networks*, vol. 52, 2008, p.2292-2330.
2. A. Dewan, S.U. Ay, M.N. Karim, H. Beyenal, Alternative power sources for remote sensors: a review, *Power Sources*, vol. 245, 2014, p.129-143.
3. I.F. Akyildiz, W. Su, Y. Sankarasubramaniam, E. Cayirci, Wireless sensor networks: a survey, *Computer Networks*, vol. 38, 2002, p.393-422.
4. Q. Wang, M. Hempstead, W. Yang, A realistic power consumption model for wireless sensor network devices, *Sensor and Ad Hoc Communications and Networks*, vol. 1, 2006, p. 286-295.
5. A. Dementyev, S. Hodges, S. Taylor, J. Smith, Power consumption analysis of Bluetooth low energy, ZigBee and ANT sensor nodes in a cyclic sleep scenario, *Wireless Symposium (IWS), 2013 IEEE International*, 2013, p. 1-4.
6. A.J. Odey, D. Li, Low power transceiver design parameters for wireless sensor networks, *Wireless Sensor Networks*, vol. 4, 2012, p. 243-249.
7. G. Deng, *Receiver cost cognizant maximal lifetime routing in embedded networks: model and solutions*, PhD Thesis, Arizona State University, 2009.
8. C. Kompis, S. Aliwell, Energy harvesting technologies to enable remote and wireless sensing, report in *Sensors and Instrumentation* series, 2008, p. 1-72.
9 J.A. Paradiso, T. Starner, Energy scavenging for mobile and wireless electronics, *IEEE Pervasive Computing*, vol. 4, 2005, p. 18-27.
10. D. Zhu, Vibration energy harvesting: machinery vibration, human movement and flow induced vibration, *Sustainable Energy Harvesting Technologies - Past, Present and Future*, 2011, p. 1-54.
11. H. Wang, Z. Ren, J.D. Park, Power electronic converters for microbial fuel cell energy extraction: effects of inductance, duty ratio, and switching frequency, *Power Sources*, vol. 220, 2012, p. 89-94.
12. S. Roundy, P.K. Wright, J. Rabaey, *Energy scavenging for wireless sensor networks with special focus on vibrations*, 2004.
13. S.P. Beeby, M.J. Tudor, N. M. White, Energy harvesting vibration sources for microsystems applications, *Measurement Science and Technology*, vol. 17, 2006, p. 175-195.
14. S. Roundy, P. K. Wright, J. Rabaey, A study of low level vibrations as a power source for wireless sensor nodes, *Computer Communications*, vol. 26, 2003, p. 1131–1144.
15. C. Williams, R. Yates, Analysis of a micro-electric generator for microsystems, *Sensors and Actuators*, vol. 52, 1996, p. 8-11.
16. X. Cao, Y. Lee, Design and fabrication of mini vibration power generation system for micro sensor networks, *IEEE International Conference on Information Acquisition*, 20-23 August, 2006, p. 91-95.
17. S. D. Nguyen, *Wideband MEMS energy harvesters utilizing nonlinear springs*, PhD Thesis, University of Oslo, 2012, p. 1-146.
18. Y. Chiu, C.T. Kuo, Y.S. Chu, MEMS design and fabrication of an electrostatic vibration-to-electricity energy converter, *Microsystem Technologies*, vol.13, 2007, p. 1663-1669.
19. S. Meninger, J. Mur-Miranda, R. Amirtharajah, A. Chandrakasan, J. Lang, Vibration-to-electric energy conversion, *IEEE Transactions on very large scale integration systems*, vol.9, 2001, p. 64-76.
20. S. Boisseau, G. Despesse, B. Ahmed Seddik, Electrostatic conversion for vibration energy harvesting, *Small-Scale Energy Harvesting*, Intech, 2012, p. 1-39.

21. W.H. Ko, *Piezoelectric energy converter for electronic implants*, US Patent 3 456 134, 1969.

22. P. Glynne-Jones, S. Beeby, N. White, Towards a piezoelectric vibration-powered microgenerator, *Science, Measurement and Technology,* IEE Proceedings, vol. 148, 201, p. 68-72.

23. N.M. White, P. Glynne-Jones, S.P. Beeby, A novel thick-film piezoelectric micro-generator, *Smart Materials and Structures*, vol. 10, 2001, p. 850-852.

24. L. Mateu, F. Moll, Review of energy harvesting techniques and applications for microelectronics (Keynote Address), *Proceedings of the SPIE*, vol. 5837, 2005, p. 359-373.

25. D. Guyomar, A. Badel, E. Lefeuvre, C. Richard, Toward energy harvesting using active materials and conversion improvement by nonlinear processing, *IEEE Transactions on Ultrasonics, Ferroelectrics and Frequency Control*, vol. 52, 2005, p. 584 – 595.

26. P.D. Mitcheson, E.M. Yeatman, G.K. Rao, A. S. Holmes, T. C. Green, Energy harvesting from human and machine motion for wireless electronic devices, *Proceedings of the IEEE*, vol. 96, 2008, p. 1457 – 1486.

27. A. Erturk, D.J. Inman, A distributed parameter electromechanical model for cantilevered piezoelectric energy harvesters, *Vibration and Acoustics*, vol. 130, 2008, p. 041002 1-15.

28. IEEE Ultrasonics, Ferroelectrics, and Frequency Control Society, 176-1987 - *IEEE Standard on Piezoelectricity*, 1988.

29. J.M. Gilbert, F. Balouchi, Comparison of energy harvesting systems for wireless sensor networks, *Automation and Computing*, vol. 5, 2008, p. 334 – 347.

30. A. Erturk, *Electromechanical modelling of piezoelectric energy harvesters*, PhD thesis, Virginia Polytechnic Institute and State University, 2009.

31. *HC Materials*, *Giant-piezo crystals*, Catalog, [interactive] [last accessed 29 May 2014], available online in www.hcmat.com.

32. A.G. Holmes-Siedle, P.D. Wilson, A.P. Verrall, PVdF: An electronically-active polymer for industry, *Materials and Design*, vol. 4, 1984, p. 910-918.

33. Y. Ito, *Piezoelectricity*, Wiley Encyclopedia of Electrical and Electronics Engineering, NY, 1999.

34. S.R. Anton, H.A. Sodano, A review of power harvesting using piezoelectric materials (2003–2006), *Smart Materials and Structures*, vol. 16, 2007, 10.1088/0964-1726/16/3/R01.

35. L. Mateu, F. Moll, Optimum piezoelectric bending beam structures for energy harvesting, *Intelligent Material Systems and Structures*, vol. 16, 2005, p. 835-845.

36. P. Glynne-Jones, S.P. Beeby, A novel thick film piezoelectric microgenerator, *Smart Materials and Structures*, vol. 10, 2001, p. 850-852.

37. S. Roundy, On the effectiveness of vibration-based energy harvesting, *Intelligent Materials and Structures*, vol. 16, 2005, p. 809-823.

38. K. Mossi, C. Green, C. Ounaies, E. Hughes, Harvesting energy using a thin unimorph prestressed bender: geometrical effects, *Intelligent Material Systems and Structures*, vol. 16, 2005, p. 249-261.

39. H.S. Yoon, G. Washington, Modelling, optimization, and design of efficient initially curved piezoceramic unimorphs for energy harvesting applications, *Intelligent Materials and Structures*, vol. 16, 2005, p. 877-888.

40. H.P. Lee, S.P. Lim, Modelling and analysis of micropiezoelectric power generators for MEMS application, *Smart Material Structures*, vol. 13, 2004, p. 57.

41. Y. B. Jeon, R. Sood, J. Jeong, S. G. Kim, MEMS power generator with transverse mode thin film PZT, *Sensors and Actuators*, vol. 122, 2005, p. 16-22.

42. S. Jiang, X. Li, Y.Hu, Performance of a piezoelectric bimorph for scavenging vibration energy, *Smart Materials and Structures*, vol. 14, 2005, p. 769-771.

43. T.A. Anderson, D.W. Sexton, A vibration energy harvesting sensor platform for increased industrial efficiency, *Proceeding of Smart Structures and Materials*, 2006, p. 6174.

44. S.P. Gurav, Uncertainty based design optimization of a micro piezoelectric energy reclamation device, *Multidisciplinary Analysis and Optimization Conference*, 2004, p. 3559-3570.

45. S. Roundy, P.K. Wright, J. Rabaey, *Energy scavenging for wireless sensor networks with special focus on vibrations*, 2004.

46. J. Twiefel, H. Westermann, Survey on broadband techniques for vibration energy harvesting, *Intelligent Material Systems and Structures*, 2013, in press.

47. J.Q. Liu, H.B. Fang, Z.Y. Xu, X.H. Mao, H.C. Shen, D. Chen, H. Liao, B.C. Cai, A MEMS-based piezoelectric power generator array for vibration energy harvesting, *Microelectronics*, vol. 39, 2008, p. 802-806.

48. Z. Yang, J.S. Yang, Connected vibrating piezoelectric bimorph beams as a wide-band piezoelectric power harvester, *Intelligent Material Systems and Structures*, vol. 20, 2009, p. 569-574.

49. S. Stanton, C. McGehee, B.P. Mann, Reversible hysteresis for broadband magnetopiezoelastic energy harvesting, *Applied Physics Letters*, vol. 95, 2009.

50. R. Elfrink, T.M. Kamel, M. Goedbloed, S. Matova, D. Hohlfeld, Y. van Andel, R. van Schaijk, Vibration energy harvesting with aluminium nitride-based piezoelectric devices, *Micromechanics and Microengineering*, vol. 19, 2009, 094005.

51. M. Umeda, K. Nakamura, S. Ueha, Analysis of the transformation of mechanical impact energy to electric energy using piezoelectric vibrator, *Applied Physics (Jpn.)*, vol. 15, 1996, p. 3267-3273.

52. H. Liu, C.J. Tay, C. Quan, T. Kobayashi, C. Lee, A new S-shaped MEMS PZT cantilever for energy harvesting from low frequency vibrations below 30 Hz, *Microsystem Technologies*, vol. 18, 2012, p. 497-506.

53. K.H. Mak, S. McWilliam, A. A. Popov, Experimental model validation for a nonlinear energy harvester incorporating a bump stop, *Sound and Vibration*, vol. 331, 2012, 26022623.

54. J. Blystad, E. Halvorsen, A piezoelectric energy harvester with a mechanical end stop on one side, *Microsystem Technologies*, vol. 17, 2011, p. 505-511.

55. H. Liu, C.J. Tay, C. Quan, T. Kobayashi, C. Lee, Piezoelectric MEMS energy harvester for low-frequency vibrations with wideband operation range and steadily increased output power, *Microelectromechanical systems*, vol. 20, 2011, p. 1131-1142.

56. M. Pozzi, M. Zhu, Plucked piezoelectric bimorphs for knee-joint energy harvesting: modelling and experimental validation, *Smart Materials and Structures*, vol. 20, 2011, 055007.

57. L. Gu, C. Livermore, Impact-driven, frequency up-converting coupled vibration energy harvesting device for low frequency operation, *Smart Materials and Structures*, vol. 20, 2011, 045004.

58. M. Ferrari, V. Ferrari, M. Guzzetti, B. Ando, S. Baglio, C. Trigona, Improved energy harvesting from wideband vibrations by nonlinear piezoelectric converters, *Sensors and Actuators A: Physical*, vol. 162, 2010, p. 425-431.

59. S. Moss, A. Barry, I. Powlesland, S. Galea, G.P. Carman, A broadband vibro-impacting power harvester with symmetrical piezoelectric bimorph-stops, *Smart Materials and Structures*, vol. 20, 2011, 045013.

60. S. Moss, A. Barry, I. Powlesland, S. Galea, G. Carman, A low profile vibro-impacting energy harvester with symmetrical stops, *Applied Physics Letters*, vol. 97, 2010.

61. E.A. Jacquelin, S. Adhikari, M.I. Friswell, A piezoelectric device for impact energy harvesting, *Smart Materials and Structures*, vol. 20, 2011, 105008.

62. M. Renaud, P. Fiorini, C. Van Hoof, Optimization of a piezoelectric unimorph for shock and impact energy harvesting, *Smart Materials and Structures*, vol. 16, 2007, p. 1125–35.

63. G. Manla, *Design, modelling and characterization of impact based and non-contact piezoelectric harvesters for rotating objects*, PhD Thesis, University of Southampton, 2010.

64. L.V. Minh, M. Hara, H. Oguchi, H. Kuwano, Lead-free (K, Na)NbO$_3$ based impact type energy harvesters integrated with a cylindrical cavity for metal ball, *MEMS 2013*, 2013, p. 833-836.

65. N.G. Elvin, Equivalent electrical circuits for advanced energy harvesting, *Intelligent Material Systems and Structures*, 2014, p.1-12.

66. J. Dicken, I. Stoianov, P.D. Mitcheson, E.M. Yeatman, Power extraction circuits for piezoelectric energy harvesters in miniature and low-power applications, *IEE Transactions on Power Electronics*, vol. 27, 2012, p. 4514 - 4529.

67. L. Zhao, L. Tang, H. Wu, Y. Yang, Synchronized charge extraction for aeroelastic energy harvesting, *Active and Passive Smart Structures and Integrated Systems*, 2014.

68. S. Priya, Advances in energy harvesting using low profile piezoelectric transducers, *Electroceramics*, vol.19, 2007, p. 165–182.

69. V. Ostasevicus, R. Dauksevicius, *Microsystem Dynamics*, Springer, 2010.

70. A. Nechibvute, A. Chawanda, P.Luhanga, Finite Element Modelling of a Piezoelectric Composite Beam and Comparative Performance Study of Piezoelectric Materials for Voltage Generation, *Materials Science*, 2012, doi:10.5402/2012/921361.

71. R.A Islam, Realization of high-energy density polycrystalline piezoelectric ceramics, *Applied Physics*, vol. 88, 2006, p. 3.

72. J. Inderherbergh, Polyvinylidene fluoride (PVDF) appearance, general properties and processing, *Ferroelectrics*, vol. 115, p. 295-302.

73. *Catalogue of Ferroperm Piezoceramics A/S*, [interactive] [last accessed 20 May 214], available at www. ferroprm-piezo.com.

74. V. Piefort, *Finite Element Modelling of Piezoelectric active structures*, PhD Thesis, Active Structures Laboratory, Université Libre de Bruxelles, 2001, p. 126.

75. A. Erturk, D.J. Inman, An experimentally validated bimorph cantilever model for piezoelectric energy harvesting from base excitations, *Smart Materials and Structures*, vol. 18, 2009. p. 1-18.

76. A. Erturk, P.A. Tarazaga, J.R. Farmer, D.J. Inman, Effect of strain nodes and electrode configuration on piezoelectric energy harvesting form cantilevered beams, *Vibration and Acoustics*, vol. 11, 2009, 011010/1-11.

77. S. Kim, W.W. Clark, Q.M. Wang, Piezoelectric energy harvesting with a clamped circular plate: experimental study, *Intelligent Material Systems and Structures*, vol. 16, 2005, p. 847-854.

78. Holography system PRISM, [interactive] [last accessed 20 May 2014], available at http://ktu.edu/im/turinys/holografine-sistema-prism.

79. B. Narijauskaite, A. Palevicius, G. Janusas, R. Sakalys, Numerical investigation of dynamical properties of vibroactive pad during hot imprint process, *Vibroengineering*, vo. 15, 2013, p.1983.

80. M. Steinzig, A. Palevicius, Holographic PRISMA system for investigation of mechatronic systems, *Vibroengineering 2006*: proceedings of the 6th International Conference, October 12-14, 2006, Kaunas, Lithuania, 2006, p. 27-29.

81. *Resato, Waterjet technology*, [interactive] [last accessed 20 May 2104], available at http://www.resato.com/waterjet/en/producten/cat/waterjet-cutting-machines/,

82. *Resato, Waterjet technology*, brochure, [interactive] [last accessed 20 May 2014], available at http://www.resato.com/waterjet/fileadmin/resato/Waterjet-cutting/ Brochures_PDF / Waterjet_UK.pdf.

83. *Piezo systems Inc*, Product Catalogue, [interactive] [last accessed 20 May 2014], available at www.piezo.com.

84. G.A. Lesieutre, L. Davis, Can a coupling coefficient of a piezoelectric device be higher than those of its active material? *Smart Structures and Materials 1997*: Smart Structures and Integrated Systems, vol. 281, 1997.

85. *Piezosystems Inc.*, PSI-5H4E piezoceramic sheets, [interactive] [last accessed 20 May 2014], available at http://www.piezo.com/prodsheet2sq5H.html.

86. A. Preumont, Mechatronics: *Dynamics of Electromechanical and Piezoelectric Systems*, 2006.

87. Y.R. Wang, T.X. Wu, Analysis on the effect of system parameter on double cantilevers vibro-impact system response, *Advanced Materials Research*, vol. 518 – 523, 2012.

88. T.G. Ritto, Choice of measurement locations of nonlinear structures using proper orthogonal modes and effective independence distribution vector, *Shock and Vibration*, vol. 2014, 2014.

89. M. Elmegård, B. Krauskopf, H.M. Osinga, J. Starke, *Bifurcation analysis of a smoothed model of a forced impacting beam and comparison with an experiment*, Cornel University Library, Mathematics, Dynamical Systems, 2013.

90. R. Szalai, *Impact Mechanics of Elastic Structures with Point Contact*, University of Bristol, 2014.

91. R.R. Trivedi, M.M. Joglekar, R.P. Shimpi, D.N. Pawaskar, Shape optimization of electrostatically actuated micro cantilever beam with extended travel range using simulated annealing, *Proceedings of the World Congress on Engineering 2011*, vol. 3, 2011.

92. R. Patel, *Modelling, analysis and optimisation of cantilever piezoelectric energy harvesters*, PhD Thesis, The University of Nottingham, 2012.

93. D. Barton, S. G. Burrow, Numerical continuation in a physical experiment: investigation of a nonlinear energy harvester, *Computational Nonlinear Dynamics*, vol. 6, 2010.

94. N.A. Khovanova, I.A. Khovanov, The role of excitations statistic and nonlinearity in energy harvesting from random impulsive excitations, *Applied Physics Letters*, vol. 99, 2011.

95. S. Moss, A. Barry, I. Powlesland, S. Galea, G.P. Carman, A low profile vibro-impacting energy harvester with symmetrical stops, *Applied Physics Letters*, vol. 97, 2010, doi. 234101.

96. E. Jacquelin, S. Adhikari, M.I. Friswell, A piezoelectric device for impact energy harvesting, *Smart Materials and Structures*, vol. 20, 2011.

97. B. Li, J.H. You, Y.J. Kim, Low frequency acoustic energy harvesting using PZT piezoelectric plates in a straight tube resonator, *Smart Materials and Structures*, vol. 22, 20113.

98. H. Lv, X. Tian, M.Y. Wang, L. Dichen, Vibration energy harvesting using a phononic crystal with point defect states, *Applied Physics Letters*, vol. 102, 2013.

99. L. Zhang, *Analytical modelling and design optimization of piezoelectric bimorph energy harvester*, PhD Thesis, The University of Alabama, 2010.

100. R.J.M. Vullers, R. van Schaijka, I. Doms, C. Van Hoof, R. Mertens, Micropower energy harvesting, *Solid-State Electronics*, vol. 53, 2009.

101. S. Roundy, P.K. Wright, A piezoelectric vibration based generator for wireless electronics, *Smart Materials and Structures*, vol. 42, 2004.